Phosphorylation of Rab7 at serine 72 and its role in the regulation of the late endocytic pathway

Martin Wallace

University College London

and

Cancer Research UK London Research Institute

PhD Supervisor: Giampietro Schiavo

A thesis submitted for the degree of

Doctor of Philosophy

University College London

September 2014

Declaration

I, Martin Wallace, confirm that the work presented in this thesis is my own. Where information has been derived from other sources, I confirm that this has been indicated in the thesis.

Abstract

The small GTPase Rab7 is a key component of the endocytic pathway that controls endosomal maturation and fusion of late endosomes with lysosomes. Rab7 also regulates growth factor signaling by modulating receptor levels at the plasma membrane. While it is known how Rab7 is regulated through the GTPase cycle and interaction with its GEF and GAP, little is known about its regulation by post-translational modifications.

In this study, I identified two kinases, TBK1 and IKKε, which phosphorylate Rab7 at S72 in *in vitro* kinase assays. Both kinases are highly homologous and are activated in the innate immune response to bacterial and viral infection. Importantly, phosphorylation of Rab7 at S72 was increased by approximately 4-fold in mouse embryonic fibroblasts following 4 h stimulation of Toll-like receptor (TLR)3 with poly(I:C), a synthetic analog of viral dsRNA. A similar increase was also seen following stimulation of TLR4 with bacterial lipopolysaccharide after 8 h stimulation.

Through a pull-down and mass spectrometry analysis of differential interactors of unphosphorylated and S72-phosphorylated GST-Rab7, I found that phosphorylation of Rab7 at S72 inhibited interaction with RILP, one of its best known effectors, while, it increased interaction with the p150(Glued) subunit of the dynactin complex. The mass spectrometry analysis also identified a novel interactor, TNFR associated factor 3 (TRAF3), which is activated via the MyD88-independent pathway following stimulation of various TLRs. TRAF3 also leads to the downstream activation of TBK1 and IKKε.

Using subcellular fractionation and immunofluorescence with an anti-phospho-Rab7(S72) antibody, I found that the ratio of phosphorylated to unphosphorylated Rab7 is significantly higher on the membrane compared to the cytosol. Furthermore, the membrane staining of the S72-phosphorylated Rab7 indicates that it is a subpopulation of the total Rab7 that is associated with

vesicular structures. These results indicate that phosphorylation may occur on the membrane and could be a mechanism of controlling late endosome/lysosome transport and/or fusion.

As the S72 site is highly conserved and located in the switch II region, which is required to bind the switch I region upon GTP binding and activation, I performed an *in vitro* GTP hydrolysis assay using [α-P^{32}]GTP to determine the GTPase activity of S72-phosphorylated Rab7 compared to the unphosphorylated protein. Interestingly, there was a significant increase in GTP hydrolysis over time in the phosphorylated Rab7 compared to the unphosphorylated protein.

The results of this study indicate that phosphorylation of Rab7 at S72 promotes differential interaction of Rab7 with certain effectors, which may promote its recruitment for specific functions. These results also indicate that phosphorylation may increase Rab7 turnover *in vivo* by stimulating the intrinsic GTPase activity.

Acknowledgements

I would like to give a big thank you to my supervisor Giampietro Schiavo for being very supportive of me over the past 4 years and for not going too mad over my total lack of organisation. I've really enjoyed my time In the MNP lab and everyone I have met through my time here.

I would also like to thank all of the past and present members, who have been so helpful throughout my 4 years. To Matthew and Claire babysitting in the beginning and to the current members, Kinga, Katherine, Nathalie, and Solène for always being there to chat, debate, drink coffee…and beer, for the last 3/4 years. Your friendship has helped this experience never feel like too much 'work'.

Most importantly, I would like to thank my parents for being so supportive throughout my many years of university. I would never have lasted this long if it hadn't been for you both and I am very grateful for everything you have done for me. To my brothers, Cian and Eimhin, Pamela and my godson Ethan, I am lucky for all of you in my life and when I win the Nobel Prize I'll be sure to thank you all I the speech!

And final huge thank you to all the friends and colleagues who have made the last 4 years in London so memorable!

Table of figures

List of tables

Abbreviations

AIDS	autoimmune disorder syndrome
ALS	amyotrophic lateral sclerosis
APC	antigen-presenting cell
APP	amyloid precursor protein
BAFFR	B cell-activating factor receptor
BDNF	brain-derived neurotrophic factor
CI-MPR	cation-independent mannose 6-phosphate receptor
CMT2B	Charcot-Marie-Tooth type 2B
CORVET	class C core vacuole/endosome tethering
COX-2	cyclooxygenase 2
DAMP	danger-associated molecular pattern
DIC	dynein intermediate chain
DRG	dorsal root ganglion
dsRNA	double-stranded RNA
DUBs	deubiquitinating enzymes
ECM	extracellular matrix
EDTA	ethylenediaminetetraacetic acid
EEA1	early endosome antigen-1
EGF	epidermal growth factor
EGFR	epidermal growth factor receptor
ELISA	enzyme-linked immunosorbent assay
ER	endoplasmic reticulum
ESCRT	endosomal sorting complexes required for transport

FACS	fluorescent-activated cell sorting
FFAT	two phenylalanines (FF) in an acidic tract
FYCO1	FYVE and coiled-coil (CC) domain containing 1
GAP	GTPase-activating protein
GAS	Group A *Streptococcus*
GcAVs	GAS-containing autophagosome-like vacuoles
GDF	GDI dissociation factor
GDI	GDP-dissociation inhibitor
GDP	guanosine diphosphate
GEF	guanine nucleotide exchange factor
GTP	guanosine triphosphate
HB-EGF	heparin-binding EGF-like growth factor
HBSS	Hank's balanced salt solution
H_CT	tetanus toxin binding fragment
HEK293	human embryonic kidney 293 cells
HER2	human epidermal growth factor receptor 2
HIV	human immunodeficiency virus
HRP	horseradish peroxidase
IFN-γ	interferon γ
IGF2R	insulin-like growth factor receptor 2
IκB	inhibitor of NF-κB (nuclear factor κB)
IKK	IκB kinase
IL	interleukin
IL-1R	interleukin-1 receptor

iNOS	inducible nitric oxide synthase
IPTG	isopropyl β-D-1-thiogalactopyranoside
IRF	interleukin regulatory factor
IRAK	IL-1R-associated kinase
KIF3A	kinesin family member 3A
KLC1	kinesin light chain 1
LAMP	lysosomes-associated membrane protein
LBPA	lysobisphosphatidic acid
LRRK2	leucine-rich repeat kinase 2
LTβR	lymphotoxin-β receptor
Lys	lysine
MAPK	mitogen-activated protein kinase
MDA5	melanoma differentiation-associated gene 5
MD-2	myeloid differentiation factor 2
MEF	mouse embryonic fibroblast
MHC-I	major histocompatibility complex class I
MHC-II	major histocompatibility complex class II
mTOR	mammalian target of rapamycin
MVB	multivesicular body
MyD88	myeloid differentiation primary response gene 88
NGF	nerve growth factor
NT	neurotrophin
OPTN	optineurin
ORP1L	OSBP–related protein 1L

OSBP	oxysterol-binding protein
PAMP	pathogen-associated molecular pattern
PBS	phosphate-buffered saline
PH	pleckstrin homology
PI3K	phosphatidylinositol-4,5-bisphosphate 3-kinase
PI(3)P	phosphatidylinositol-3-phosphate
PI(4)P	phosphatidylinositol-4-phosphate
PI(3,4)P2	phosphatidylinositol-3,4-bisphosphate
PI(3,5)P2	phosphatidylinositol-3,5-bisphosphate
PI(4,5)P2	phosphatidylinositol-4,5-bisphosphate
PI(3,4,5)P3	phosphatidylinositol-3,4,5-trisphosphate
PKC	protein kinase C
pRab7(S72)	S72-phosphorylated Rab7
PVDF	polyvinylidene fluoride
PX	phox homology
$p75^{NTR}$	p75 neurotrophin receptor
RabF	Rab family motif
RabSF	Rab subfamily motif
RabGGTase	Rab geranylgeranyl transferase
REP	Rab escort protein
RHD	Rel homology domain
RIG-I	retinoic acid-inducible gene-I
RILP	Rab-interacting lysosomal protein
ROS	reactive oxygen species

SCV	*Salmonella*-containing vacuole
SDS-PAGE	sodium dodecyl sulfate polyacrylamide gel electrophoresis
Ser	serine
shRNA	short-hairpin RNA
Sifs	*Salmonella*-induced filaments
SNARE	soluble *N*-ethylmaleimide-sensitive factor activating protein receptor
Snx	sorting nexin
SOD1	superoxide dismutase 1
SPTN1	spectrin alpha chain, non-erythrocytic 1
SPTB2	spectrin beta chain, non-erythrocytic 1
STX6	syntaxin 6
TAB	TAK1-binding protein
TBC1D15	TBC domain family, member 15
TBS	tris-buffered saline
TCR	T cell receptor
TfR	transferrin receptor
TGFα	transforming growth factor-α
TGFβ	transforming growth factor-β
TGN	trans-Golgi network
TIP47	tail-interacting protein of 47 kDa
TNFα	tumour necrosis factor-α
TNFR	tumour necrosis factor receptors
TRAF	TNFR associated factor

TRIF	TIR domain-containing adapter inducing IFN-β
Trk	tropomyosin-related kinase
Tyr	tyrosine
ULK	unc-51-like kinase
VAMP	vesicle-associated membrane protein
VAP	VAMP-associated ER protein
Vps	vacuolar protein sorting-associated protein

Chapter 1. Introduction

1.1 Rab GTPases & the endocytic pathway

The Rab family of small Ras-like GTPases is an important regulator of vesicular transport along the endocytic pathway. Rabs were initially discovered as important regulators of membrane trafficking; however, they are now believed to be key players in cell signalling, growth, survival and development (Romero Rosales et al., 2009; Tu et al., 2010; Wang et al., 2012). These processes are controlled by the endocytosis of a large variety of cargoes, including activated receptors, nutrients and their carriers, lipids, extracellular matrix proteins, fluids, viruses and bacteria. Once internalised, these molecules can be sorted via a number of different routes, including recycling back to the plasma membrane or to the lysosome for degradation. In mammals, more than 60 Rabs have been identified, each of which functions in an organelle-specific manner to control the passage and sorting of different cargoes (Hutagalung and Novick, 2011) (Figure 1.1). The initial internalisation of cargoes and the fusion of early endosomes are controlled by Rab5. Cargo is then sorted and recycled back to the plasma membrane by Rab4, Rab11, and Rab25, or sent to the lysosome for degradation by Rab7. Other important vesicular transport pathways in cells include transport between the endoplasmic reticulum (ER), Golgi and lysosomal networks. The ER is a major site of protein and lipid synthesis that forms a vast network throughout the cell. It is also a major site of synthesis of membranes for all organelles of the endocytic pathway. Thus, transport between the ER and other compartments is fundamental for the correct functioning of intracellular transport. The Golgi apparatus is composed of a stack of four to six membrane-bound flattened cisternae, which are usually classified as cis- medial- or trans-Golgi networks (Gu et al., 2001). The Golgi is responsible the post-translational modification of many proteins, while the trans-Golgi network (TGN) is also involved in the sorting of proteins to their final destinations, including numerous signalling receptors that are destined for the plasma membrane (Figure 1.1).

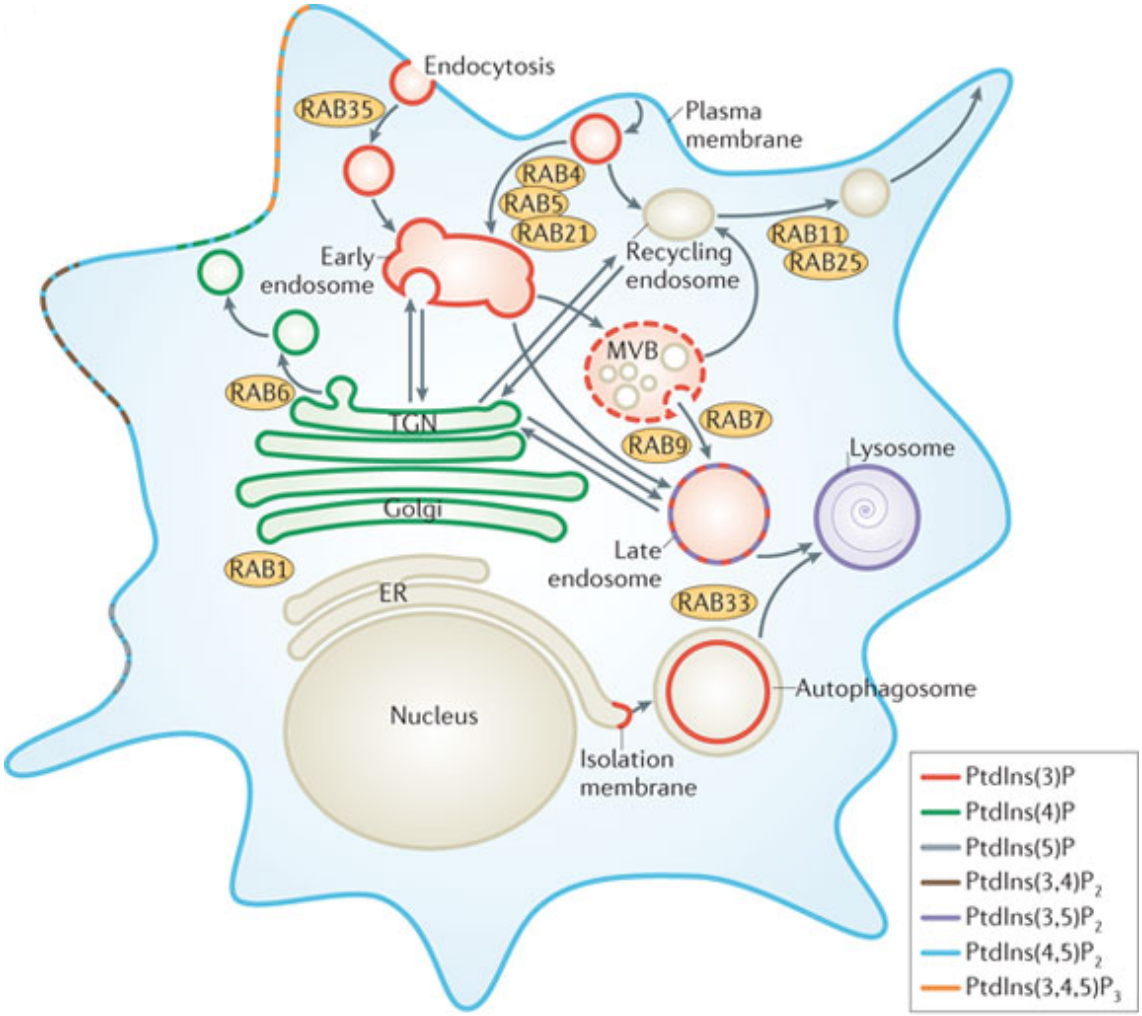

Figure 1.1. The endocytic pathway.

The endocytic pathway is controlled by over 60 members of the Rab family, which function in organelle specific manner to control the trafficking and sorting of different cargo. The membranes of these organelles are also characterised by their different phosphoinositide composition, which also controls the recruitment of different proteins and their effectors. Figure generated from Jean and Keger, 2012.

Rab6 is an important regulator of this secretory pathway, while Rab1 functions in ER-Golgi transport and Rab9 mediates trafficking between the ER and the lysosome.

Rab proteins are GTPases, which cycle between guanosine diphosphate (GDP)-inactive and guanosine triphosphate (GTP)-active forms (Figure 1.2). Newly synthesised GDP-bound Rabs interact with a Rab escort protein (REP) in the cytosol, which binds and presents the Rab to Rab geranylgeranyl transferase (RabGGTase). The RabGGTase transfers one or two geranylgeranyl groups to C-terminal cysteines for correct insertion of the Rab into its target membrane (Pereira-Leal et al., 2003). Following prenylation, REP chaperones the GDP-bound Rab to the correct membrane, where it becomes a substrate for a guanine nucleotide exchange factor (GEF), which catalyses the conversion of GDP to GTP. The active Rab can then interact with its effector(s) proteins to perform its specific function(s). Following interaction with its effectors, molecules, a GTPase-activating protein (GAP) binds the Rab and catalyses the hydrolysis of GTP to GDP, thereby converting it back to an inactive state. Inactive Rab7 then dissociates from the membrane back into the cytosol, where it is bound to a GDP-dissociation inhibitor (GDI). While in this state the Rab binds a GDI dissociation factor (GDF), which removes the GDI and allowing the Rab to re-enter the cycle.

Common structural elements and the presence of specific motifs are important for the correct binding of shared interactors and specific effectors of Rabs. They have similar structural features to other Ras-related GTPases, containing a six-stranded β sheet, with five parallel strands and one anti-parallel strand, flanked by five α helices. Rabs are distinguished from other GTPases by the presence of five distinct motifs, known as Rab family motifs (RabFs) (Pereira-Leal et al., 2003) (Figure 1.3). These motifs are proposed to mediate binding of Rabs to common interactors, such as Rab escort protein 1 (REP1). Indeed, it was shown that residues within the RabF1, RabF3, and RabF4 motifs of Rab3A

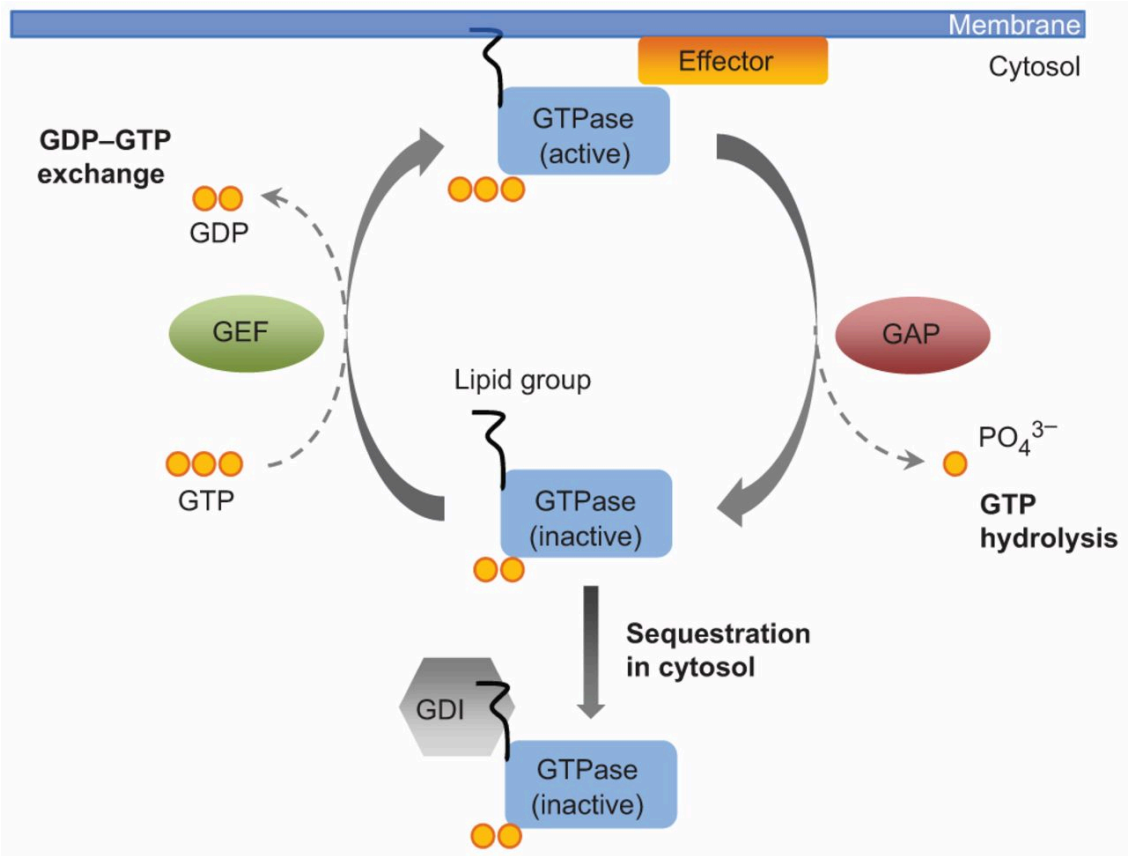

Figure 1.2. The Rab GTPase cycle.

Rab proteins cycle between active GTP-bound and GDP-bound forms, which are characterised by different affinities with the cellular membranes. GTP-bound Rabs are recruited to their respective membranes where they interact with different effectors to perform specific functions. Following this step, a GAP catalyses the conversion of GTP to GDP and the Rab is recycled back into the cytosol. Figure generated from Bento et al., 2007.

mediate binding to REP1 (Pereira-Leal et al., 2003). Some of these regions also contain sites of the switch I and II regions of Rab3A. These switch regions are responsible for changes in conformation of Rabs in their GTP- and GDP-bound forms. In the active GTP-bound form the conformation is stabilized by hydrophobic contacts between the switch I and II regions (Dumas et al., 1999). The orientation of the switch I and II domains distinguishes Rabs from Ras. The Rab family is further subdivided based on the presence of four subfamily motifs (RabSFs), which are highlighted in yellow inFigure 1.3 These RabSF motifs,

along with the switch I and II regions, are responsible for the specificity of binding differential interactors for each Rab protein.

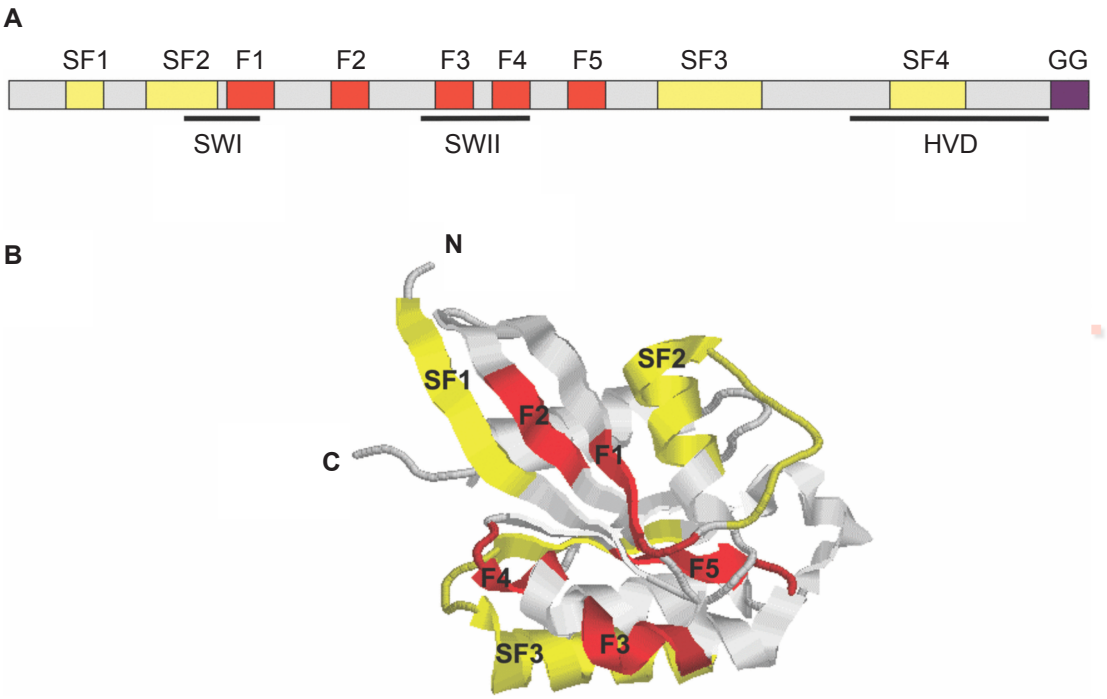

Figure 1.3. Generic structure of Rab proteins.

A. Schematic representation of the domain structure of Rab proteins, showing the RabF (red) and the RabSF (yellow) regions, and the switch I and II regions (SWI and SWII) and the hypervariable domain (HVD), as indicated by black bars. The prenylation motif (GG) is located at the C-terminal region. B. A three-dimensional model showing the positions of the RabF and RabSF motifs. Figure adapted from Zhu et al., 2004.

Rab proteins mostly differ in their C-terminal region, which are approximately 35 to 40 amino acids in length. This region, known as the hypervariable domain, was proposed to be responsible for the specific membrane targeting of different Rabs. It was originally shown that swapping the C-terminal 35 amino acids of Rab5 with that of Rab7 resulted in relocalisation of the hybrid Rab to Rab7-positive vesicles. However, a subsequent study created a series of hybrid Rabs by swapping the hypervariable domains of Rab1, Rab2, Rab5, Rab7 and Rab27 (Ali et al., 2004). They found that certain hybrids retained their original

subcellular localisation and function, indicating that other regions of the protein or effector proteins may recruit them to their respective membranes.

Other major components of the machinery controlling the endocytic pathway include soluble *N*-ethylmaleimide-sensitive factor activating protein receptor (SNARE) proteins, which are crucial for membrane fusion, scaffolding proteins mediating the formation of endosomal organelles and their fission from the plasma membrane, sorting complexes such as endosomal sorting complexes required for transport (ESCRT), homotypic fusion and protein-sorting (HOPS) and retromer, and the numerous effector molecules that interact different Rabs. Importantly, regulatory roles are not only restricted to protein complexes, but extend to specialised lipid moieties, such as phosphoinositides and lysobisphosphatidic acid (LBPA) (Billcliff and Lowe, 2014; Chevallier et al., 2008). Phosphoinositides are critical regulators of the endocytic pathway. There are seven different forms of phosphoinositide, generated by differential phosphorylation of the phosphatidylinositol head group at one or more of three positions (D-3, D-4 or D-5). The different phosphoinositide species are localized to distinct subcellular compartments or domains within different compartments, similar to the Rab family (Figure 1.1). Numerous effector proteins specifically bind the different phosphoinositides, making them important regulators of signal transduction, membrane trafficking, cell migration, and other cellular functions (Billcliff and Lowe, 2014). Phosphatidylinositol-3,4-bisphosphate (PI(3,4)P2) and phosphatidylinositol-3,4,5-trisphosphate (PI(3,4,5)P3) are signalling molecules involved in cell proliferation and survival, which are generated in response to the stimulation of receptors at the plasma membrane. Changes in the levels of phosphatidylinositol-3-phosphate (PI(3)P), phosphatidylinositol-4-phosphate (PI(4)P), phosphatidylinositol-3,5-bisphosphate (PI(3,5)P2) and phosphatidylinositol-4,5-bisphosphate (PI(4,5)P2) can also occur through external stimuli, but they mostly remain stable and are distributed at specific membranes throughout the cell (Mayinger, 2012) (Figure 1.3). The production and regulation of the different phosphoinositide species is controlled by various phosphoinositide kinases and phosphatases.

1.2 The early endocytic pathway

There are numerous mechanisms of endocytosis, including clathrin-mediated, caveolae-dependent, flotillin-dependent, or Arf6-dependent endocytosis, phagocytosis, macropinocytosis and entosis. Clathrin-mediated endocytosis is probably the most widely understood mechanism of endocytosis. Cargo internalised by clathrin-mediated endocytosis are taken up into clathrin-coated pits, where they subsequently form clathrin-coated vesicles. Clathrin, which is located on the cells limiting membrane, forms a polyhedral lattice as it binds to the cytoplasmic surface of the plasma membrane. Binding of clathrin to the membrane is mediated by interaction with a number of adaptor proteins, including the AP-2 complex, which links clathrin to the plasma membrane and is capable of binding the cytoplasmic domain of cargo proteins. Other members of the AP family of adaptors, (AP-1, -3, -4), serve as clathrin adaptors in other parts of the cell, such as the TGN and endosomes (Owen et al., 2004). Other clathrin adaptors at the plasma membrane include amphiphysins 1 and 2, β-arrestins 1 and 2, epsins 1, 2, and 3, and sorting nexin 9 (Snx9). The clathrin lattice acts as a scaffold for the binding of proteins that are important for membrane curvature and the formation of the clathrin-coated pit. Upon formation of the pit, the cytoplasmic GTPase dynamin forms a ring around the top of the pit to pinch off the clathrin-coated vesicle from the membrane.

Many plasma membrane receptors, such as receptor tyrosine kinases and G-protein-coupled receptors are internalised by clathrin-mediated endocytosis; however, some of these receptors can be internalised by alternative mechanisms. For example the epidermal growth factor receptor (EGFR), which has eight different ligands, can still be internalised following clathrin knockdown by stimulation with betacellulin and heparin-binding EGF-like growth factor (HB-EGF), but this is not the case following stimulation with epidermal growth factor (EGF) and transforming growth factor-α (TGF-α) (Henriksen et al., 2013). It has

also been shown that stimulation of fibroblasts and epithelial cells with EGF causes internalisation of the EGFR by macropinocytosis (Orth et al., 2006).

Rab5 is one of the key regulators of the early endocytic pathway, regulating endocytosis, homotypoic fusion of endocytic vesicles with themselves or early endosomes, along with uncoating of clathrin-coated vesicles, and initiates early sorting events and intraluminal vesicle formation. Rab5 has a number of different effectors, including hRME-6, which promotes AP-2 uncoating of clathrin-coated vesicles (Semerdjieva et al., 2008), early endosome antigen-1 (EEA1) (Merithew et al., 2003), required for membrane fusion, and Hrs, a component of the ESCRT-0 complex, required for intraluminal vesicle formation (Pons et al., 2008). It also interacts with vacuolar protein sorting-associated protein (Vps)34, Vps45, and Rabex-5, the Rab5 GEF. The recruitment of Hrs and EEA1 occurs prior to binding of Vps34, a phosphoinositide 3 [PI(3)] kinase, which is responsible for the generation of PI(3)P on early endosomal membranes.

Early endosomes have a complex structure, with vacuolar and tubular domains, which are responsible for the sorting of specific cargo towards different routes to which they are destined. A number of different proteins, including sorting nexins (Snxs) are phox homology (PX) domain-containing proteins, are believed to be involved in the sorting of cargo along the endocytic pathway. Indeed, it has been shown that Snx1 has the ability to form dimers and sense membrane curvature, which allows it to form tubular microdomains on early endosomes (Carlton et al., 2004). This is important for endosome-TGN transport of the cation-independent mannose 6-phosphate receptor (CI-MPR), with no effects of EGFR and transferrin receptor (TfR) sorting. Other microdomains will be discussed in the following section, which are required for the recycling of cargo back to the plasma membrane.

1.3 The recycling pathway

The majority of internalised cargo is recycled back to the plasma membrane, via fast and slow recycling endosomes. Rab4 and Rab11 are two of the main Rabs involved in the recycling route. The role of Rab4 has been widely investigated, but its exact function remains unclear. Most studies have looked at the involvement of Rab4a in the recycling of the TfR, which is constitutively recycled back to the plasma membrane. However, different studies have found that both the overexpression and knockdown of Rab4a results increased levels of TfR at the plasma membrane (Deneka et al., 2003). In contrast, Rab11 knockdown has been shown to increase the number of recycling endosomes unable to tether and fuse with the plasma membrane (Takahashi et al., 2012). This indicate that Rab4 plays a role in the sorting of different cargoes in different domains of the endosomal compartment for recycling at an earlier stage than Rab11, which is more important for transport and fusion of these vesicles with the plasma membrane. Indeed, it has been recently shown by D'Souza *et al.* that Rab4 recruits Arl1, which in turns recruits the Arf GEFs BIG1 and BIG2 to early endosomes to promote the formation of elongated tubules or sorting domains (D'Souza et al., 2014). Furthermore, Ward *et al.* showed that the major histocompatibility complex class I (MHC-I)-related receptor, FcRn, initially leaves sorting endosomes in Rab4/Rab11- or Rab11-positive endosomes, following which the Rab4/Rab11-positive endosomes segregate into two distinct compartments which eventually separate. The Rab11-positive recycling endosomes fuse with the plasma membrane, whereas the Rab4-positive carriers do not (Ward et al., 2005).

The recycling pathway plays an important role in many different functions. In the case of signalling receptors, it allows for further activation of the pathway following their reintegration at the plasma membrane. It has also been shown to participate in cell migration and tumour invasion, through integrin recycling. Integrins are a family of receptors that mediate cell adhesion to extracellular matrix (ECM). They play key roles in numerous processes, including cell

migration, differentiation, proliferation and survival, and in pathological conditions, such as cancer progression and metastasis. Integrins are constantly undergoing endocytosis and recycling back to the plasma membrane, a process that is very important in cell migration. Syntaxin 6 (STX6) is a SNARE located in the TGN that is responsible for transport of integrins to the plasma membrane. STX6 has been shown to be upregulated in numerous types of cancers, and its depletion inhibits chemotactic cell migration (Riggs et al., 2012).

1.4 The late endocytic pathway

1.4.1 Ubiquitination & targeting for degradation

Receptors internalised by the endocytic pathway are targeted for degradation by ubiquitination. Ubiquitination occurs via the covalent addition of one or more ubiquitin moieties to lysine (Lys) residues, in a three-step process by the sequential action of E1 ubiquitin-activating, E2 ubiquitin-conjugating and E3 ubiquitin-ligating enzymes. Ubiquitin itself contains several Lys residues (Lys6, Lys11, Lys27, Lys29, Lys33, Lys48 and Lys63), all of which can be modified with ubiquitin to form chains of varying lengths. Therefore, proteins can be ubiquitinated by three different modifications: monoubiquitination, the attachment of a single ubiquitin, multiple monoubiquitination, the attachment of multiple single ubiquitin molecules to different Lys residues, and polyubiquitination, modification with ubiquitin chains of different lengths and linkages. Ubiquitination is a reversible process via the action of deubiquitinating enzymes (DUBs) that recycle ubiquitin back into the cytosol (Haglund and Dikic, 2012). As such, ubiquitination targets protein substrates to many different fates such as lysosomal or proteasomal degradation or specific intracellular routing, and controls many cellular functions, including endocytosis, sorting, NF-κB signalling and DNA repair.

1.4.2 Intraluminal vesicle formation & the ESCRT machinery

The correct targeting of ubiquitinated proteins for degradation is controlled by interaction with proteins containing ubiquitin-binding domains, which include the ESCRT machinery (Haglund and Dikic, 2012). The ESCRT machinery is responsible for the formation of intraluminal vesicles, which begins in the early endosome and is one of the main characteristic steps of the maturation of early-to-late endosomes. It is for this reason that late endosomes are often referred to as multivesicular bodies (MVBs). The ESCRT pathway is characterised by five complexes (ESCRTs -0, -I, -II, and -III, and Vps4), which play key roles in cargo recognition and sorting (Henne et al., 2011). Interestingly, although ESCRTs bind ubiquitinated proteins to target them for degradation, ESCRT-0 and ESCRT-III also interact with DUBs to remove ubiquitin prior to sorting into intraluminal vesicles and targeting to the lysosome. ESCRT-0, ESCRT-I and ESCRT-II all contain ubiquitin-binding domains and function in the early stages of cargo recognition and clustering. ESCRT-III subunits do not contain ubiquitin-binding domains, but the ESCRT-III complex plays a crucial role in membrane deformation and scission through its Snf7 subunit, which can form oligomeric assemblies similar to dynamin. ESCRT-I and ESCRT-II can induce membrane deformation *in vitro* but are unable to perform membrane scission (Henne et al., 2011). ESCRTs also play an important role in cytokinesis and are hijacked by viruses, such as HIV budding at the surface of infected host cells.

1.4.3 Intraluminal acidification & lysosomal hydrolases

The maturation of endosomes is accompanied by intraluminal acidification and the formation of intraluminal vesicles. Early endosomes are mildly acidic at pH 5.9–6.8, whereas late endosomes/lysosomes can range between pH 4.9–6.0. Acidification is largely dependent on the vacuolar V-type ATPases, which is a proton pump that also regulates the intake of cations, such as Na^{+}, Ca^{2+} and Cd^{2+}, from the cytosol into the lumen of the lysosome (Beyenbach and Wieczorek, 2006). Endosomal acidification is responsible for a number of

processes, including the uncoupling of ligands from their receptors, which occurs around pH 6.5 for TGF-α and HER2/EGFR, with EGF dissociating at pH5.5, while the degradation of cargoes in the lysosome occurs between pH 4.5–5.0. Lysosomes contain about 50 different acid hydrolases, which include proteases, glycosidases, lipases, nucleases and phosphatases, which break down macromolecules in the lysosome. Mutations in the genes that encode these enzymes cause over 30 different diseases, called lysosomal storage diseases, such as Gaucher's disease, which is caused by a mutation in glucocerebrosidase, an enzyme involved in the digestion of glycolipids. Many of these enzymes are synthesised in the ER and pass through the TGN before trafficking to the late endosome/lysosome. Rab9, together with its effector tail-interacting protein of 47 kDa (TIP47), is located on late endosomes, and is involved in regulating transport to the TGN (Ganley et al., 2004). TIP47 binds MPR, which transports newly synthesized lysosomal enzymes from the Golgi to late endosomes. Rab9, TIP47 and MPRs all reside in a microdomain of late endosomes that does not contain Rab7 (Ganley et al., 2004). Transport of MPR back to the Golgi is mediated by the retromer complex, which is composed of two functional sub-complexes: the cargo-selective trimer of Vps35, Vps29, Vps26, and the membrane tubulating dimer of sorting nexin (Snx)1 and Snx2. Seaman *et al.* identified an interaction between Vps35/29/26 complex and Rab7, which was required for its recruitment to the membrane to complex with Snx1/2 (Seaman et al., 2009). They also found that the Rab-GAP TBC1D5 interacts with Vps25/29/26 to inhibit its recruitment to the membrane.

1.4.4 Rab7 recruitment and membrane fusion

The recruitment of Rab7 and simultaneous dissociation of Rab5 controls early-to-late endosome maturation and fusion with the lysosome (Hutagalung and Novick, 2011). Rab7 also mediates the fusion of mature autophagosomes with the lysosome, see section 1.6.2 (Jager et al., 2004). Fusion of endosomal membranes is usually performed by the interaction of Rabs, SNAREs, and different tethers. The HOPS complex is an important tethering complex involved

in the fusion of late endosomes and phagosomes with lysosomes. It is a conserved hexatetrameric complex composed of Vps11, Vps16, Vps18, Vps33, Vps39, and Vps41. Rab7 binds the Vps39 and Vps41 subunits of the HOPS complex. It was originally believed that the Vps39 subunit of the HOPS complex acted as the GEF for Rab7, as it increased the rate of nucleotide exchange on Ypt7 *in vitro* (Wurmser et al., 2000). However, subsequent work indicates that Vps39 serves as an effector rather than a GEF, as Vps39 preferentially binds GTP-bound Ypt7 and the addition of Gyp7, the Ypt7 GAP, causes release of Vps39 from the vacuolar membrane (Ungermann et al., 2000).

Interestingly, Rab5 also binds a hexatetrameric complex known as class C core vacuole/endosome tethering (CORVET) complex, which also contains the VPS-C core subunits, Vps11, Vps16, Vps18, Vps33, as well as the Rab5-binding subunits, Vps3 and Vps8 (Balderhaar and Ungermann, 2013). Both the HOPS and CORVET complexes contain subunits with SNARE binding domains. SNAREs are membrane-bound proteins that enable membrane fusion (Balderhaar and Ungermann, 2013). It has been proposed that there may be an intermediate complex based around the VPS-C core complex between Rab5-CORVET and Rab7-HOPS that helps mediate the maturation of early to late endosomes. Following this, Rab7-HOPS mediates fusion of the late endosome and autophagosome with the lysosome.

1.4.5 TBC1D15 and the Mon1-Ccz1 complex - the Rab7 GAP and GEF

TBC domain family, member 15 (TBC1D15) was first identified by Zhang *et al*. as the GAP for Rab7 using an in vitro [γ-^{32}P]GTP hydrolysis assay, where is stimulated the GTPase activity of Rab7 by approximately 90-fold compared to its intrinsic abilities (Zhang et al., 2005). They also tested it against Rab4, Rab6 and Rab11, with Rab11 exhibiting an approximately 8-fold increase in activity, whereas there was no effect on the other two Rabs. This was confirmed by Peralta *et al*. using a Rab-interacting lysosomal protein (RILP) pull-down assay for GTP-bound Rab7, which showed that overexpression of TBC1D15

significantly reduced the amount of active Rab7 (Peralta et al., 2010). They also showed that overexpression of TBC1D15 had no effect on TfR recycling, which requires Rab4, Rab5 and Rab11, indicating its specificity for Rab7 in this pathway.

Most of the insight into the GEF for Rab7 has been through studies using the yeast homolog of Rab7, Ypt7. Only recently, Nordmann *et al*. identified the Mon1-Ccz1 complex as the GEF for Ypt7, with neither being able to perform the activity on their own (Nordmann et al., 2010). Furthermore, knockdown of *MON1* or *CCZ1* both result in lysosomal fragmentation, consistent with an inhibition of Rab7 activity. Interestingly, this study also used an *in vitro* GEF assay, whereby a fluorescent GDP analog MANT-GDP is lost from Ypt7 upon incubation with the GEF, to show that Mon1-Ccz1 was indeed the GEF for Ypt7, while neither Vps39 nor the HOPS complex were active in the assay (Nordmann et al., 2010). This same group showed in a later study that the Mon1-Ccz1 GEF activity for Ypt7 was highly stimulated by the presence of PI3P, a major component of cellular membranes, which both Mon1 and Ccz1 could also bind individually (Cabrera et al., 2014). Poteryaev *et al.* showed that the loss of Rab5 from early endosomes and the acquisition of Rab7 are controlled by SAND-1/Mon1, while knockdown of Mon1a/b causes an accumulation of enlarged early endosomes in mammalian (HeLa) cells (Poteryaev et al., 2010). They also showed that Mon1a/b overexpression in HeLa cells caused a redistribution of Rabex5 to smaller vesicles and an increase in cytosolic Rab5. They concluded that SAND-1/Mon1 acts as a switch to control the localization of Rab5 and Rab7 GEFs. However, this group were basing their findings on the belief that the HOPS complex was the GEF for Rab7, while more recent data indicates that it is actually Mon1 itself (Cabrera et al., 2014). Thus, SAND-1 may regulate the Rab5-Rab7 conversion, while Mon1 simultaneously acts as the GEF for Rab7.

1.4.6 Rab7 and its protein interactions in the dynamics of late endosomes and lysosomes

RILP was first identified as a Rab7 interactor in a yeast two-hybrid screen using the constitutively active $Rab7^{Q67L}$ to identify specific interactors of GTP-Rab7. Its binding to Rab7 occurs through the C-terminal domain of RILP and the expression of a truncated form lacking the N-terminal domain results in dispersal of late endosome/lysosomes similar to overexpressing dominant-negative Rab7 (Cantalupo et al., 2001). This was subsequently shown to be caused by the fact that the N-terminal domain of RILP interacts with the p150(Glued) subunit of the dynactin complex and drives the recruitment of the dynein-dynactin motor to late endosomes (Jordens et al., 2001). It was shown from the crystal structure of the Rab7-RILP interaction that the Rab7-binding domain of RILP forms a coiled-coil homodimer that interacts with two separate GTP-bound Rab7 molecules, resulting in a complex of Rab7-RILP-RILP-Rab7 (Wu et al., 2005).

While the Rab7-RILP complex is sufficient to recruit p150(Glued), it is not sufficient to drive microtubule minus-end directed transport. The complex must also recruit oxysterol-binding protein (OSBP)–related protein 1L (ORP1L) and βIII spectrin (Rocha et al., 2009). ORP1L contains three major domains, a pleckstrin homology (PH) domain that binds phosphoinositides, a FFAT (two phenylalanines [FF] in an acidic tract) motif that binds various proteins, and a C-terminal OSBP-related domain (ORD) that binds cholesterol. The FFAT motif of ORP1L also binds VAMP (vesicle-associated membrane protein)-associated ER protein (VAP)-A and VAP-B, which are involved in the ER export of proteins and lipids (Rocha et al., 2009). It was originally believed that ORP1L was a cholesterol sensor that bound to VAP-A or VAP-B on the ER membrane, resulting in the removal of p150(Glued) to allow for binding of kinesin motors and transport in the opposite direction. However, Vihervaara *et al.* showed that ORL1L also binds several oxysterols and cholesterols, with the overexpression of a sterol binding-deficient mutant of ORP1L causing scattering of late endosomes/lysosomes, while still colocalising with Rab7 (Vihervaara et al.,

2011). In contrast to this, overexpression of ORP1L causes perinuclear aggregation of late endosomes/lysosomes. This study also revealed that ORP1L is capable of recruiting both p150(Glued) and KIF3A for dynein- and kinesin-mediated transport. Overexpression of the sterol binding-deficient ORP1L mutant recruited both p150(Glued) and KIF3A to late endosome, whereas these proteins were mostly cytosolic in untransfected cells. Thus, binding of ORP1L to Rab7 appears to be the major factor determining transport of late endosome/lysosomes, with the recruitment of other factors possibly influencing the choice of direction and/or the efficiency of the transport process by influencing the processivity of the motor complexes.

Furthermore, although the role of RILP in transport and recruitment of p150(Glued) and the dynein motor may not be as important as previously believed, it may be involved in regulating other important functions. Most recently, RILP was shown to interact with the V-ATPase, by regulating recruitment of its V1G1 subunit to the late endosomal/lysosomal membrane, while also regulating the proteasomal degradation of ubiquitinated V1G1; however, this only appears to occur upon overexpression of RILP and not Rab7 (De Luca et al., 2014). Furthermore, they showed that RILP can bind both p150(Glued) and V1G1 in the same complex *in vitro*. Thus, RILP could stabilise the V-ATPase on the membrane during transport of late endosomes/lysosomes towards the MTOC to help promote acidification of these vesicles.

Interestingly, RILP is also an effector of Rab34 and Rab36, two highly similar Rabs (56% amino acid identity) located on the Golgi, who are responsible for the correct positioning of late endosomes and lysosomes. Expression of the constitutively active forms of Rab34 or Rab36 causes the perinuclear aggregation of late endosomes/lysosomes, whereas the dominant-negative forms are cytosolic and have not effect on late endosome/lysosome distribution (Chen et al., 2010; Wang and Hong, 2002). Both of these proteins could serve as tethering factors between late endosomes/lysosomes and the Golgi allowing for the recruitment of factors for cargo sorting and exchange.

1.5 Rab7 in axonal retrograde transport

Another important function of Rab7 is in sustaining axonal retrograde transport of motor and sensory neurons(Deinhardt et al., 2006)(Deinhardt et al., 2006)(Deinhardt et al., 2006). Intracellular transport of proteins and organelles is more important in neurons than any other cell in the body, as proteins synthesised in the cell body need to transported over long distances, sometimes over 1 metre, to the distal parts of the axon or dendrites. Axonal retrograde transport is essential for the transport of signalling molecules, including members of the neurotrophin family: nerve growth factor (NGF), brain-derived neurotrophic factor (BDNF), neurotrophin (NT)-3 and NT-4/5; and their receptors, the tropomyosin-related kinases TrkA, TrkB, and TrkC, and the p75 neurotrophin receptor ($p75^{NTR}$), over long distances from distal sites to the soma where they relay signals for survival and growth Figure 1.4). Deinhardt *et al*. showed that TrkB, $p75^{NTR}$, and their ligand BDNF all travel together in the same compartment as the binding fragment of tetanus toxin (H_CT), which is just one example of how pathogens can highjack the normal transport pathways of a cell during infection. The transport of these 'axonal signalling endosomes' is controlled by the sequential action of Rab5 and Rab7. Rab5 is involved in the early sorting step, whereas Rab7 is crucial for the transport of fast retrograde carriers (Deinhardt et al., 2006). Expression of the dominant-negative GFP-$Rab5^{N133I}$ in motor neurons completely abolished H_CT retrograde transport, but did not inhibit internalisation, indicating that Rab5 is essential for the early sorting steps prior to retrograde transport. In contrast, expression of the constitutive-active GFP-$Rab7^{Q67L}$ gave a similar profile as the wild-type, whereas the dominant-negative GFP-$Rab7^{N125I}$ completely blocked H_CT, $p75^{NTR}$, and TrkB transport, without affecting mitochondrial morphology or dynamics, indicating that this inhibition was specific to a subset of transport carriers (Deinhardt et al., 2006).

Following this, another study showed that Rab7 interacts with TrkA to regulate signalling and neurite outgrowth (Saxena et al., 2005). Expression of dominant-

negative Rab7^{T22N} resulted in significantly enhanced neurite outgrowth in PC12 cells following stimulation with NGF, the ligand of TrkA.

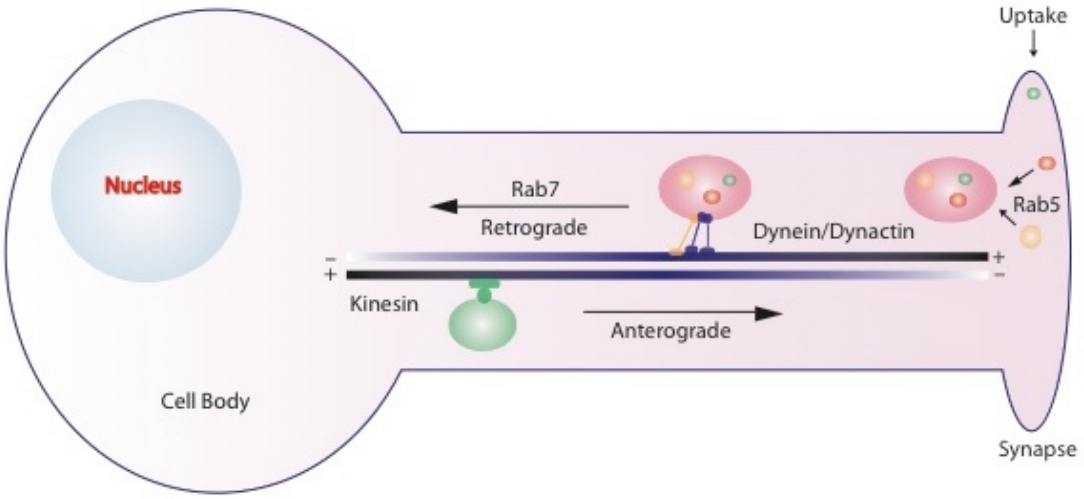

Figure 1.4. Axonal transport pathways.
Cargo internalised at distal sites in neurons must be trafficked to the cell body over long distances. Rab7 is required for the dynein-mediated retrograde transport of signalling endosomes, known to contain growth factor receptors and their ligands, including TrkA, NGF and p75^{NTR}.

Interestingly, TrkA has also been shown to phosphorylate dynein intermediate chain (DIC) 1B on serine (Ser) 80, for the recruitment of cytoplasmic dynein and the axonal retrograde transport of signalling endosomes (Mitchell et al., 2012). This phosphorylation did not affect transport of recruitment of dynein to mitochondria, indicating that this was specific for the transport of signalling endosomes to promote neuron survival. These results were interesting as it had been previously indicated that phosphorylation of dynein subunits inhibited its recruitment to membrane-bound organelles. Thus, phosphorylation may be a mechanism of promoting interaction with recruitment factors specific to certain organelles, thus providing an organelle-specific mechanism of recruiting transport machinery.

1.6 Rab7 in disease

1.6.1 Charcot-Marie Tooth type 2B & other neurological disorders

Charcot-Marie-Tooth type 2B (CMT2B) is a common inherited peripheral neuropathy, characterized by sensory loss, with distal muscle weakness and wasting. A direct link between Rab7 and CMT2B was established with the identification of four missense mutations, L129F, V162M, N161T, and K157N, in four different families with this hereditary sensory neuropathy (Verhoeven et al., 2003; Zhang et al., 2013). Follow-up studies have investigated the differences in activities of these mutant forms of Rab7, where they observed higher nucleotide exchange rates and slower GTP hydrolysis than wild-type Rab7 (Spinosa et al., 2008). However, this mechanism is not completely agreed upon. A crystal structure of the GTP-bound $Rab7^{L129F}$ suggested an alteration in the nucleotide-binding pocket that would affect GTP-binding (McCray et al., 2010). They also showed by biochemical analyses that the $Rab7^{L129F}$ did not have an intrinsic GTPase defect, but allowed for unregulated nucleotide exchange leading to both excessive activation and hydrolysis-independent inactivation. All mutations were also shown to exhibit a marked inhibition of neurite outgrowth in PC12 and Neuro2A cells. Although the exact mechanism behind the neurodegeneration in CMT2B is not know, it has been shown that the four known mutations all exhibit faster axonal anterograde transport, without increasing the speed of retrograde movements, in dorsal root ganglion (DRG) neurons (Zhang et al., 2013). Furthermore, this study also showed that TrkA transport was suppressed in both directions, while also reducing surface levels of TrkA, and inhibiting NGF binding and internalization. CMT2B Rab7 mutants inhibit NGF-induced differentiation in PC12M cells and cause axonal degeneration in DRG neurons, based on retraction of neurons by approximately 80%, three days after transfection with CMT2B mutants (Zhang et al., 2013).

Rab7 has also been shown to interact with peripherin, a 57 kDa type III neuronal intermediate filament protein, primarily expressed in peripheral neurons and CNS neurons that project towards peripheral structures. This interaction is inhibited in CMT2B. Interestingly, a frameshift deletion and a neurotoxic splice variant of peripherin have also been discovered in amyotrophic lateral sclerosis (ALS), a common, neurodegenerative disorder characterized by degeneration of motor neurons in the cortex, brainstem, and spinal cord, leading to progressive muscle weakness, atrophy, and ultimately paralysis and death, usually within 3–5 years of disease onset. Most cases of ALS are sporadic; however, approximately 10% are familial. Mutations in the superoxide dismutase gene (*SOD1*) gene have been the most well-characterised, with the $SOD1^{G93A}$ mouse being commonly used as a model for the investigation of mechanisms and potential therapies. Bilsland *et al*. that the $SOD1^{G93A}$ mouse exhibits slower retrograde transport compared with its wild-type counterpart at an early pre-symptomatic stage, with no decrease in KIF5A-mediated anterograde transport (Bilsland et al., 2010). The exact mechanism how mutant SOD1 affects axonal transport is not yet understood, but it is known that it affects transport of specific cargoes differently. For example, a common pathological finding of ALS is the accumulation of neurofilaments in the cell body as a result of a defect in its anterograde transport, whereas fast transport vesicles exhibit defects in both directions, and mitochondria exhibit defects in anterograde only (De Vos et al., 2008).

Defects in endocytic transport resulting in the accumulation of organelles and proteins in axons and cell bodies have also been implicated in a number of other neurological disorders, including frontotemporal lobar degeneration, Alzheimer’s, Huntington’s, and Parkinson’s disease (De Vos et al., 2008). In Alzheimer's disease, the presence of neurofibrillary tangles containing paired helical filaments, which are assembled from hyperphosphorylated tau, is a common hallmark of the disease. The other major hallmark is the presence of amyloid plaques, which are areas of degenerating neurites surrounding a core of amyloid-β peptide, which is produced by proteolytic cleavage of the amyloid

precursor protein (APP) (De Vos et al., 2008). Mutations in the *tau* and *APP* gene have been associated with familial forms of Alzheimer's. Furthermore, defects in axonal transport have been shown to be an early pathological feature in animal models, while amyloid-β peptide has been shown to disrupt transport of a variety of cargoes, including mitochondria, possibly even damaging them (Manczak et al., 2006). Mutant huntingtin may also damage axonal transport, as huntingtin has been shown to interact with huntingtin-associated protein 1 (HAP1), which interacts with kinesin light chain 1 (KLC1) and p150(Glued). In addition, Smith *et al.* found changes in the levels of proteins associated with axonal transport and microtubules, including kinesin family member 3A (KIF3A), dynein and dynactin, in the striatum, motor cortex, prefrontal cortex and hippocampus in a mouse model of Huntington's disease in the early stages of onset (6 months) (Smith et al., 2014). This was associated with neuronal degeneration and dense mutant huntingtin inclusion formation, along with decreased striatal dopamine levels and loss of striatal BDNF, indicating a defect in axonal transport.

Parkinson's disease is characterised by the presence of Lewy Bodies, which are cytoplasmic accumulations of proteins in neurons. Interestingly, α-synuclein is one of the main proteins that accumulate in Lewy Bodies. It is a long-lived protein that is degraded by the lysosome, through chaperone-mediated autophagy, and its upregulation is a cause of autosomal dominant Parkinson's disease. Furthermore, mutant forms of α-synuclein involved in the pathogeneisis of Parkinson's disease have been shown to inhibit its degradation, resulting in accumulation and neurotoxicity. Interestingly, the brains of Parkinson's disease patients have also been shown to have reduced numbers of lysosomes, characterised by decreased lysosomes-associated membrane protein (LAMP)1- and LAMP2-positive vesicles (Chu et al., 2009). This indicates that both axonal transport and lysosomal dysfunction are impaired in a number of neurological disorders, with Rab7 being an essential regulator of both.

1.6.2 Rab7 in autophagy & infection

The endocytic and autophagic pathways are both membrane trafficking pathways that are crucial for cell survival, and Rab7 plays a crucial role in both. Autophagy is a catabolic process that involves the formation of double-membrane vesicles, called autophagosomes, which surround and engulf cytosolic components, following which they fuses with lysosomes for degradation. This results in the generation of nutrients, from the recycling of damaged organelles, mitochondria, and proteins back into the cell to maintain cellular homeostasis. Under normal conditions, the cell energy sensor AMP-activated protein kinase (AMPK), and the cell growth regulator mammalian target of rapamycin (mTOR), are key players in the regulation of autophagy. Under conditions of stress, AMPK is activated, subsequently inhibiting mTOR, which leads to phosphorylation and activation of the unc-51-like kinase (ULK) complex and, consequently, the rapid induction of autophagy. The ULK complex is one of the key regulators of the initial steps in the formation of the autophagosome. Under periods of stress, such as amino acid starvation, hypoxia, oxidative stress, and infection, autophagy can be significantly upregulated. Fusion of the autophagosomes with the lysosome is a key process in autophagy induced by many mechanisms, and Rab7 is a key regulator of this process (Lin and Zhong, 2011).

Approximately 30 autophagy-related (Atg) proteins were identified in yeast that are essential for autophagosome biogenesis, most of which function in the initiation steps. PI3P is also extremely important in autophagosome biogenesis and it recruits and activates proteins with FYVE and PX (Phox) domains. Pankiv *et al*., identified FYCO1 (FYVE and coiled-coil [CC] domain containing 1) as a LC3-, Rab7-, and PI3P-interacting protein, which is required for the transport of autophagosomes in the microtubule plus-end direction (Pankiv et al., 2010). This study also showed that overexpression of FYCO1 was shown to redistribute LC3- and Rab7-positive vesicles to the periphery in a microtubule-dependent manner. It is still unknown if FYCO1 also plays a role in the transport of late endosomes and lysosomes.

Autophagy is the cells first line of defence against a number of invading pathogens, such as Group A *Streptococcus* (GAS) and *Salmonella* (Wild et al., 2011). Invading bacteria enter non-phagocytic cells by pathogen-induced endocytosis. Maturation of these endocytic vesicles will eventually lead to fusion with the lysosome and degradation of the bacteria. Thus, numerous bacteria have evolved mechanisms to avoid this process. *Streptococcus* can escape into the cytosol, where they are engulfed by GAS-containing autophagosome-like vacuoles (GcAVs). These GcAVs can be up to 10-fold the size of normal autophagosomes and their formation requires Rab7, which is not normally involved at such an early stage in the formation of autophagosomes. In contrast, upon infection with *Salmonella* most of the bacteria survive and proliferate within a phagosome-like organelle, known as the *Salmonella*-containing vacuole (SCV). However, some are released into the cytoplasm upon entry and damage to the SCV membrane. The cytosolic bacteria are rapidly ubiquitinated and recognised by at least three autophagy receptors, p62, NDP52, and optineurin (OPTN), resulting in their clearance by autophagy. Loss of either one of these receptors results in hyperproliferation of *Salmonella* within the cytosol (Wild et al., 2011). In contrast, SCVs form tubular structures by recruiting Arl8B for kinesin-mediated elongation in *Salmonella*-induced filaments (Sifs), which somehow inhibit fusion with the lysosome (Kaniuk et al., 2011). These Sifs subsequently migrate to the cell periphery to fuse with the membrane infect neighbouring cells. Interestingly, Rab7 and Arl8 are both required for the tubulation of lysosomes in macrophages following their activation by bacterial lipopolysaccharide (LPS). Furthermore, the class II major histocompatibility complex compartment, a lysosome-related organelle, of dendritic cells also requires Rab7 and Arl8 for the formation of a tubular network following their activation (Mrakovic et al., 2012).

Rab7 and a number of autophagy proteins, including Atg5, Atg7, Atg4B and LC3, also play an important role in osteoclastic bone resorption. Osteoclasts degrade bone via the action of secretory lysosomes, which deliver lysosomal

hydrolases and hydrochloric acid into the extracellular resorptive area. This secretion occurs in ruffled borders, which is also the same region where resorption occurs. It was previously found that the localisation of Rab7 to these ruffled borders is Atg5-dependent, and efficient secretion required Atg5, Atg7, and Atg4B/LC3 (DeSelm et al., 2011).

Mycobacterium tuberculosis is responsible for the most deadly bacterial disease in history, tuberculosis. Worldwide, millions of people are latently infected with *M. tuberculosis*, with the number of people with active disease in the millions. A large proportion of HIV-infected individuals are also infected with *M. tuberculosis*, with the combination of tuberculosis and AIDS being recognised as a global health emergency by the World Health Organisation (WHO). *M. tuberculosis* infects cells by phagocytosis and can infect and survive in macrophages by inhibiting fusion of the phagosome with the lysosome. Seto *et al*. showed that Rab7 is transiently recruited to *M. tuberculosis* phagosome, where it recruits cathepsin D, lysosomal protease (Seto et al., 2009). They showed that at 30 min approximately 80% of phagosomes are Rab7-positive, whereas at 6 h it is absent from most. This is in contrast to *Staphylococcus aureus,* which localises to approximately 80% of phagosomes at 6 h. This indicates that Rab7 is actively removed from *M. tuberculosis* phagosomes (Seto et al., 2009). Interestingly, the interaction between Rab7 and RILP is also disrupted in *M. tuberculosis* infected cells, which could contribute to the inhibition of acidification via the recent findings of RILP effects on the V-ATPase. Furthermore, it has been shown that the induction of autophagy in infected macrophages by starvation, or treatment with rapamycin or interferon (IFN)-γ, resulted in acidification of phagosomes and fusion with the lysosomes to inhibit bacterial survival (Gutierrez et al., 2004).

Human immunodeficiency virus (HIV) has the ability to cause a chronic disease that can lead to the more progressive autoimmune disorder syndrome (AIDS). To do this, HIV must evade the immune system of infected individuals. HIV encodes a protein Nef that has the ability to downregulate the levels of a

number of important surface molecules, such as the MHC-I and MHC II on antigen-presenting cells (APCs) and target cells, and CD4 and CD28 on helper T cells. Schaefer *et al*. showed that Nef binds CD4 and removes it from the cell surface of T cells, while also inhibiting MHC-I transport from the TGN to the plasma membrane (Schaefer et al., 2008). Furthermore, they showed that the Nef-interacting protein, β-COP, targets CD4 and MHC-I to Rab7-positive vesicles for lysosomal degradation. This process is highly efficient with 94% of CD4-positive vesicles being also positive for Rab7. HIV has also been show to colocalise and replicate in early autophagosomes, while Nef also interacts with Beclin-1, an essential autophagic factor, to inhibit their maturation and fusion with lysosomes in macrophages (Kyei et al., 2009).

1.6.3 Rab7 implications in cancer

With the importance of the endocytic pathway in controlling cell signalling pathways that govern proliferation, differentiation and survival, it is no surprise that defects in this pathway have been implicated in numerous types of cancer. Rab7 has been linked to melanoma (Alonso-Curbelo et al., 2014), breast (Wang et al., 2012), prostate (Steffan et al., 2014), and lung (Steffan et al., 2014) cancers, with an increasing number of publications in recent years. Indeed, EGFR signalling is tightly controlled by the endocytic pathway, by both the recycling and degradative routes. Both EGFR and human epidermal growth factor receptor 2 (HER2), are frequently overexpressed or activated by mutations in lung and breast cancers and promote cancer cell survival by activating PI3K/Akt signalling. Approximately 20-25% of breast cancers overexpress HER2, which when activated, stimulates cell proliferation and inhibits apoptosis. Using short-hairpin RNA (shRNA)-mediated knockdown of Rab7 in several breast cancer tumour cells lines, Wang *et al*. found that inhibition of HSP90 reduced the level of EGFR and Her2, and promoted apoptosis in Rab7 knocked-down cells but had no effect in control cells (Wang et al., 2012). Thus, Rab7 appears to stabilise EGFR-Her2 to sustain Akt survival signalling in breast cancer cells. This is a surprising finding, as Rab7 is

involved in the degradation of EGFR, whereas in these breast cancers this does not appear to be occurring indicating they have possibly evolved to bypass lysosomal degradation.

Many cancers deregulate proliferation and differentiation-related genes to drive invasion and metastasis. However, some studies believe that cancers can hijack lineage-specification genes to promote malignancy, and this is why some genes are involved in only certain types of tumours. Alonso-Curbelo *et al*. examined human cells, clinical specimens, and mouse models to look for melanoma-enriched genes. They found a lysosomal cluster of genes, and examined the role of Rab7 in this type of cancer. They found that inhibition of Rab7 reduced tumour cell proliferation and colony formation, whereas it increased cell motility and invasiveness. They also showed that melanoma cells had a significantly higher level of Rab7 expression compared with normal surrounding skin, and that its activity was regulated by the oncogenic transcription factor Myc and an early melanocytic lineage specification transcription factor, Sox10 (Alonso-Curbelo et al., 2014).

The increased invasiveness of tumour cells following the downregulation of Rab7 was also seen in prostate cancer invasion (Steffan et al., 2014). The same group had previously shown that the distribution of lysosomes in a tumour cell correlate with invasiveness, with less invasive cells having lysosomes clustered in the perinuclear region and more invasive cells having lysosomes near the periphery. Invasive cells secrete lysosomal enzymes into the extracellular space to facilitate invasion by decreasing cell-cell adhesion. Stefan *et al.* proposed that Rab7 is a potential tumour suppressor *in vivo*, as shRNA expressing cells formed larger tumours *in vivo* (Steffan et al., 2014). These tumours were associated with increased proliferation, decreased apoptosis, and increased invasiveness. Rab7 shRNA tumours also exhibited an upregulation of the proto-oncogene c-Met, which could lead to increased oncogenesis.

1.7 Rab7 Regulation by Phosphorylation

One of the main mechanisms of protein regulation by post-translational modification is through phosphorylation at serine (S), threonine (T) or tyrosine (Y) residues. The human kinome contains 518 kinases, most of which are either serine/threonine or tyrosine kinases, while a select few phosphorylate both. Numerous Rab proteins have been previously reported as being phosphorylated at different residues, including Rab4 (van der Sluijs et al., 1992), Rab24 (Ding et al., 2003), Rab3, Rab6, Rab8 (Karniguian et al., 1993) and Rab5a (Ong et al., 2014). Most recently, Rab5a was shown to be phosphorylated by PKCε on its Thr7 residue in response to integrin or chemokine stimulation, in a process that results in Rac1 activation, actin rearrangement, and T-cell motility (Ong et al., 2014). In another study, Rab3b, Rab6 and Rab8 were all shown to be phosphorylated following thrombin-induced activation of human platelets, which leads to the secretion of the dense- and α-granule contents (Karniguian et al., 1993). Both Rab6 and Rab8 proteins were preferentially targeted to the plasma membrane and the α-granules, whereas Rab3b was mainly cytosolic. Rab4 was also found to be phosphorylated by p34cdc2 kinase on S196 during mitosis, which regulates its cycling between the membrane and cytoplasm, as the phosphodeficient $Rab4^{S196A,}$ mutant preferentially localised to membranes (van der Sluijs et al., 1992). Thus, phosphorylation appears to play diverse role in regulating the GTPase activity and/or interaction with effectors, GAPs or GEFs for different Rab proteins.

Rab7 has been previously identified in a number of phosphoproteomic screens as being phosphorylated on 11 different sites, S17, Y37, T40, S72, S101, T168, T178, Y183, S201, S204 and S206, with S72 and Y183 being detected in significantly more screens that any other position. Phosphorylation of Rab7 at S72 was identified 22 independent screens, covering a diverse range of cellular processes and signalling pathways, including basal conditions in numerous tissues throughout the body, such as the liver, brain, lung, pancreas, spleen

and testis (Huttlin et al., 2010; Villen et al., 2007). Although phosphorylation of Rab7 at S72 has been identified in numerous screens, there are no publications to date that have investigated this mechanism further.

Mayya *et al*. performed a phosphoproteomic screen to identify proteins that were phosphorylated in response to T cell receptor (TCR) stimulation human Jurkat T cell leukaemia cells (Mayya et al., 2009). The found that the proteins identified were involved in processes controlling endocytosis of the TCR, F-actin cup formation, integrin activation, microtubule polarization, cytokine production, and alternative splicing of mRNA, all of which are associated with TCR signalling. For example, the polarisation of microtubules towards antigen-presenting cells occurs following TCR activation to facilitate exocytosis of effector proteins, and they found that tubulin was phosphorylated during this process on six different serine residues. Rab7 phosphorylation also increased following TCR activation, but this was not examined as it was below the threshold. Interestingly, Rab7 knockout T cells show deceased proliferation in response to TCR activation, It has been suggested that this may be the result of increased reactive oxygen species (ROS) generation secondary to mitophagy or through an inhibition of autophagy, which may be upregulated following TCR activation to generate energy from internal stores (Roy et al., 2013).

Increased phosphorylation of Rab7 at S72 was also detected in lipopolysaccharide (LPS)-stimulated macrophages (Weintz et al., 2010). LPS stimulates Toll-like receptor (TLR)4 on the plasma membrane, which is internalised by clathrin-mediated endocytosis, and undergoes ubiquitin-mediated lysosomal degradation (Husebye et al., 2006). Furthermore, trafficking of TLR4 via the degradative pathway, which is highly dependent on Rab7, is required for signal termination and LPS-associated antigen presentation. In the results of the phosphoproteomic screen, the authors also noted that the annotation term ‘Rho GTPase cycle’ was significantly enriched for LPS□regulated phosphoproteins, along with the term ‘cytoskeletal’ (Weintz et al., 2010). TLR4 also induces activation of mTOR, which is interesting as

increased phosphorylation of Rab7 at S72 was also detected in two independent phosphoproteomic screens using insulin to active mTORC1 (Hsu et al., 2011; Yu et al., 2011). This is also interesting, as it has been previously shown that inhibition of endosomal maturation by overexpression of constitutively active Rab5 or knockdown of the Rab7 effector Vps39 inhibits activation of mTORC1/S6K1 by insulin- or amino acid-stimulation (Flinn et al., 2010).

Two independent phosphoproteomic screens also detected increased levels of phosphorylation of Rab7 at S72 during mitosis (Dephoure et al., 2008; Olsen et al., 2010). Both groups used stable isotope labeling of amino acids in cell culture (SILAC) to examine changes in phosphorylation between cells arrest in G_1 phase by double-thymidine and M phase by nocodolzole. Both screens identified phosphorylation at S72 during the G_1 phase, but not in the M phase. Interestingly, it has been shown that endosomal fusion is inhibited during mitosis, and one of the mechanisms by which it is inhibited is the phosphorylation of vimentin, a class III intermediate filament protein, on S459 by Polo-like kinase 1 (Plk1) (Ikawa et al., 2014). Another study also found that Rab7 directly interacts with vimentin, resulting in increased phosphorylation of vimentin and inhibition of its assembly into filaments (Cogli et al., 2013). Furthermore, Rab11 has been shown to regulate dynein-dependent endosome localization at the mitotic spindle, and its depletion delays mitosis, causing disruption of astral microtubules and redistribution of spindle pole proteins (Hehnly and Doxsey, 2014). In addition, phosphorylation of Rab7 at S72 has also been detected in the DNA damage response after ionizing radiation, which causes massive changes in cellular pathways including DNA replication, cell cycle progression, and gene expression (Bennetzen et al., 2010). These results indicate that endosomal transport undergoes big changes during the cell cycle, which may be mediated by phosphorylation of different Rabs, such as Rab7.

Most recently, phosphorylation of Rab7 at S72 was detected in a screen investigating the role of TANK-binding kinase 1 (TBK1)-induced

phosphorylation in lung cancer cells (Kim et al., 2013). TBK1 is a potential therapeutic target for a subset of lung cancers cells, as it appears to promote prosurvival signalling through the activation of nuclear factor-κB (NF-κB) and AKT signalling pathways. This study also identified Plk1 as a target of TBK1 phosphorylation during mitosis, as knockdown of TBK1 decreased mitotic phosphorylation of Plk1. Thus, TBK1 may be a regulator of mitosis through Plk1, indicating that it may also regulate endosomal dynamics during the cell cycle.

From these studies, phosphorylation of Rab7 at S72 occurs during multiple regulatory events, and can be induced by various stimulations. From the results of studies investigating other Rab proteins, it is difficult to hypothesise exactly what effect this may have of Rab7 activity, as for other Rabs, phosphorylation appears to have different effects for different members. Thus, the aim of this thesis was to examine the effect S72 phosphorylation has on Rab7 activity and determine the cellular mechanisms responsible for this process.

Chapter 2. Materials & Methods

2.1 Materials

2.1.1 Reagents

Laboratory reagents were purchased from the following companies, unless otherwise stated: Biorad, Calbiochem, Clontech, Fisher Scientific, GE Healthcare, Gibco, Life Technologies, Millipore, Qiagen, Sigma, Thermo Scientific. Distilled water (dH_2O), phosphate-buffered saline (PBS), tris-buffered saline (TBS), glutamine, Lurai Bertani (LB) broth, 2YT broth, Super Optimal broth with Catabolite repression (SOC) medium, ethylenediaminetetraacetic acid (EDTA; pH 7.5, 8.0, 9.5), trypsin, versene, Hank's balanced salt solution (HBSS), and penicillin/streptomycin were provided by Cancer Research UK.

2.1.2 Cells lines

HEK293 cells and SV40-immortalised mouse embryonic fibroblasts (MEFs) were a gift from Sharon Tooze (Secretory Pathways, Cancer Research UK London Research Institute, London, UK).

2.1.3 Bacteria

Escherichia coli strain XL1-Blue was used for DNA amplification, and strain BL-21 was used for protein expression.

2.1.4 Vectors & expression plasmids

pEGFP-Rab7 and pcDNA3.1-HA-Rab7, containing the canine sequence of Rab7, and pGFP-RILP were gifts from Cecilia Bucci (Università del Salento, Department of Biological and Environmental Sciences and Technologies (DiSTeBA), Italy); Raichu-Rab7-A441 was a gift from Takeshi Nakamura (Tokyo

University of Science, Research Institute for Biomedical Sciences, Japan); and pEGFP-ORP1L was a gift from Vesa Olkkonen.

2.1.5 Primers

The following primers were used for site-directed mutagenesis of the pEGFP-Rab7, pcDNA3.1-HA-Rab7 and Raichu-Rab7-A441 plasmids:

Table 2.1. Site-directed mutagenesis primers.

Primer	Direction	Sequence
S72A	Forward	CAGGAACGGTTCCAGGCCCTTGGTGTGGCCT
S72A	Reverse	AGGCCACACCAAGGGCCTGGAACCGTTCCTG
S72E	Forward	CAGGAACGGTTCCAGGAACTTGGTGTGGCCT
S72E	Reverse	AGGCCACACCAAGGTTCTGGAACCGTTCCTG
S72P	Forward	CAGGAACGGTTCCAGCCCCTTGGTGTGGCCT
S72P	Reverse	AGGCCACACCAAGGGGCTGGAACCGTTCCTG

The following primers were used for genotyping the Rab7^{S72P} mice:

Table 2.2. Genotyping primers.

Primer	Direction	Sequence
Wild-type	Forward	CCGGTCAAGAACGGTTCCAGT
S72P	Forward	CCGGTCAAGAACGGTTCCAGC
Both	Reverse	ACGACAACGACGCCCACCTG

The following primers were used for sequencing the pEGFP, pcDNA3.1, and pGEX-4T2 plasmids:

Table 2.3. Sequencing primers.

Primer	Direction	Sequence
EGFP	Forward	CATGGTCCTGCTGGAGTTCGTG
EGFP	Forward	CAGTCCGCCCTGAGCAAAGAC
SP6	Forward	ATTTAGGTGACACTATAG
T7	Forward	GTAATACGACTCACTATAGGGC
T7	Forward	TAATACGACTCACTATAGGG
pGEX	Forward	GTGGCAAGCCACGTTTGGTG
pGEX	Reverse	GGAGCTGCATGTGTCAGAGG

2.1.6 Antibodies

Flourescently-conjugated secondary antibodies were from Life Technologies, and used at a concentration of 1:500. HRP-conjugated secondary antibodies eere from DAKO or GE Healthcare, and used at 1:4000. The primary antibodies used are shown in Table 2.4.

Table 2.4. Primary antibodies.

Antigen	Name	Species	Supplier	Dilution
Actin	clone AC 15	Mouse (monoclonal)	Sigma	1:4000 WB
EEA1	610457	Mouse (monoclonal)	BD Transduction Laboratories	1:250 IF
EGFR	DB831	Rabbit (monoclonal)	Cell Signalling	1:1000 WB
GAPDH	mab374	Mouse (monoclonal)	Millipore	1:4000 WB
GFP	Cone 4E12/8	Mouse (monoclonal)	Monoclonal antibody facility, CRUK	1:4000 WB
HA	Clone 3F10	Rat (monoclonal)	Roche	1:1000 WB
HA	Clone 12CA5	Mouse (monoclonal)	Monoclonal antibody facility, CRUK	1:1000 WB
LAMP2	CD107B	Mouse (monoclonal)	BD Pharmingen	1:250 IF
ORP1L		Rabbit (polyclonal)	Gift from Vesa Olkkonen	1:1000 WB
phospho-Rab7(S72)		Rabbit (polyclonal)		1:100 WB
Rab7	9367S	Rabbit (monoclonal)	Cell Signalling	1:100 IF
Rab11				1:250 IF
RILP	ab54559	Rabbit (monoclonal)	Abcam	1:500 WB
Vps26		Rabbit	Gift from Matthew Seaman	1:250 IF

WB: western blot, IF: immunofluorescence.

2.2 Methods

2.2.1 Mouse breeding & genotyping

The Rab7^{S72P} strain were a kind gift from Abraham Acevedo-Arozena (MRC Harwell, UK). The mice were generated via N-ethyl-N-nitrosourea (ENU) mutagenesis. The colony was maintained by crossing Rab7$^{S72P+/-}$ mice with wild-type C57BL/6 mice for over 10 generations.

The extraction of DNA from adult ear snips, or tail and yolk sac from embryos, was performed in a 120 µl reaction mixture of Viagen Biotech DirectPCR® tail lysis reagent, with 0.1 mg/ml proteinase K, overnight at 55°C in a shaking hotblock. The reaction was inactivated at 85°C for 30 min.

Genotyping was performed using MegaMix-Blue (Microzone Ltd.), which a Taq polymerase-based PCR mixture. Each reaction contained 15 µl Megamix-Blue, 2 µl extracted DNA and 1.6 µl of each primer (2 µM stock).

The reaction conditions were as follows:

1.	Initial denaturation	95°C	3 min
2.	Denaturation	95°C	30 s
3.	Annealing	Tm - 5°C	1 min
4.	Extension	72°C	1 min
5.	Repeat steps 2–4	29 times	
6.	Final extension	72°C	5 min

2.2.2 Generation of the anti-pRab7(S72) antibody

A peptide sequence corresponding to the region surrounding the S72 site, which is completely conserved in human, mouse, rat, dog, and rabbit, was produced by the Peptide Synthesis facility at Cancer Research UK London Research Institute, with the S72 site phosphorylated. The peptide was sent to

Biogenes GmBH (Berlin, Germany) for immunisation of two rabbits. Pre- and post-bleeds were sent for testing of the antibody specificity.

The peptide sequence was as follows: CERFQpSLGVA-$CONH_2$

2.2.3 DNA techniques

2.2.3.1 Site-directed mutagenesis

Site-directed mutagenesis of the pEGFP-Rab7, pcDNA3.1-HA-Rab7 and Raichu-Rab7-A441 plasmids were performed according to the QuikChange® Site-Directed Mutagenesis Kit (Stratagene) protocol. The QuikChange site-directed mutagenesis method is performed using PfuTurbo® DNA polymerase, which replicates both plasmid strands with high fidelity and without displacing the mutant oligonucleotide primers. This reduces the chances of amplifying the original construct without the mutation.

The reaction mixture contained the following:

5 µl	10× reaction buffer
5–50 ng	dsDNA template
0.5 µM	each oligonucleotide primer
200 µM	each deoxynucleoside triphosphate (dNTP)
1 µl	PfuTurbo
up to 50 µl	ddH_2O

A control reaction without the polymerase was also prepared.

The PCR conditions were as follows:

1.	Initial denaturation	95°C	30 s
2.	Denaturation	95°C	30 s
3.	Annealing	55°C	1 min
4.	Extension	68°C	1 min/kb plasmid length
5.	Repeat steps 2–4	16 times	

Following the PCR reaction, the original plasmid was digested by addition of 1 µl DpnI restriction enzyme for 2 h at 37°C. DpnI digests methylated DNA from dam$^+$ *E. coli* strains, and will therefore only digest the parental DNA. 2 µl of the final reaction mix after DnI digestion was then transformed in *E. coli* XL1-Blue.

2.2.3.2 Ligation of DNA

Subcloning of constructs used for site-directed mutagenesis was performed by digesting the insert and original vector with the same restriction enzymes and ligating overnight with T4 DNA ligase at 16°C, with a vector to insert ratio of 1:5. Samples were then transformed in E. coli XL1-Blue and selected for on kanamycin or ampicillin agar plates. All newly ligated plasmids were sequenced to ensure the correct insert was obtained.

2.2.3.3 Agarose gel electrophoresis

DNA from all PCR reactions and restriction digest analyses were subjected agarose gel electrophoresis in 0.8–2% agarose in TBE buffer (90 mM Tris/HCl, 90 mM boric acid, 2 mM EDTA pH 8.0), with one drop ethidium bromide per 50 ml. Gels were run at 80–120V for various time periods, depending on the size of the DNA being analysed.

2.2.3.4 DNA extraction from agarose gels

DNA bands were cut from the agarose gels using a clean scalpel and the DNA was extracted using the QIAquick Gel Extraction kit (Qiagen), according to the manufacturer's instructions. The extracted DNA was quantified using a Nanodrop® spectrophotometer.

2.2.3.5 Plasmid sequencing

DNA sequencing was performed using BigDye® Terminator Cycle Sequencing kit (Applied Biosystems). The reaction was performed using, 200 ng DNA, 3.2 pmol of primer, 8 µl of BigDye® Terminator, in a reaction volume made to 20 µl with dH_2O.

The PCR reaction was as follows:

1.	Initial denaturation	95°C	2 min
2.	Denaturation	95°C	30 s
3.	Annealing	47°C	15 s
4.	Extension	72°C	4 min
5.	Repeat steps 2–4	25 times	
6.	Cooling	12°C	

The DNA was purified from the reaction using DyeEx™ 2.0 Spin kit (Qiagen), according to the manufacturer's instructions. Following this, the reaction was dried in a speed vacuum and sequenced by the Cancer Research UK Sequencing facility. Sequence alignment was performed using ApE software (M. Wayne Davis).

2.2.3.6 Bacterial transformation

Both electro-competent XL1-Blue bacteria and chemically-competent XL1-Blue and BL-21 strains of E. coli were used throughout this project. For electro-competent transformation, 2 µl of the DNA mixture were added to 50 µl bacteria for 20 min on ice, prior to electroporating at 2.5 kV. Bacteria were recovered by adding 500 µl SOC medium to and incubating at 37°C and 1,000 rpm for 1 h. Transformants were then selected by plating on LB agar plates containing, 50 µg/ml kanamycin or 100 µg/ml ampicillin, depending of the plasmid resistance.

For the chemically-competent transformations, 2 µl DNA mixture was mixed with 120 µl bacteria in $CaCl_2$ + 20% glycerol for 20 min on ice. Bacteria were then heat-shocked for 45 s at 42°C, following which they were cooled on ice for 1 min. 500 µl of prewarmed SOC medium was then added and bacteria were recovered and selected for as above.

2.2.4 Cell culture

2.2.4.1 Cell culture

Both HEK293 cells and MEFs were maintained in Dulbecco's Modified Eagle's medium (DMEM; Gibco), containing 10% foetal bovine serum (FBS) and 2 mM L-glutamine. Cells were passaged when almost confluent at 1:10–20 dilutions, by trypsinisation, which was inhibited by addition of normal growth medium containing FBS. Medium was changed every 3–4 days.

2.2.4.2 Transfection procedures

Three different transfection reagents were used throughout this study. Initially, FuGENE® 6 (Promega) was used to transfect HEK293 cells, as it transfected >70% of cells but at lower levels than Lipofectamine 2000, which can be extremely strong. FuGENE® 6 is a nonliposomal reagent that has very low toxicity, but it is very poor at transfecting MEFs. Thus, Lipofectamine 2000, which can exhibit high toxicity when cells are below 70% confluency, was used to transfect MEFs. Thus, FuGENE® 6 was used to transfect HEK293 cells for the EGFR degradation assay, and Lipofectamine 2000 was used for all MEF experiments. Both transfection mixes were prepared similarly, with a 3:1 ratio of transfection reagent (µl) to plasmid (µg) in Opti-MEM® I Reduced Serum Media (Life Technologies), which were incubated at room temperature for 20–30 min before adding to cells in antibiotic-free DMEM, containing 10% FBS and L-glutamine. Cells were incubated in the transfection mixture for 24 h, before assaying or medium change.

2.2.4.3 Poly(I:C) & bacterial lipopolysaccharide stimulation of MEFs

MEFs were transfected with GFP-Rab7^{Wt} for 48 h, then stimulated with 10 µg/ml LMW poly(I:C) (Invivogen) or 1 µg/ml LPS from *Escherichia (E.) coli* strain 0111:B4 (Sigma) for various time periods. In experiments using BX795 or MRT67307, cells were preincubated for 2 h or overnight with 2 µM of each inhibitor prior to stimulation. Cells were lysed in RIPA buffer containing HALT™ Protease & Phosphatase Inhibitor Cocktail, and incubated with GFP-Trap® beads to immunoprecipitate GFP-Rab7 prior to western blotting with the anti-pRab7(S72) antibody.

2.2.4.4 EGFR degradation assay

HEK293 cells in 24-well plates were transfected with GFP-Rab7^{Wt}, GFP-Rab7^{S72A} and GFP-Rab7^{S72E} overnight. The next day, cells were serum-starved DMEM containing L-glutamine for 4 h, following which they were stimulated with 100 ng/ml EGF (Preprotech) at 37°C for 0, 15, 30, 60 and 90 min. Cells were lysed in RIPA buffer containing HALT™ Protease & Phosphatase Inhibitor Cocktail, and boiled with Laemmli sample buffer for 5 min. Immunoblotting was performed with antibodies to EGFR, and actin.

2.2.5 Biochemical techniques

2.2.5.1 Preparation of cell lysates

Adherent cells were placed on ice, washed once with ice-cold HBSS and lysed using either RIPA (10 mM Tris/HCl pH 7.5 150 mM NaCl, 0.1% SDS, 1% Triton X-100, 1% deoxycholate, 5 mM EDTA) or TNTE (20mM Tris pH 7.4, 150 mM NaCl, 150 mM EDTA, 5 mM 1% Triton X-100) lysis buffers containing HALT™ Protease & Phosphatase Inhibitor Cocktail. Samples were incubated on ice for 20 min, following which they were centrifuged at maximum speed for 10 min to

pellet the nuclear material. The supernatants were removed and placed in fresh tubes. Protein concentration was measured by Bradford assay, using Bio-Rad Protein Assay Reagent (Bio-Rad). Briefly, 1 µl of each sample was added to 1 ml of diluted assay reagent (200 µl regent + 800 µl dH_2O) and incremental dilutions of BSA (1–10 µg/ml) were used as a standard. Samples were incubated for 5 min. and then the absorbances were read at 595 nm using a spectrophotometer (BioPhotometer, Eppendorf). Concentrations of samples were determined from the BSA standard curve.

2.2.5.2 SDS-PAGE

Laemmli sample buffer (60 mM Tris-Cl pH 6.8, 2% SDS, 10% glycerol, 5% β-mercaptoethanol, 0.01% bromophenol blue) was prepared as a 5× solution and added to protein samples to a minimum final concentration of 2×, or 5× if adding to beads for immunoprecipitation or pull-down experiments, and samples were boiled for 5 min at 100°C or at 65°C for 10 min for membrane proteins. Samples were then loaded in precast 4–12% NuPAGE® gels (Life Technologies), or 12% NuPAGE® gels for subcellular fractionation. Proteins were separated at 200 V for 60–70 min in MES (2-ethanesulfonic acid) buffer (Life Technologies).

2.2.5.3 Western blot analysis

Following SDS-PAGE, proteins were transferred to a methanol-activated polyvinylidene fluoride (PVDF) membrane in NuPAGE® transfer buffer containing 15% methanol for 120 min at 30V. The efficiency of transfer was monitored by Ponceau S staining, following which nonspecific binding sites were blocked with 5% milk (Marvel) or 5% membrane blocking agent (GE Healthcare) for phospho-antibodies for 1 h at room temperature. Membranes were then incubated with primary bodies diluted in blocking buffer overnight at 4ºC, following which they were washed extensively with TBS containing 1% Triton X-100 (TBST) and incubated with horseradish peroxidase (HRP)-conjugated secondary antibodies (1:4000) for 1 h at room temperature.

Membranes were then washed extensively with TBST, followed by a brief final wash in dH_2O.

Immunoreactivity of blots was measured using enhanced chemiluminescence (ECL) reagent (GE Healthcare). The intensities of bands on the blots were quantified using ImageJ software (National Institutes of Health, USA).

2.2.5.4 Production of recombinant His-Rab7

E. coli BL-21 transformed with pcDNA3.1-His^6-$Rab7^{Wt}$ and pcDNA3.1-His^6-$Rab7^{S72P}$ were grown overnight in 5 ml 2YT containing 100 µg/ml ampicillin. The following morning, the 5 mL was added to 200 ml 2YT containing 100 µg/ml ampicillin and grown to log phase (OD_{600nm} ~0.6–0.8). 1 mM isopropyl β-D-1-thiogalactopyranoside (IPTG) was added to induce protein expression for 4 h. Bacteria were harvested by centrifugation at 5,000 rpm for 15 min at 4°C, washed in ice-cold PBST, and lysed by passing through a French Press machine twice at 1300 psi. Bacterial lysates were then centrifuged at 17,500 rpm for 25 min at 4°C. The supernatant was then added to a column containing 1.5 ml Ni^{2+}-agarose resin, pre-equilibrated with buffer containing 50 mM Na_xP_i and 300 mM NaCl (pH 7.8), and placed on a rotator for 2 h at 4°C. The column was washed once with 15 ml of high-salt buffer (50 mM Na_xP_i, 600 mM NaCl, pH 7.8) containing 1 mM ATP and 1 mM Mg^{2+} to remove chaperones, followed by a wash with 15 ml 50 mM Na_xP_i, 300 mM NaCl, 20 mM imidazole, pH 7.8). Proteins were eluted with 50 mM Tris pH 7.8, 100 mM NaCl). Concentrations were determined using the Bradford assay. Proteins were subjected to SDS-PAGE on a 4–12% NuPAGE® gels to determine purity of different fractions (P1–3), using Coomassie staining method.

2.2.5.5 Production of recombinant GST-Rab7

E. coli BL-21 transformed with pGEX-4T2-Rab7 were grown overnight in 5 ml 2YT containing 100 µg/ml ampicillin. The following morning, the 5 mL was

added to 200 ml 2YT containing 100 µg/ml ampicillin and grown to log phase (OD_{600nm} ~0.6–0.8). 1 mM IPTG was added to induce protein expression for 4 h. Bacteria were harvested by centrifugation at 5,000 rpm for 15 min at 4°C, washed in ice-cold PBST, and centrifuged again. Bacteria were then resuspended in resuspension buffer (0.05% PBST, 2 mM EDTA, 0.1% β-mercaptoethanol, 1 mM phenylmethylsulfonyl fluoride, 2 µg/ml pepstatin A). Bacteria were lysed by sonication at 90% power for 3 × 20 s, and 1 × 40 s. Bacterial lysates were then centrifuged at 15,000 rpm for 15 min at 4°C, and the supernatant was incubated with 2 ml 50% reduced glutathione (GSH)-agarose beads for 2 h at 4°C. The beads were then washed 3 × 10 ml ice-cold PBST, then added to a column the bound GST-Rab7 was eluted in 3 × 1 ml elution buffer (10 mM GSH, 50 mM Tris/HCl pH 8.0). Proteins were dialysed overnight in dialysis buffer (10 mM HEPES-NaOH pH 7.4, 100 mM NaCl) using Slide-A-Lyzer® Dialysis Cassettes (Thermo Scientific), with a molecular weight cut-off of 10,000 kDa. Proteins were subjected to SDS-PAGE on a 4–12% NuPAGE® gels to determine purity of different fractions (P1–3), using Coomassie staining method.

2.2.5.6 Anti-phospho-Rab7(S72) antibody purification

Around 4–8 mg of the phosphorylated peptide used for immunisation of the rabbits to produce the anti-pRab7(S72) antibody, and the corresponding unphosphorylated peptide, which was also produced by the Peptide Synthesis Facility, were dissolved 2 ml coupling buffer (50mM Tris/HCl pH 8.5, 5mM EDTA). The dissolved peptides were added to 0.5 mL 100% Sulpholink resin (Thermo Scientific), which was pre-equilibrated by washing twice with coupling buffer using 2 × 1 mL washes. These were placed on a rotator for 60 min to bind the peptides. The beads were washed once with 2 mL of wash buffer 1 (50 mM cysteine-HCL in coupling buffer) and placed on a rotator for 30 min at RT to remove non-covalently bound peptide. All procedures after this step were performed at 4°C. The supernatant was eluted and the column was washed

once with 5 ml dH_2O, followed by wash buffer 2 (1M NaCl, 200 µM glycine pH 2.4), and another wash with 5 ml dH_2O.

Samples were routinely taken during the above process to check coupling efficiency by Ellman's method. Briefly, samples were prepared containing 86 µl coupling buffer, 4 µl Ellman's reagent, and 10 µl of each sampling. These were incubated at room temperature for 15 min and measured on the Nanodrop at 410 nm.

The antibody serum was diluted 1:1 with TBS and centrifuged at maximum speed for 10 min to pellet any debris. 1 mL was added per column and placed on a rotator at 4°C for 2 hrs for the antibody to bind the peptide. The supernatant was eluted, which would for the unphosphorylated peptide column, should contain serum that has been depleted of unphosphorylated anti-Rab7 antibody. The columns were washed twice with 10 ml ice-cold TBS, followed by elution in 3 × 0.5 mL 200mM glycine (pH2.4). The eluants were neutralised on ice with 140 µl 1.5 M TCl (pH 8.8). The purified antibody samples were desalted in a Centricon® (Millipore) using 10 mM HEPES, 100 mM NaCl (pH 7.4), and centrifugation at 4,000 × g for 5 min at 4°C.

2.2.5.7 ELISA for antibody testing

The anti-pRab7(S72) antibodies were examined by ELISA to determine whether they were specific for pS72 of S72-OH. 0.01–10 ng dilutions of the unphosphorylated and S72 phosphorylated peptides were diluted in TBS and added to well of a 96-well plate in 50 µl volume and allowed air dry overnight. Plates were blocked for 1 h with 100 µl of TBST + 1% BSA at room temperature, followed by two washes with TBST. Each bleed was incubated at 1:200 dilution in TBST for 2 h, followed by 3 washes in TBST, and incubation with the anti-rabbit peroxidase secondary antibody (1:2,000 in TBST + 1% BSA). The plates were then washed 5–-6 times for 3 min each with TBST, followed by blocking in TBST + 1% BSA for 10 min. After rinsing in water, 75 µl of SIGMA*FAST*™ OPD

Substrate (Sigma) was added to each well and the plate was covered from light. After incubation for 10 min, the reaction was stopped by addition of 50 µl 2 M HCl. Absorbances were read at 490 nm.

2.2.5.8 Antibody testing by western blot

After the ELISA revealed that the anti-pRab7(S72) antibody serum from rabbit 192 was more specific for pRab7(S72), the antibody was tested against recombinant His-Rab7 +/- TBK1 phosphorylation by western blot. The non-phosphoantibody was firstly saturated with 1 mg/ml unphosphorylated peptide for 1 h at 4°C on a rotator. Recombinant protein was loaded corresponding to 80, 160 and 320 ng protein per lane. The anti-pRab7(S72) antibody serum was used at a dilution of 1:100 overnight at 4°C. The same blot was stripped and reprobed with a mouse anti-Rab7 antibody (1:1000) fro 1 h at room temperature as a control.

2.2.5.9 In vitro phosphorylation

Phosphorylation of Rab7 *in vitro* by His-TBK1 or GST-IKKε was performed in a reaction buffer containing 20 mM TCl pH 7.5, 10 mM $MgCl_2$, 1 mM EGTA, 10 µM Na_3VO_4, 0.5 mM β-glycerophosphate, 2 mM dithiothreitol (DTT) and 0.01% Triton X-100, with 100 µM ATP and > 100 ng kinase per 50 µl reaction. Samples were incubated at 30°C for 30–60 min, depending on the amount of protein used.

2.2.5.10 Immunoprecipitation experiments

Immunoprecipitation was performed using GFP-Trap® for GFP-Rab7 expressing samples of Dynabeads with the mouse anti-HA antibody for HA-Rab7. Both will be described separately. For most immunoprecipitations, equal amounts of cells were seeded per condition and the amount used was based on the volume lysed in and not quantification. This method was consistent for

loading as quantified by known standards, actin, GAPDH or GFP or HA transfection.

Immunoprecipitation for GFP-Rab7:

Following protein extraction, lysates were incubated with 10–15 µl GFP-Trap® beads for 1–2 h, depending on volume of sample, at 4°C on a rotator. Following this the beads were pelleted and the supernatant was removed and sampled to determine efficient of binding, and the beads were washed three times with ice-cold TBS contain 0.1% Triton X-100. Samples were then boiled in Laemmli sample buffer for 5 min, and analysed by SDS-PAGE western blot.

Co-immunoprecipitation of HA-Rab7 and effectors:
5 µg/ml mouse anti-HA antibody per sample was bound to 20 µl Dynabeads® (Life Technologies).

2.2.5.11 Pull-down experiment

For the GST-Rab7 pull-down of differential interactors of unphosphorylated Rab7 and pRab(S72), 1 µg GST-Rab7 was bound to 50 µl GSH-agarose beads per condition, which had been prewashed twice with 10 volumes of wash buffer (TBS containing 0.1% NP-40). These were placed on a rotator for 30 min to bind the proteins. The beads were then washed twice with ice-cold wash buffer, followed by one wash with reaction buffer (20 mM TCl pH 7.5, 10 mM $MgCl_2$, 1 mM EGTA, 10 µM Na_3VO_4, 0.5 mM β-glycerophosphate, 2 mM dithiothreitol (DTT) and 0.01% Triton X-100). The phosphorylated sample was then incubated with TBK1 reaction buffer containing 100 µM ATP and 1 µl of TBK1 (0.14 mg/ml) at 30°C for 1 h with gentle shaking. The nonphosphorylated sample was incubated with reaction buffer only. The samples were then washed once with ice-cold reaction buffer, followed by two quick washes with 10 volumes of 1M guanidine-HCl at 4°C to remove bound nucleotides, and then twice with ice-cold GTPγS loading buffer (20 mM Tris-HCl pH7.8, 100 mM NaCl,

5 mM $MgCl_2$, 1 mM NaH_2PO_4, 10 mM β-mercaptoethanol). Bound proteins were then loaded with 10 µM GTPγS in loading buffer for 30 min at 4°C on a rotator. Following this, they were washed three times with ice-cold TNTE buffer, and incubated with the cell lysates for 2 h at 4°C on a rotator for the effector pull-down. Following this, samples were washed three times with wash buffer and boiled in 5× Laemmli sample buffer.

The sample was split into two, one for mass spectrometry analysis and the other for western blot. The mass spectrometry sample was separated on a precast 10% NuPAGE® gel at 200 V for approximately 10 min, followed by staining in GelCode Blue Stain Reagent (Thermo Scientific) and destaining with HPLC grade water (Fisher Scientific). The lanes were then cut into 8 equal sections, which were then placed in a 96-well plate in HPLC grade water and sent for mass spectrometry analysis. The results were analysed using Scaffold 4.3.4 software analysis (Proteome Software, Inc.). Change in levels of protein associations with unphosphorylated Rab7 or pRab7(S72) were compared using intensity-based absolute quantification (iBAQ) values, which calculates protein intensities as the sum of total peptide intensities of a protein.

2.2.5.12 Subcellular fractionation

To examine subcellular localisation of phospho-Rab7(S72), GFP-$Rab7^{Wt}$ was transfected in MEFs and cells were stimulated with poly(I:C) to see if any changes occur compared with unstimulated controls. On day 1, MEFs were seeded on 1 × 150 cm^2 dish per condition. On day 2, GFP-$Rab7^{Wt}$ was transfected for 48 h, following which they were stimulated with 10 µg/ml poly(I:C) for 4 h. Cells were then placed on ice, washed once with ice-cold HBSS, and scraped in subcellular fractionation buffer (250 mM sucrose, 20 mM HEPES (7.5), 10 mM KCl, 2.5 mM MgOAc, 1 mM EDTA, 1mM DTT) containing HALT™ Protease & Phosphatase Inhibitor Cocktail. The cells were allowed to swell on ice for 20 min, following which they were lysed by passing through a

17.5-gauge needle (15-20 times). Nuclei and any remaining whole cells were removed by two centrifugations at 1000 × *g,* for 10 min each.

2.2.5.13 Immunofluorescence staining

Cells on coverslips were fixed by adding equal volume of 8% paraformaldehyde (PFA), which had been prewarmed to 37°C, to the culture medium in each well for 10 min at room temperature. Membranes were then permeabilised for 10 min with 0.1% Triton X-100, followed by blocking in 5% bovine serum albumin (BSA) for 1 h at room temperature. The cells were then incubated with the primary antibodies fro 1 h at room temperature or overnight at 4°C. After washing 3 × 5 min with PBS, they were incubated with the appropriate AlexaFlour secondary antibodies for 1 h at room temperature. Immunofluorescence was visualised using Zeiss LSM 710 or 780 confocal microscopes, using a 63× 1.4 NA Plan-Apochromat oil immersion objective.

2.2.5.14 Fluorescent-activated cell sorting

HEK293 cells were transfected with GFP-Rab7^{Wt}, GFP-Rab7^{S72A} and GFP-Rab7^{S72E} overnight, following which they were fixed in 4% PFA, washed three times with PBS for 5 min each, and incubated with the primary antibodies against Vps26 and LAMP2 for 2 h at room temperature. Cells were washed again as before, followed by incubation with the corresponding AlexaFlour secondary antibodies for 1 h at room temperature. Cells were then washed again and analysed by fluorescent-activated cell sorting (FACS).

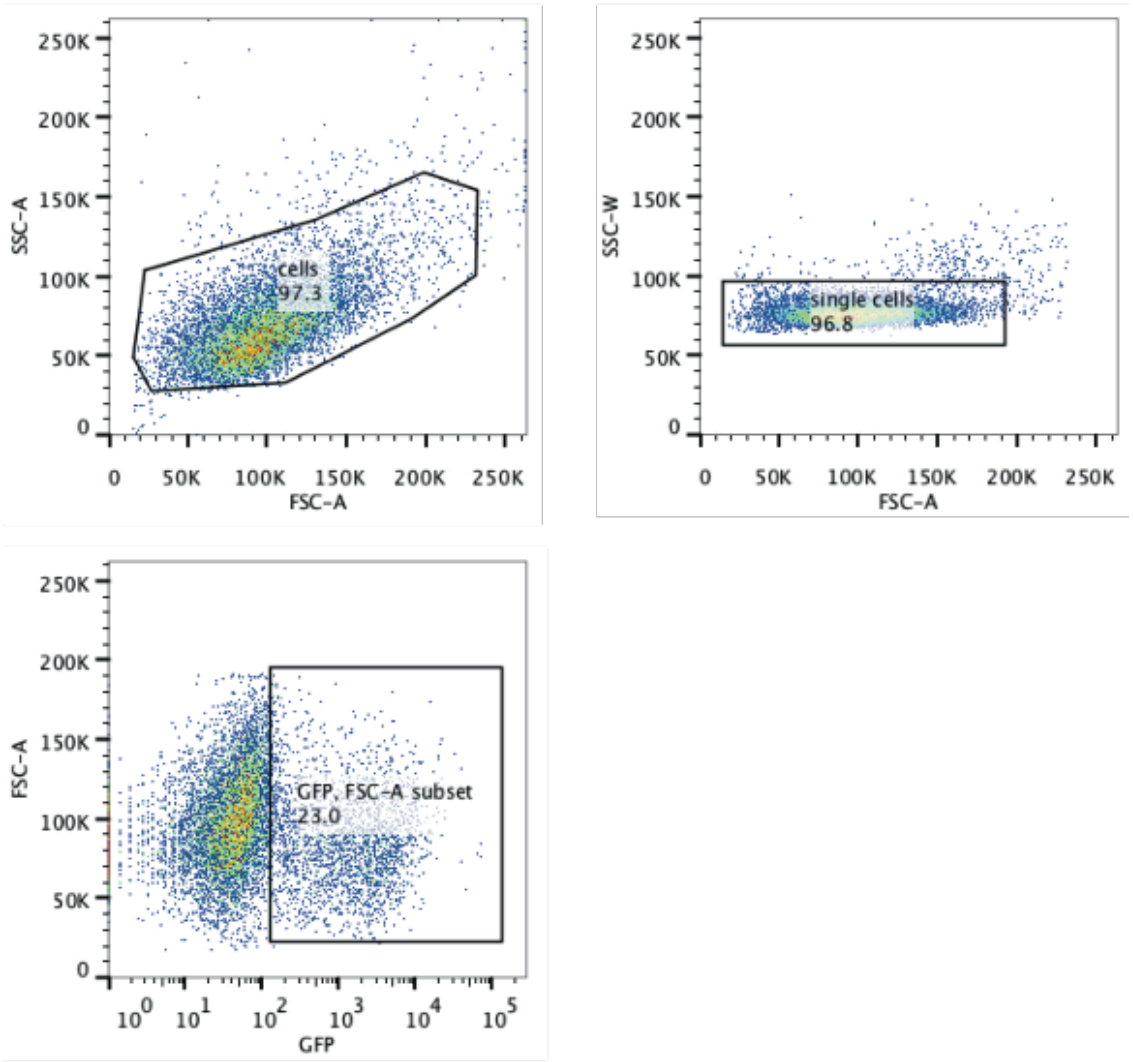

Figure 2.1. Setting of thresholds for the FACS analysis.

Cells for FACS analysis were firstly thresholded by selecting only the cell population, excluding any debris or dead cells. Following this, cells were selected based on size to include only a single cell population. From this, cells were then selected based on GFP expression (bottom panel), excluding the lowest expressing cells. These cells were than used to analyse Vps26 and LAMP2 expression.

When setting the threshold on the FloJo vX.0.6 software for the BD FACSCalibur™ flow cytometer, cells were initially selected based on their size to exclude any dead cells or debris (Figure 2.1). Following this, single cells were

selected, followed by GFP-positive only cells. These GFP-positive cells were then used to determine overall intensity of Vps26 and LAMP2 expression.

2.2.5.15 In vitro GTPase assay

In vitro hydrolysis of [α-P^{32}]GTP by unphosphorylated Rab7 and phospho-Rab7(S72) was examined using recombinant His-$Rab7^{Wt}$ ± IKKε phosphorylation. 2 × 10 µl aliquots of Ni^{2+} agarose resin, which had been preswelled in TBS overnight, were prepared for each time point (0, 15, 30, 60, 120 min) by washing twice with 10 volumes of loading buffer (20 mM Tris-HCl pH7.8, 100 mM NaCl, 5 mM $MgCl_2$, 1 mM NaH_2PO_4, 10 mM β-mercaptoethanol) and incubating them on a rotating wheel with 1 pmol of purified His-$Rab7^{Wt}$ ± IKKε phosphorylation in loading buffer for 20 min at 25°C.

Bound nucleotides were eluted by washing quickly twice with 10 volumes of 1M guanidine-HCl at 4°C and then twice with ice-cold loading buffer. After aspirating as much buffer as possible, 1 pmol of [a-^{32}P]GTP (400Ci/mmol) was added in 20 ml of ice-cold loading buffer and incubated at 0°C for 10 min. 50 ml of loading buffer was then added to each aliquot and samples were incubated at 37°C for the various time periods (0, 15, 30, 60, 120 min). After incubations, each sample was washed three times with ice-cold loading buffer, following which 8 ml of boiling buffer (0.2% SDS, 2 mM EDTA, 10 mM GDP, 10 mM GTP, pH 7.5) was then added.

Spot 2 ml of each sample onto PEI cellulose sheets and proceed with thin layer chromatography in 0.6 M Na-phosphate buffer, pH 3.5, for approximately 1 h. The thin layer chromatography sheets were placed in a PhosphorImager overnight and the radioactive spots corresponding to [a-^{32}P]GDP and [α-^{32}P]GTP were quantified by scanning the PhosphorImager and using ImageJ software (NIH) for quantification. GTP hydrolysis was calculated as the signal in the GDP spot relative to the total signal (GDP + GTP).

2.2.5.16 In vitro kinase assay

IKKα, IKKβ, TBK1 and IKKε phosphorylation of Rab7 was examined in [γ-^{32}P]ATP *in vitro* kinase assays. Each assay was performed in 50 µl of autophosphorylation buffer, containing 100 mM Tris-HCl, pH 7.5, 50mM $MgCl_2$, 50 µg/ml phosphatidylserine, 100 ng/ml TPA, with 50 ng of kinase, 2 µg His-Rab7^{Wt} or His-Rab^{S72P} (control), 10 mM cold ATP and 100 µM [γ-^{32}P]ATP (3000 Ci/mmol, Amersham). After mixing well, the samples were incubated at room temperature for 1 h, then the assay was stop by precipitating the protein 0.5µl of 5% NaDOC and 3.2 µl of TCA for 10 min. Samples were then centrifuged at maximum speed for 10 min and the supernatant was carefully discarded. The precipitated samples were boiled in sample buffer (10 mM Tris pH 8.2, 0.1 mM EDTA, 10% SDS, 0.01% bromophenol blue) for 3 min and loaded on a 4–12% NuPAGE® gel at 200 V for 40 min, following which it was stained with *Coomassie* Brilliant Blue (Bio-Rad) for 1 h on a shaker. The gel was then destained for 1 h using 40% methanol and 10% glacial acetic acid, and dried in a radioactive gel dryer for 1 h. The gel was then exposed overnight using a Biomax MR film and developed the following morning. Images were quantified with ImageJ software.

Chapter 3. Impact of phosphomimetic and phosphodeficient Rab7 proteins on the endocytic pathway

3.1 Analysis of the Rab7^{S72P} mouse model

A previous member of the Molecular Neuropathobiology laboratory, Olga Martins de Brito, together with Abraham Acevedo-Arozena (MRC Harwell) and Elizabeth Fisher (UCL Institute of Neurology), examined a collection of mouse strains obtained via a N-ethyl-N-nitrosourea (ENU) mutagenesis screen for mutations in Rab7. In particular, they identified three point mutations in Rab7 at potential phosphorylation sites, two of which had previously been identified in phosphoproteomic screens (Rab7^{S72P} and Rab7^{Y183H}). Preliminary analysis of the Rab7^{S72P} strain revealed that this mutation was lethal in homozygosis, indicating that this residue is essential for Rab7 function and for life.

ENU is a mutagen usually administered as a series of intraperitoneal injections to adult male mice, with the optimal concentration predicted to induce one mutation every 1–1.5 Mb. Premeiotic spermatogonial stem cells are one of the primary targets of ENU. To screen for mutations, ENU-treated males (G0) are crossed with wild-type females to produce G1 progeny, which have an estimated 30–50 potential functional mutations in their genome. These G1 progeny are then backcrossed to a wild-type strain for approximately 10 generations to reduce the likelihood of residual mutations that may affect the analysis of the phenotype of a particular mutation.

After backcrossing the Rab7^{S72P} strain for 10 generations into the C57BL/6 strain, I set up Rab7^{S72P} heterozygous mating pairs to analyse the specific phenotype induced by this mutation. Analysis of six litters from E13.5, three litters from E12.5, three litters from E11.5 and four litters from E10.5 revealed that no homozygous embryos were obtained for any of the days examined (Table 3.1). Furthermore, analysis of the ratios of wild-type to heterozygous

mice revealed that for all embryonic days the ratio was slightly below the 1:2 Mendelian ratio (Table 3.2), but I do not believe this was low enough to be of major concern. In almost all litters, there were also approximately 1–5 reabsorptions that I attempted to genotype, but none were homozygous. Finally, the transgenic facility at the LRI also attempted to obtain embryonic stem (ES) cells from the $Rab7^{S72P}$ strain, without success. Together, these results indicate that the $Rab7^{S72P}$ mutation is lethal at a very early stage in embryogenesis, possibly even before E4.5 when the ES cells are harvested. It is worth noting that both the male and female mice are fertile and produce heterozygous progeny when crossed with wild-type mice, so the lethality occurs after fertilisation.

The MNP group also obtained a Rab7 gene-trap clone (E284E11) from the German Genetrap Consortium. This is a knockout-first genetrap that should produce homozygous $Rab7^{-/-}$ progeny when the heterozygous mice are crossed. Unfortunately, no $Rab7^{-/-}$ mice or ES cells could be obtained from these matings. The strain was subsequently crossed with FlpO mice, which, through the expression flippase (Flp) recombinase, inverts the genetrap cassette. When the cassette is inverted, the splice acceptor site is removed and the genetrap is inactivated. These mice can then be mated to produce progeny homozygous for the inactive cassette, which can then be crossed with Cre recombinase expressing strains to invert the cassette again into the active conformation and produce conditional knockout mice for Rab7. ES cells and MEFs can also be harvested and transfected with a Cre expression plasmid to produce knockout cells. However, the insertion site for the cassette is not known, so we could not distinguish between heterozygous and homozygous mice. The Edinger laboratory at University of California, Irvine, previously produced a conditional knockout mouse for Rab7 in T cells, in which they found that Rab7 was important in negatively regulating growth or division during T cell development. Furthermore, these mice exhibited an increased rate of developing lymphomas. Prof. Edinger kindly provided us with $Rab7^{-/-}$ MEFs, but this was very recently, so they have yet to be examined.

Table 3.1. Genotype analysis of E10.5–13.5 embryos from $Rab7^{Wt/S72P}$ × $Rab7^{Wt/S72P}$ timed-matings

Litter	Embryonic Day	$Rab7^{Wt/Wt}$	$Rab7^{Wt/S72P}$	$Rab7^{S72P/S72P}$
1	13.5	3	5	0
2	13.5	3	8	0
3	13.5	4	5	0
4	13,5	3	2	0
5	13.5	3	7	0
6	13.5	3	3	0
7	12.5	4	5	0
8	12.5	3	7	0
9	12.5	3	5	0
10	11.5	5	7	0
11	11.5	4	7	0
12	11.5	4	8	0
13	10.2	3	6	0
14	10.5	6	10	0
15	10.5	5	9	0
16	10.5	6	7	0

Table 3.2. Genotype ratio analysis of $Rab7^{Wt/S72P}$ × $Rab7^{Wt/S72P}$ timed-matings

Embryonic day	$Rab7^{Wt/Wt}$	$Rab7^{Wt/S72P}$	$Rab7^{S72P/S72P}$	Ratio
13.5	19	30	0	1:1.58
12.5	10	17	0	1:1.7
11.5	13	22	0	1:1.69
10.5	20	32	0	1:1.6

3.2 Rab7 sequence conservation and structural predictions for phosphorylation at S72

Rab GTPases belong to the Ras superfamily of proteins, which contains four other members: Arf, Rab, Ran, and Rho. The Rab family is the largest of the five members, with over 60 known Rabs in mammalian cells. Of the Rab proteins known to date, around 20 appear to have been present in the last eukaryotic common ancestor. Of these 20 Rabs, only five (Rab1, Rab5, Rab6, Rab7 and Rab11) are present in most of the well-characterized genomes studied to date (Klopper et al., 2012). Of the five kingdoms (Animalia, Plantae, Fungi, Bacteria, and Protozoa), Bacteria is the only kingdom in which Rab proteins are not found.

Based on its good evolutionary conservation, I decided to examine the Rab7 sequence to see if the S72 residue was well conserved using the EMBL Clustal Omega tool (http://www.ebi.ac.uk/Tools/msa/clustalo/). The species chosen spanned the Animalia (human, mouse, rat, zebrafish, fruit fly), Plantae (*Arabidopsis thaliana*), Fungi (*Saccharomyces cerevisiae*) and Protozoa (*Entamoeba histolytica*) kingdoms, where Rab7 is found. Interestingly, the results revealed that the S72 site was conserved across all species examined, along with 16 surrounding residues, or 27 residues excluding *Saccharomyces cerevisiae* and *Entamoeba histolytica* (Figure 3.1). Thus, the S72 site and surrounding region appear to be highly important for Rab7 function, as it has been completely conserved throughout evolution.

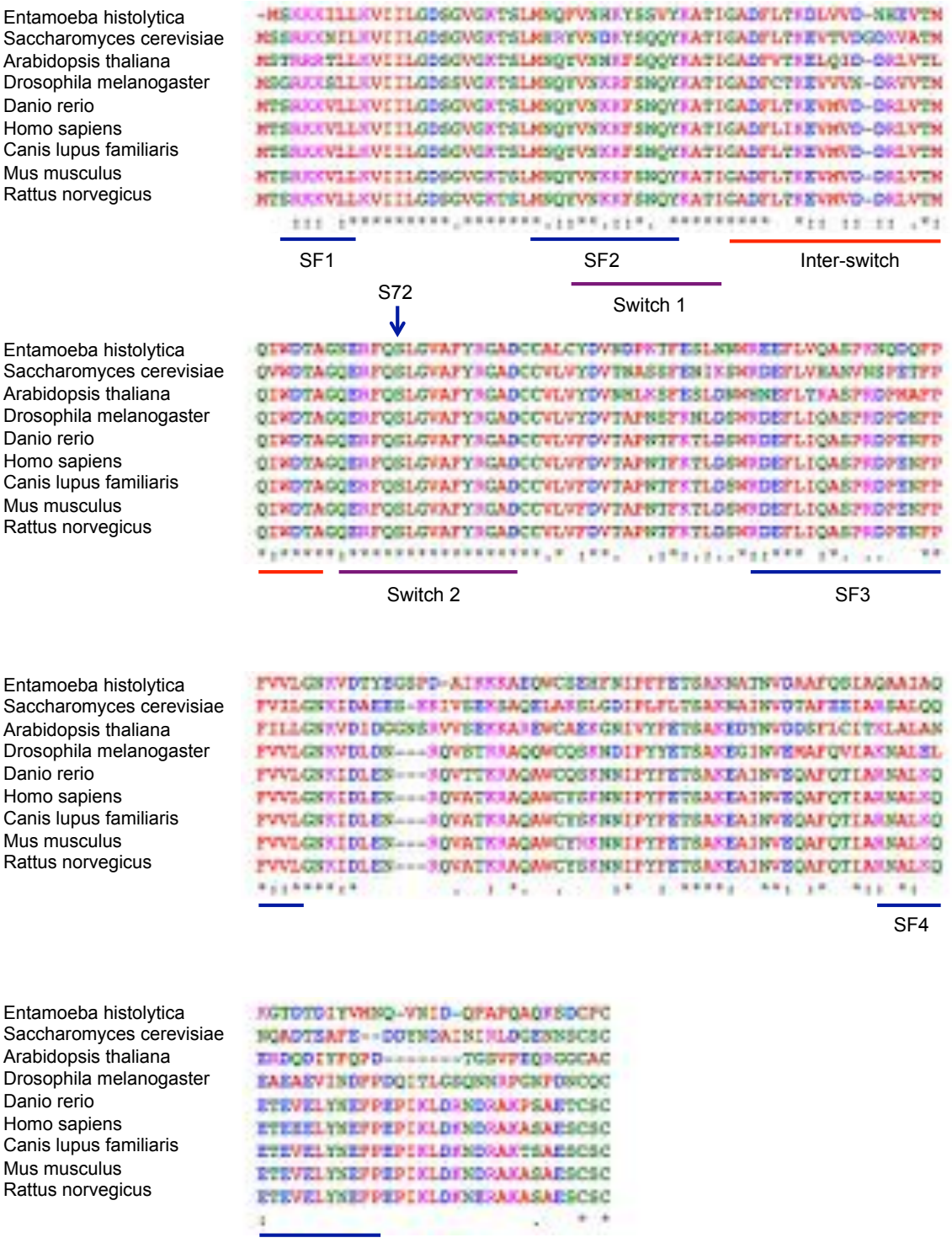

Figure 3.1. Rab7 sequence conservation.

Sequence conservation was examined by aligning sequences of various organisms from the different kingdoms where Rab7 is found. The S72 site is completely conserved, while the region surrounding it is also highly conserved. Colour coding: red indicates small, hydrophobic residues, including aromatics; blue indicates acidic

residues; magenta indicates basic residues; and green indicates hydroxyl, sulphydryl, amine and G residues. * indicates a fully-conserved residues; : indicates conservation between groups of strongly similar properties; and . indicates conservation between groups of weakly similar properties. Obtained using Clustal Omega software (EMBL-EBI).

Another insight into the importance of the S72 residue is that it is conserved in a number of other Rabs operating in the endocytic (Rab5) and the secretory (Rab6, Rab9 and Rab27) pathways; however, it is not present in two of the five most commonly found Rabs, Rab1 and Rab11 (Figure 3.2).

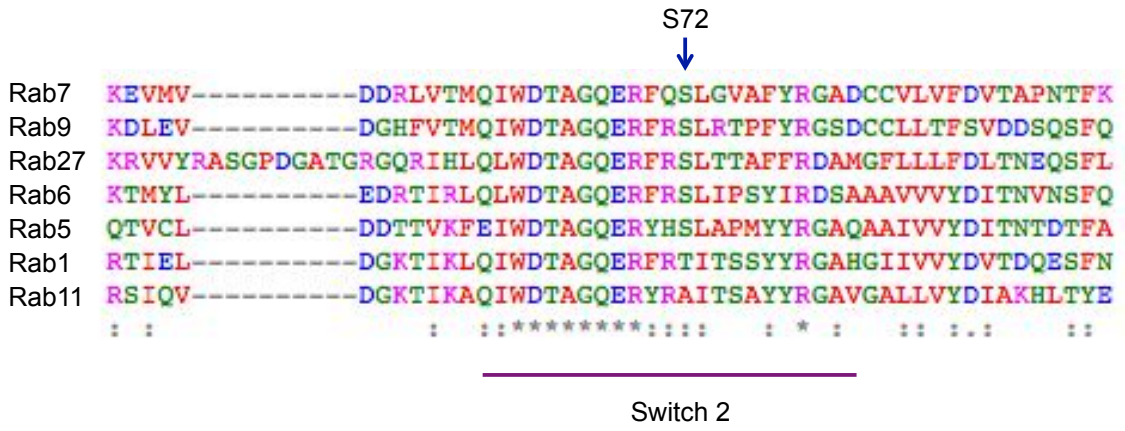

Figure 3.2. S72 conservation between different Rab proteins.
Conservation of the S72 site was examined in across the most common Rabs. The five Rabs present in most of the well-characterized genomes studied to date (Rab1, Rab5, Rab6, Rab7 and Rab11) are shown in the above alignment, along with Rab9 and Rab27, both of which have the conversed S72 site. Colour coding: red indicates small, hydrophobic residues, including aromatics; blue indicates acidic residues; magenta indicates basic residues; and green indicates hydroxyl, sulphydryl, amine and G residues. * indicates a fully-conserved residues; : indicates conservation between groups of strongly similar properties; and . indicates conservation between groups of weakly similar properties.

3.3 Cellular localisation of serine 72 phosphomimmetic and phosphodeficient Rab7 mutant proteins

Without knowing what kinases phosphorylate Rab7 at S72, I first decided to create GFP-Rab7^{S72A} (phosphodeficient), GFP-Rab7^{S72E} (phosphomimmetic) and GFP-Rab7^{S72P} (mouse model) constructs using site-directed mutagenesis of wild-type pcDNA3-GFP-Rab7^{Wt} to determine if phosphorylation at S72 could affect cellular localisation of Rab7. The mouse mutation was included to determine if it acted similarly to the phosphodeficient or phosphomimmetic mutations.

All four constructs were transfected in MEFs overnight with Lipofectamine 2000 transfection reagent and visualised by confocal microscopy on a Zeiss LSM 710 upright microscope (Figure 3.3). Both Rab7^{Wt} and Rab7^{S72A} expressed similarly and are localised to numerous puncta throughout the cell, which are reminiscent of multivesicular bodies (MBVs)/late endosomes. The distributions of both proteins were varied, exhibiting some cells with large amounts of perinuclear clustering and others with much higher cytosolic localisation. These can be seen in the lower magnification images in Figure 3.3, which show that variations were evident in cells of similar morphology in the same region. In contrast, both the Rab7^{S72E} and Rab7^{S72P} mutants are cytosolic and uniform, indicating that these cannot be recruited to endosomal membranes for activation. Both mutant proteins are also found in the nucleus; however, the reason for this is unclear. As GFP-Rab7 is below the cut-off size for diffusing through the nuclear pore (>60 kDa), these mutants may simply cross as their localisation signals could be affected. Overall, these results indicate that phosphorylation at S72 may inhibit Rab7 activity by affecting its recruitment to endosomal membranes.

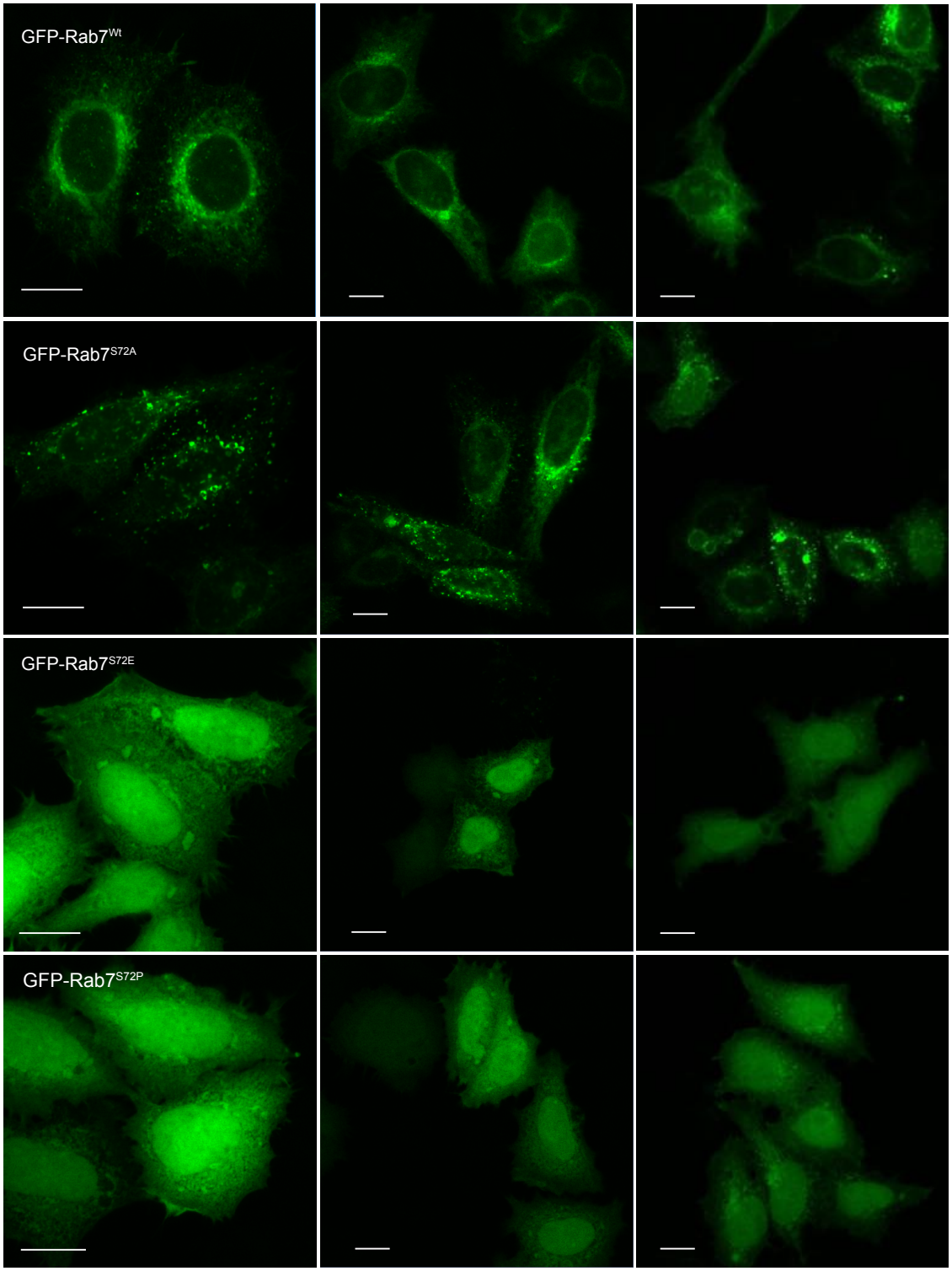

Figure 3.3. Subcellular localisation of GFP-Rab7^{Wt}, GFP-Rab7^{S72A}, GFP-Rab7^{S72E}, and GFP-Rab7^{S72P}.

GFP-Rab7^{Wt}, GFP-Rab7^{S72A}, GFP-Rab7^{S72E} and GFP-Rab7^{S72P} were transfected for 24 h in MEFs to determine whether the phosphomimetic (S72E), phosphodeficient (S72A) or mouse (S72P) mutations had any effects on subcellular localisation of Rab7. Images

were obtained by confocal microscopy. The second and third columns show lower magnification images to illustrate the variations in expression of GFP-Rab7^{Wt} and GFP-Rab7^{S72A}. Both proteins exhibit perinuclear clusters as well as scattered distributions throughout the cell. Scale bar = 10 μm.

3.4 Comparison of the effects of serine 72 phosphomimmetic and phosphodeficient mutations of Rab7 on markers of the endocytic pathway

As there were such a striking difference in the cellular localisation of Rab7^{S72E} compared to Rab7^{Wt} and Rab7^{S72A}, I decided to examine whether these mutations had any effects on the localisation and expression of other endocytic markers. The markers chosen were are follows: EEA1, a peripheral membrane protein that co-localizes with Rab5 on early endosomes; Rab11, a regulator of the trafficking of recycling endosomes; Vps26, an essential component of the retromer complex, which is required for endosome-to-Golgi retrieval of receptors, such as insulin-like growth factor receptor 2 (IGF2R) and M6PR; and LAMP2, a lysosomal membrane protein believed to play roles in protecting the membrane from proteolytic enzymes within lysosomes and aiding the import of proteins into the lumen of the lysosome.

GFP-Rab7^{Wt}, GFP-Rab7^{S72A} and GFP-Rab7^{S72E} were transfected in MEFs on coverslips overnight with Lipofectamine 2000, following which cells were fixed in 4% PFA and stained for the intracellular markers discussed above. Images were acquired using a Zeiss LSM 780 microscope. The results revealed that although there were striking differences in localisation of GFP-Rab7^{Wt} and GFP-Rab7^{S72A}, compared to GFP-Rab7^{S72E}, there appeared to be no differences in the subcellular localisation or total intensity of any of the markers tested, supporting that these mutants do not induce a rearrangement of intracellular organelles cells (Figure 3.4–3.7).

As the levels GFP-Rab7 can be quite heterogeneous when overexpressing the cells, it can be very difficult to quantify changes in the overall intensity of specific markers in cells that are expressing similar levels of GFP-Rab7. Thus, the total intensities of LAMP2 and Vps26 were examined by FACS in the total population of GFP-positive cells for GFP-Rab7^{Wt}, GFP-Rab7^{S72A} and GFP-Rab7^{S72E}. As the antibodies are from different species, both were analysed in

the same sample of cells. The results of the FACS analysis revealed that there was no difference in the total intensity of LAMP2 or Vps26 in GFP-Rab7^{Wt}, GFP-Rab7^{S72A} and GFP-Rab7^{S72E} expressing (Figure 3.8).

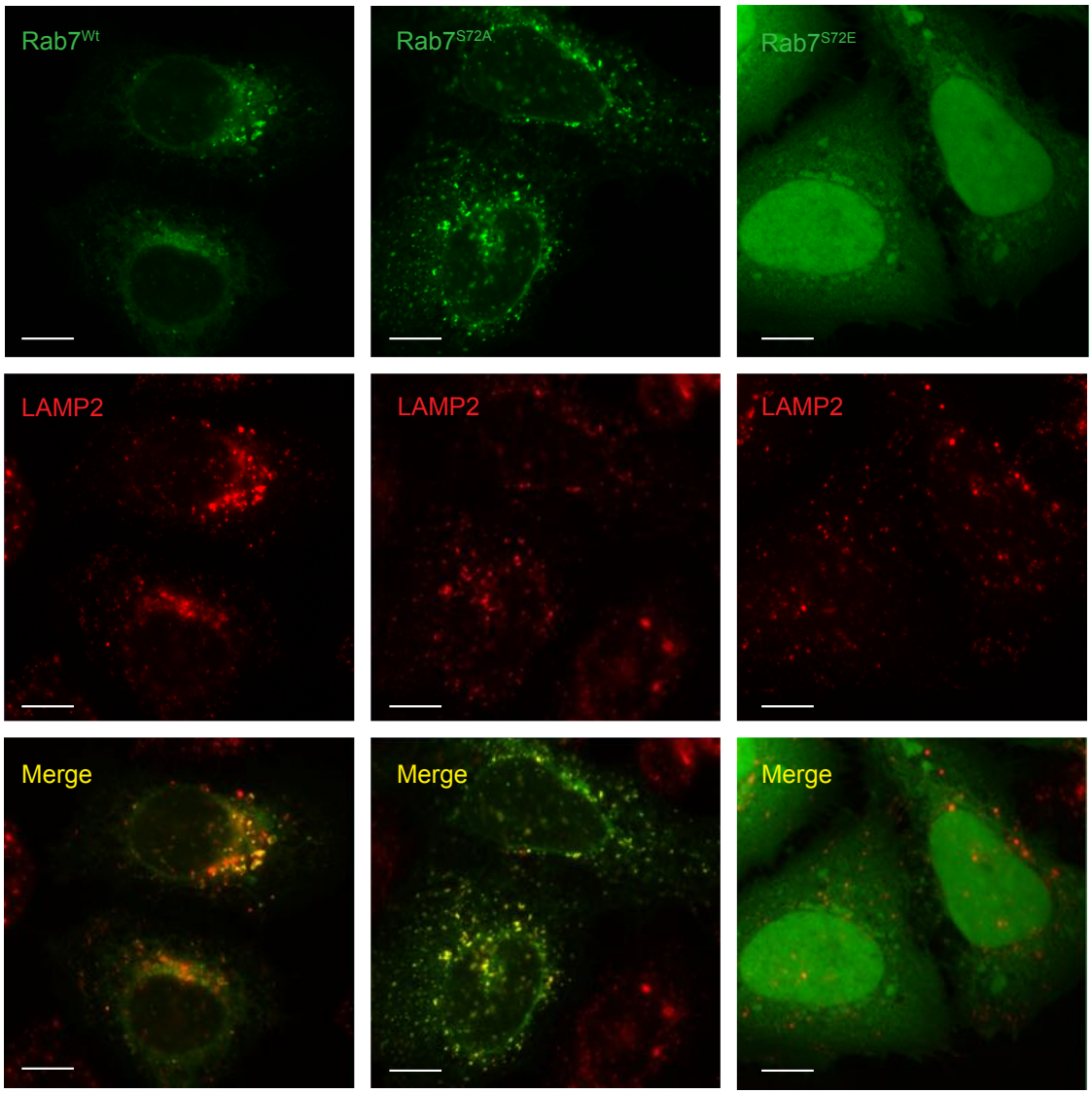

Figure 3.4. LAMP2 expression in cells overexpressing GFP-Rab7^{Wt}, GFP-Rab7^{S72A} and GFP-Rab7^{S72E}.

GFP-Rab7^{Wt}, GFP-Rab7^{S72A} and GFP-Rab7^{S72E} were transfected for 24 h in MEFs, following which LAMP2 expression was examined using a mouse anti-LAMP2 antibody. Images were obtained by confocal microscopy. Scale bar = 10 μm.

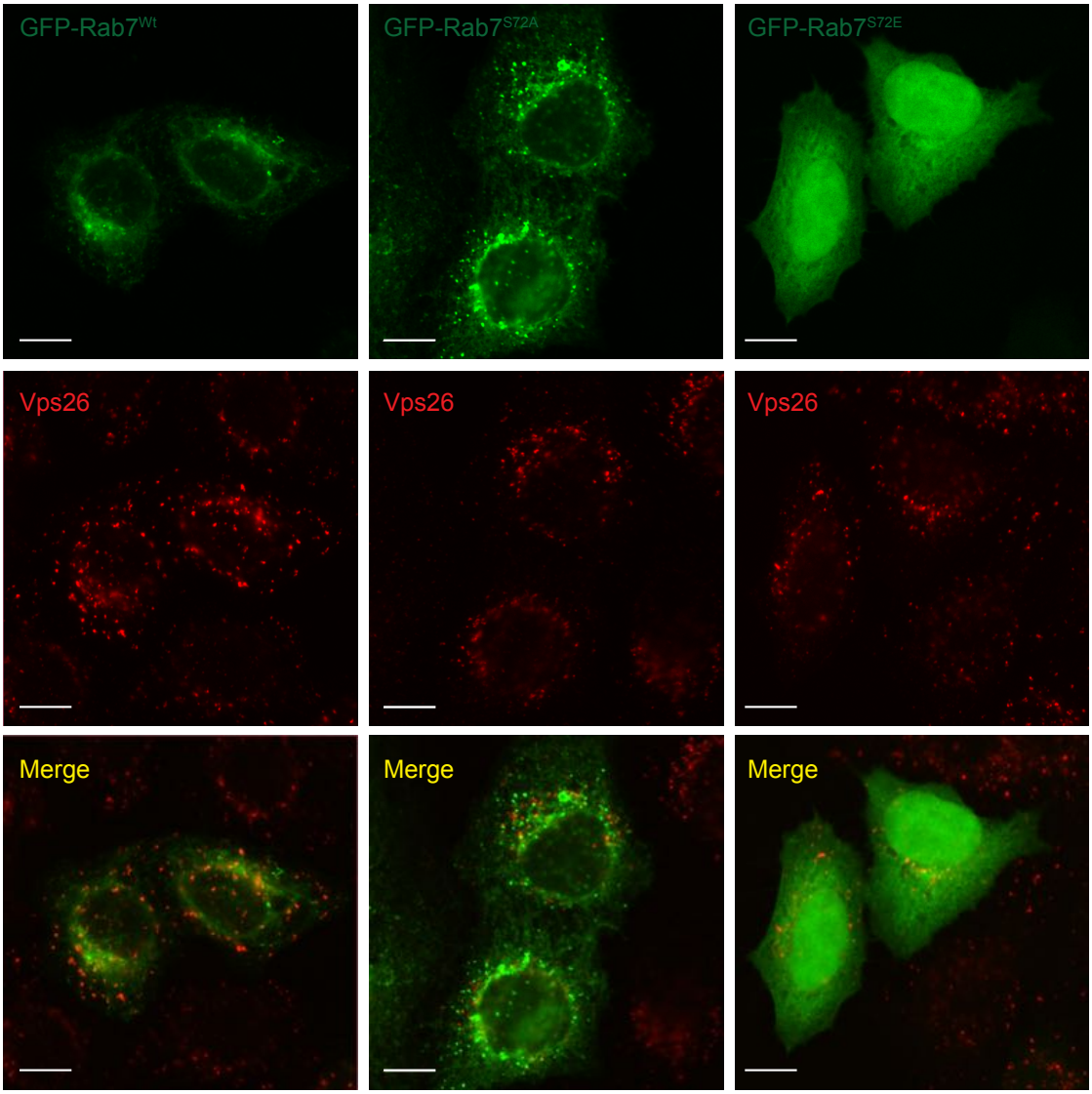

Figure 3.5. Vps26 expression in cells overexpressing GFP-Rab7^{Wt}, GFP-Rab7^{S72A} and GFP-Rab7^{S72E}.

GFP-Rab7^{Wt}, GFP-Rab7^{S72A} and GFP-Rab7^{S72E} were transfected for 24 h in MEFs, following which Vps26 expression was examined using a mouse anti-Vps26 antibody. Images were obtained by confocal microscopy. Scale bar = 10 μm.

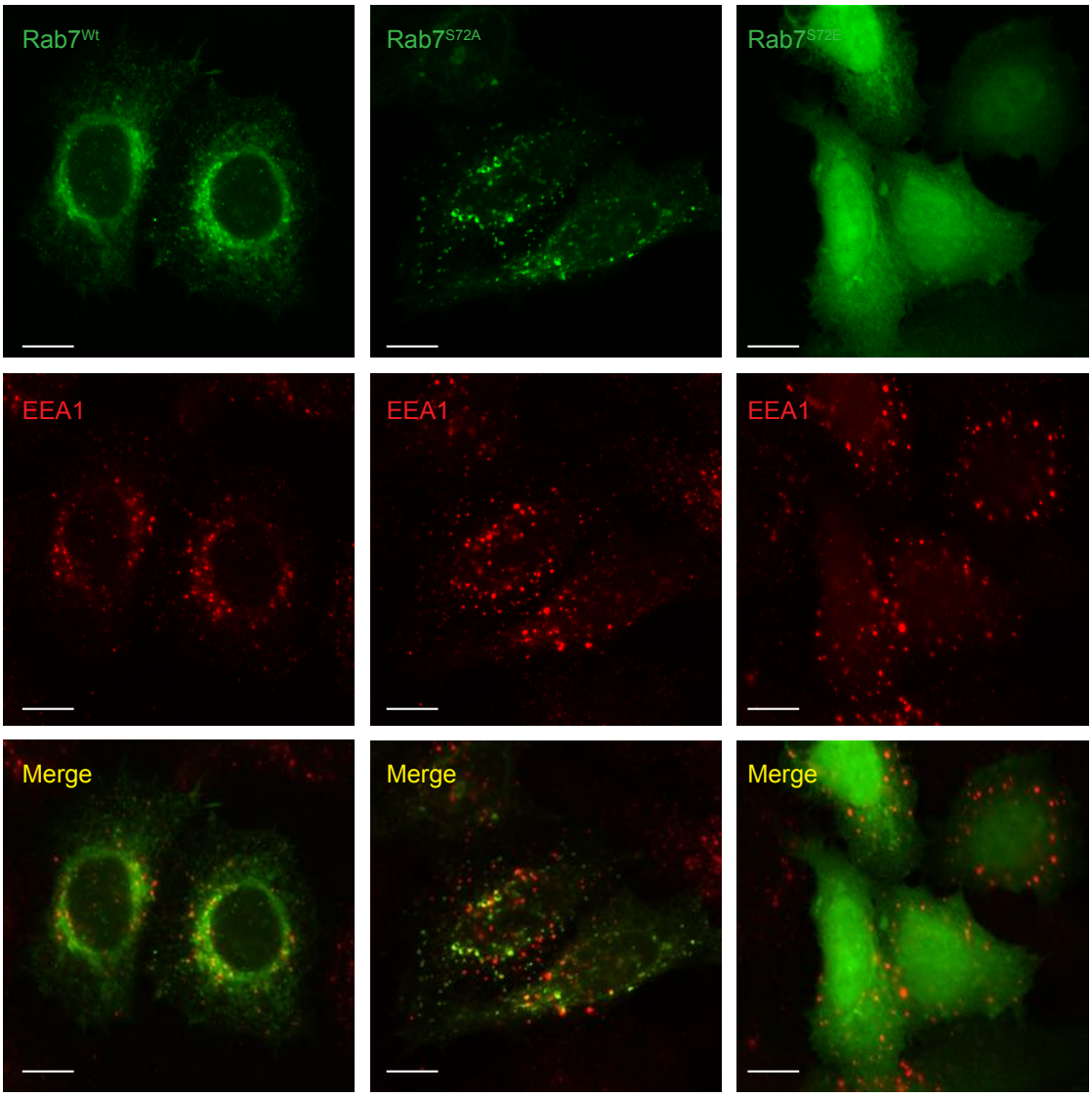

Figure 3.6. EEA1 expression in cells overexpressing GFP-Rab7^{Wt}, GFP-Rab7^{S72A} and GFP-Rab7^{S72E}.

GFP-Rab7^{Wt}, GFP-Rab7^{S72A} and GFP-Rab7^{S72E} were transfected for 24 h in MEFs, following which EEA1 expression was examined using a mouse anti-EEA1 antibody. Images were obtained by confocal microscopy. Scale bar = 10 μm.

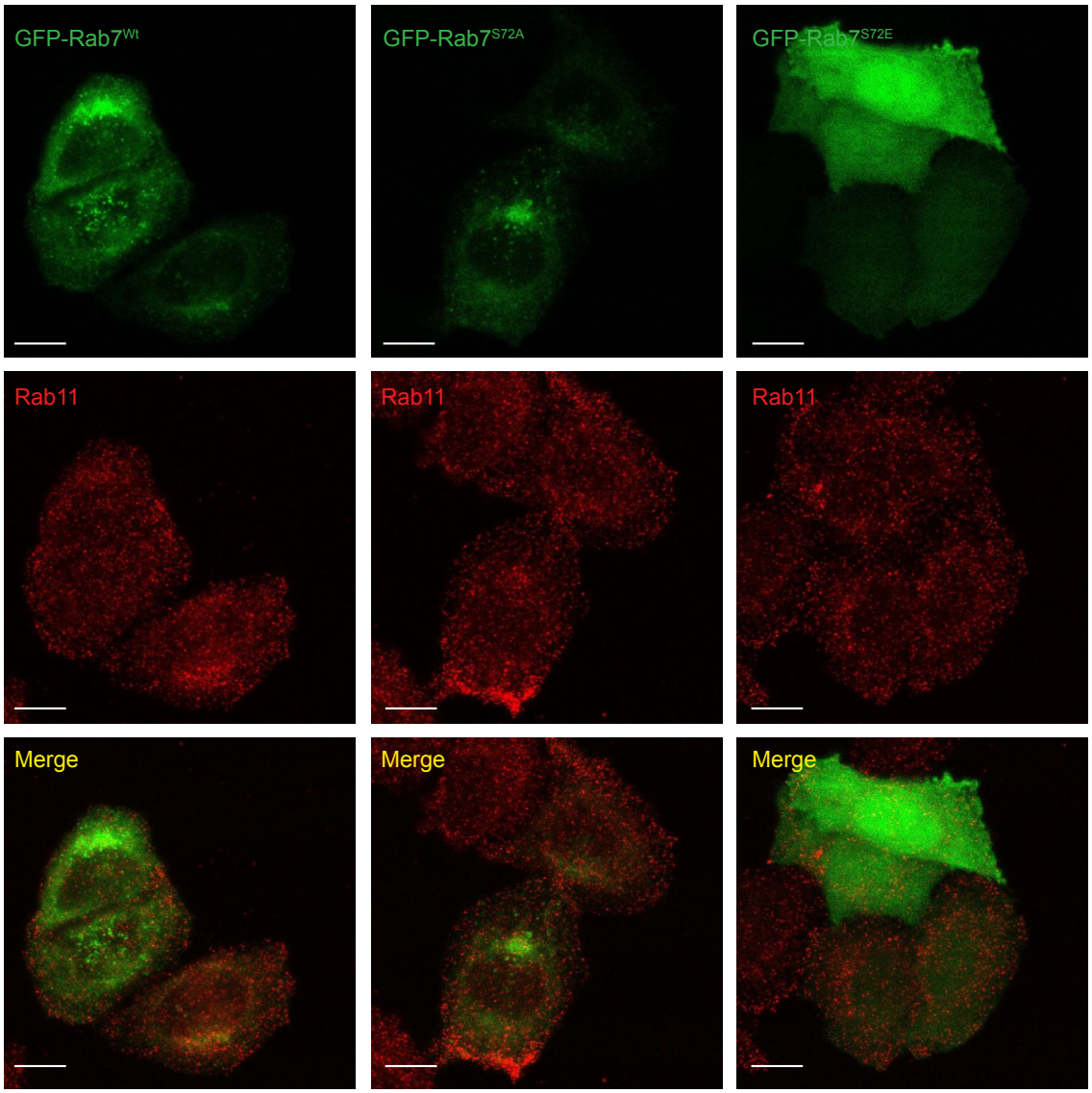

Figure 3.7. Rab11 expression in cells overexpressing GFP-Rab7^{Wt}, GFP-Rab7^{S72A} and GFP-Rab7^{S72E}.

GFP-Rab7^{Wt}, GFP-Rab7^{S72A} and GFP-Rab7^{S72E} were transfected for 24 h in MEFs, following which Rab11 expression was examined using a mouse anti-Rab11 antibody. Images were obtained by confocal microscopy. Scale bar = 10 μm.

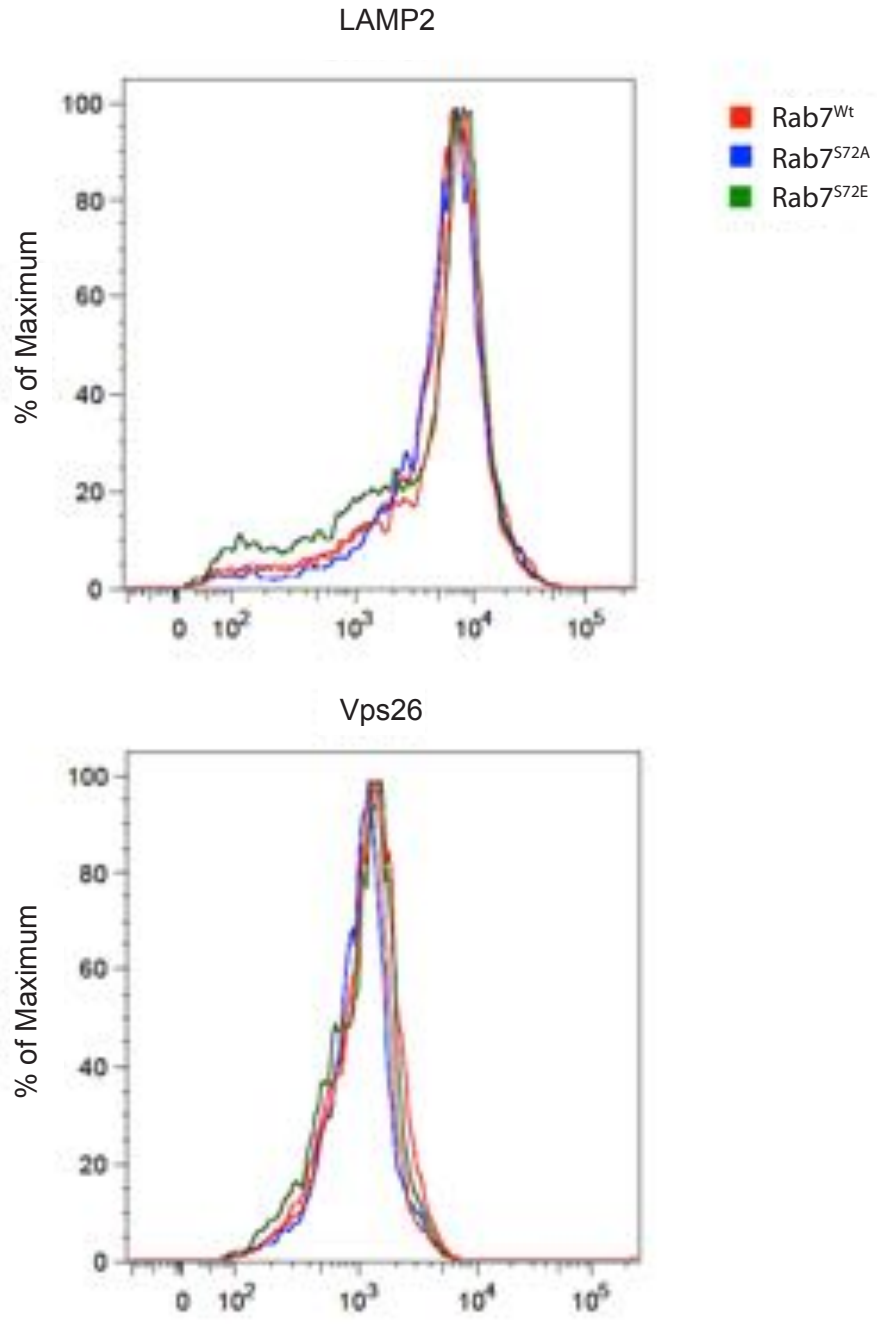

Figure 3.8. Total LAMP2 and Vps26 expression in cells expressing GFP-Rab7^{Wt}, GFP-Rab7^{S72A}, GFP-Rab7^{S72E} and GFP-Rab7^{S72P}.

GFP-Rab7^{Wt}, GFP-Rab7^{S72A} and GFP-Rab7^{S72E} were transfected for 24 h in MEFs, following which total LAMP2 and Vps26 levels were examined by FACS using mouse anti-LAMP2 and rabbit anti-Vps26 antibodies.

3.5 Comparison of the effects of serine 72 phosphomimmetic and phosphodeficient mutations of Rab7 on EGFR degradation

The endocytic pathway is highly important for the control of many signalling pathways, including the EGFR, which plays an important role in cell growth, migration, and differentiation. When the EGFR binds its ligand, EGF, it is internalised by clathrin-mediated endocytosis. Following internalisation, the EGFR can be recycled back to the plasma membrane for further activation or it can be targeted for degradation in a Rab7-dependent manner (Ceresa and Bahr, 2006).

To determine if the phosphomimetic or phosphodeficient mutations affect Rab7 activity, I decided to perform an EGFR degradation assay in HeLa cells overexpressing GFP-Rab7^{Wt}, GFP-Rab7^{S72A} or GFP-Rab7^{S72E}. Cells were transfected with the constructs for 24 h using Fugene6 transfection reagent, serum-starved for 2 h and stimulated with 100 ng/ml recombinant human EGF for 0, 15, 30, 60 and 90 min.

From the results, it appears that the phosphodeficient Rab7^{S72A} causes increased EGFR degradation at 15 min compared to the wild-type expressing cells, while the phosphomimetic Rab7^{S72E} causes decreased degradation (Figure 3.9). Following this, the levels of EGFR appear to increase, which could be the result of neosynthesis of the receptor. There is a large increase in EGFR levels at 30, 60 and 90 min with Rab7^{S72E}, with the levels at 90 min being much higher than the unstimulated condition (0 min). In contrast, Rab7^{Wt} and Rab7^{S72A} are similar to the unstimulated condition. Thus, these results indicate that phosphorylation may inhibit Rab7 activity. Ideally this experiment should be repeated in Rab7 knockout cells, as although repeats of this experiment did show the same trend in degradation, the differences reported were high, possibly due to the compensatory effects of endogenous Rab7.

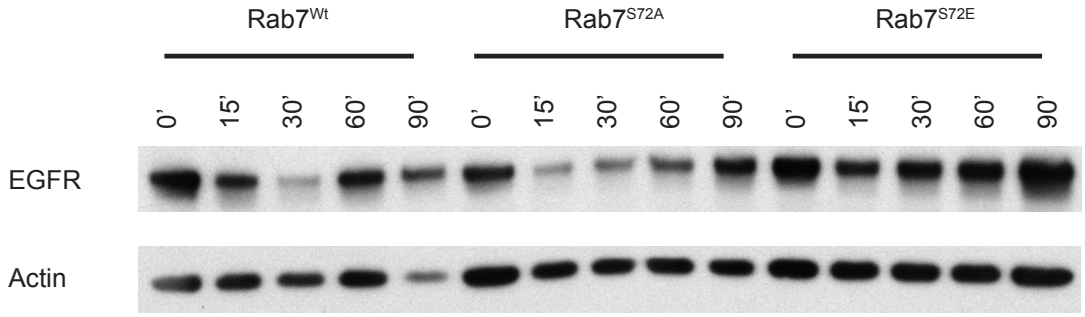

Figure 3.9. Comparison of EGFR degradation in cells overexpressing GFP-Rab7^{Wt}, GFP-Rab7^{S72A} or GFP-Rab7^{S72E}.

HEK293 cells were transfected with GFP-Rab7^{Wt}, GFP-Rab7^{S72A} or GFP-Rab7^{S72E} overnight, serum-starved for 2 h and stimulated with 100 ng/ml EGF for the indicated time-points. Cells were lysed and subjected to western blot for anti-EGFR and anti-β-actin antibodies.

3.6 Co-immunoprecipitation of wild-type, phosphomimmetic and phosphodeficient HA-Rab7 with GFP-RILP and GFP-ORP1L

RILP and ORP1L are two of the best-studied effectors of Rab7. As described in the introduction, RILP can bind both p150(Glued) and the V1G1 subunit of the V-ATPase, which may help stabilise the V-ATPase during minus-end directed transport of late endosomes/lysosomes to promote endosomal acidification. The crystal structure of the Rab7:RILP complex revealed that the interactions between these proteins involves residues directly surrounding the S72 site, indicating that phosphorylation at S72 could affect binding of RILP to Rab7. In contrast, ORP1L appears to be a master regulator of late endosomal/lysosomal transport as it recruits both p150(Glued) and KIF3A for dynein- and kinesin-mediated transport. It also binds VAP, an ER membrane protein, at ER-late endosome contact sites.

To examine whether phosphorylation of Rab7 at S72 could be a mechanism of promoting/inhibiting transport in the minus or plus direction, HA-Rab7^{Wt}, HA-Rab7^{S72A} and HA-Rab7^{S72E} were co-transfected with GFP-RILP, GFP-ORP1L or GFP-FYCO1 overnight in HEK293 cells using Lipofectamine 2000 transfection reagent. Using a mouse anti-HA antibody bound to Dynabeads, HA-Rab7^{Wt}, HA-Rab7^{S72A} and HA-Rab7^{S72E} were immunoprecipitated from cell lysates and samples were subjected to SDS-PAGE followed by western blot for GFP-RILP or GFP-ORP1L using a mouse-anti-GFP antibody. Levels of transfection of HA-Rab7^{Wt}, HA-Rab7^{S72A} and HA-Rab7^{S72E} were determined using a rat anti-HA antibody. Results were subjected to one-way ANOVA, followed by Tukey's multiple comparisons test using GraphPad Prism software. A $P < 0.05$ was considered statistically significant. Both experiments were repeated three times (n = 3).

Results revealed that there was no significant difference in the interaction between GFP-RILP and HA-Rab7^{Wt} and HA-Rab7^{S72A}, whereas there was

approximately 80% decrease in binding to HA-Rab7^{S72E} (Figure 3.10). This indicates that phosphorylation of Rab7 at S72 inhibits binding of Rab7 to RILP.

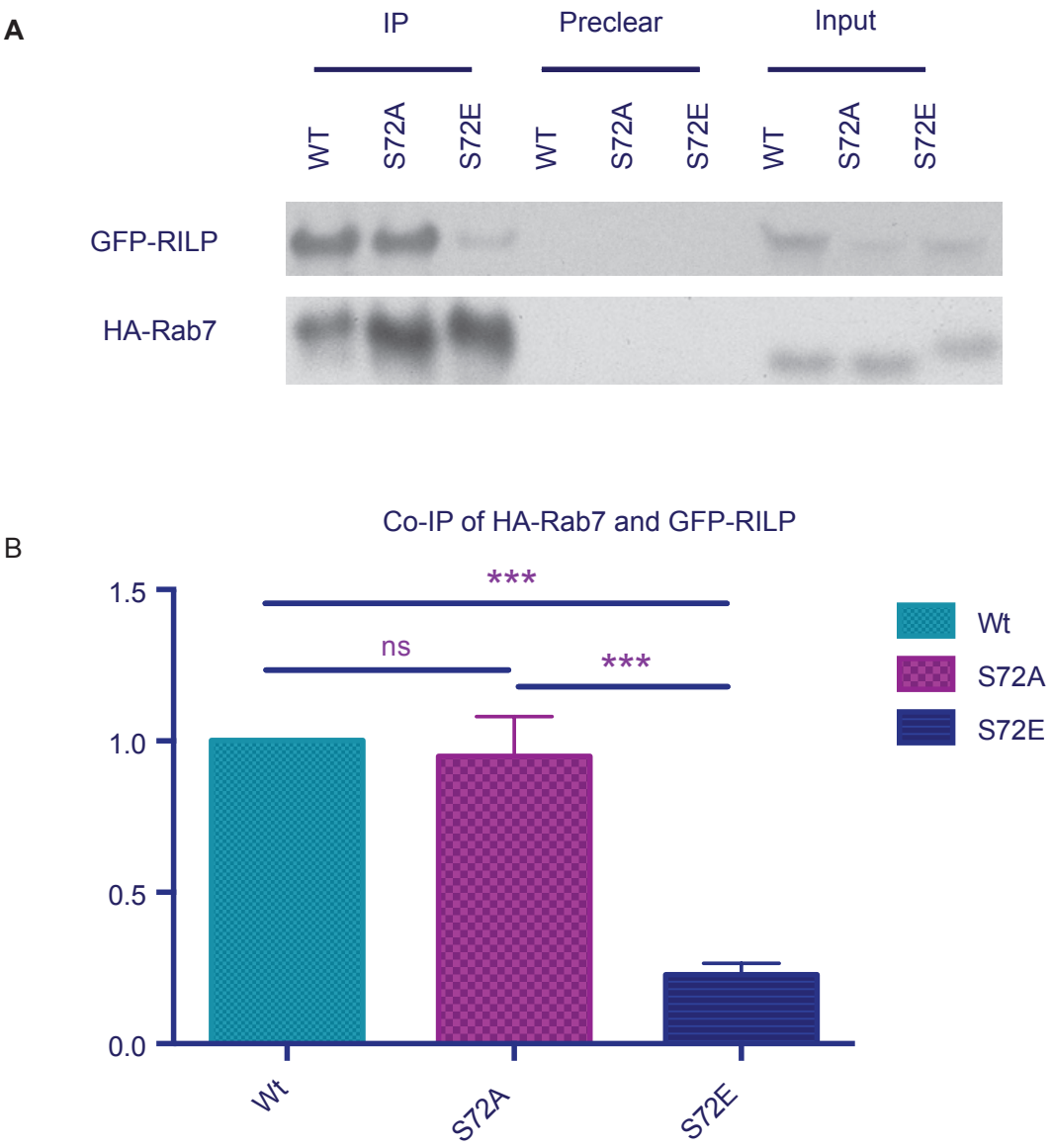

Figure 3.10. Co-IP of HA-Rab7^{Wt}, HA-Rab7^{S72A} and HA-Rab7^{S72E} with GFP-RILP. HA-Rab7^{Wt}, HA-Rab7^{S72A} and HA-Rab7^{S72E} were co-transfected with GFP-RILP overnight in HEK293 cells using Lipofectamine 2000. The HA-Rab7 variants were immunoprecipitated with anti-HA antibody on Dynabeads and the immunoprecipitates were subjected to western blot using an anti-GFP antibody to probe for GFP-RILP.

In contrast, there was no significant difference in the interaction between GFP-ORP1L and any of the three Rab7 proteins (Figure 3.11). This indicates that ORP1L binding is unaffected by phosphorylation of Rab7 at S72.

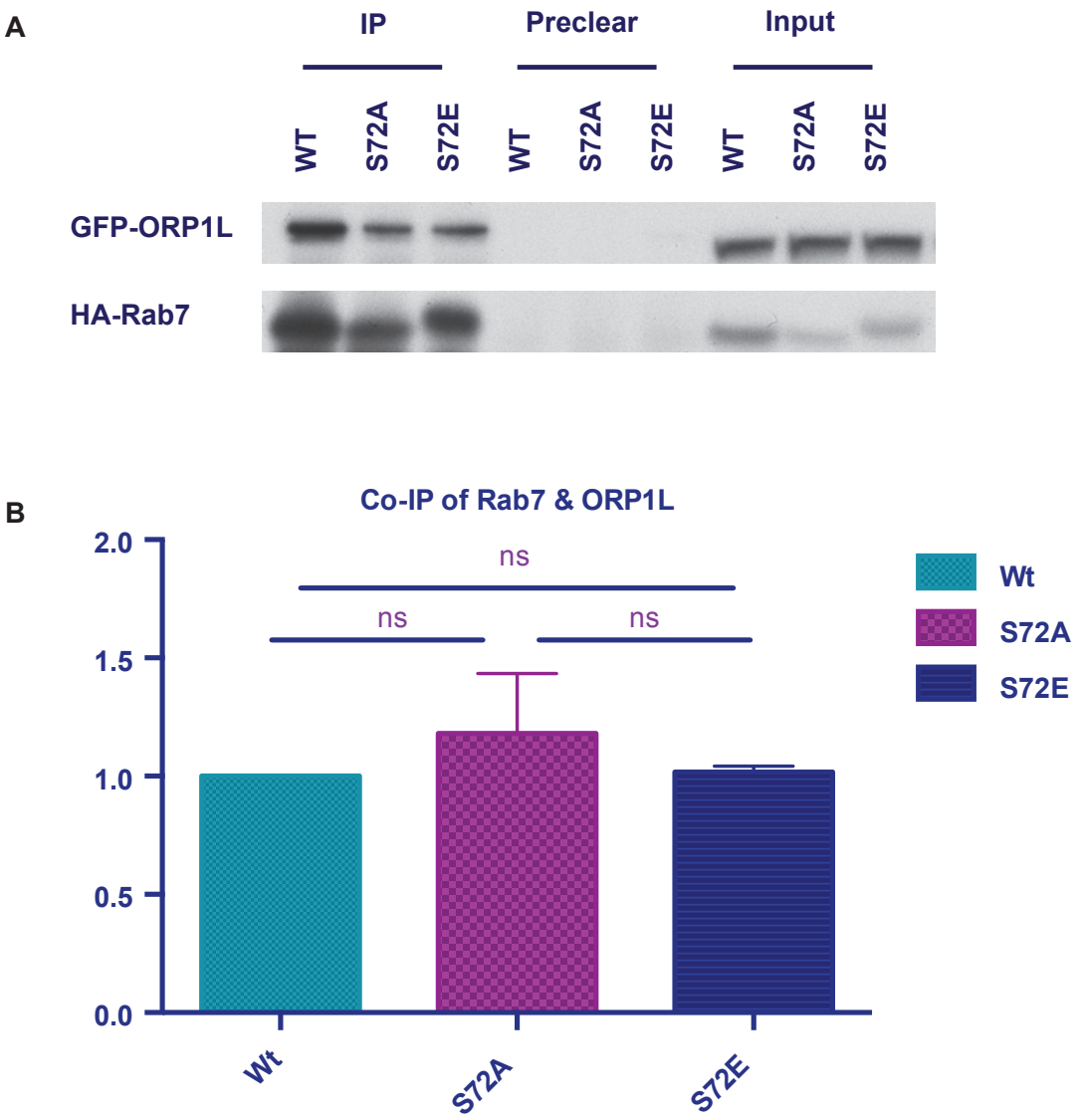

Figure 3.11. Co-IP of HA-Rab7^{Wt}, HA-Rab7^{S72E} and HA-Rab7^{S72E} with GFP-ORP1L. HA-Rab7^{Wt}, HA-Rab7^{S72A} and HA-Rab7^{S72E} were co-transfected with GFP-ORP1L overnight in HEK293 cells using Lipofectamine 2000. The HA-Rab7 variants were immunoprecipitated with anti-HA antibody on Dynabeads and the immunoprecipitates were subjected to western blot using an anti-GFP antibody to probe for GFP-ORP1L.

3.7 Analysis of the effect of serine 72 phosphomimmetic and phosphodeficient mutations on Rab7 activity using novel Raichu-Rab7 FRET sensors

The Matsuda laboratory at Kyoto University, Japan, previously produced FRET sensors for a number of small GTPases, including Ras, RhoA and Rab5, which they termed Raichu-Ras, Raichu-RhoA and Raichu-Rab5, respectively. The term Raichu is an acronym for Ras and interacting protein chimeric unit. For the Raichu-Rab5 FRET sensor Rab5 and the N-terminal Rab5-binding domain (RBD) of EEA1 were fused to YFP and CFP in the order of YFP-RBD-CFP-Rab5, with Rab5 at the C-terminus, as the REP requires access to the lipid modification site of Rab5 at the C-terminus for insertion into the endosomal membrane. This is the same organisation for the Raichu-Rab7 sensor created by the Nakamura laboratory at Tokyo University of Science, Japan, in collaboration with the Matsuda laboratory (Figure 3.12). In Raichu-Rab7, the RBD is the Rab7-binding domain of Rabring7 (Rab7-interacting RING finger protein), a Rab7 effector that specifically binds the GTP-bound form at the N-terminus. Rabring7 itself has not been very well characterised, although it its overexpression has been shown to cause increased EGFR degradation and perinuclear aggregation of lysosomes, whereas Rabring7^{C229S}, which lacks its E3 ligase activity, inhibits EGFR degradation (Mizuno et al., 2003; Sakane et al., 2007). When Rab7 is in its inactive GDP-bound state, excitation of CFP at 433 nm will result in emission at 475 nm, as the two fluorescent proteins are separated. However, in the GTP-bound state, Rab7 binds the RBD resulting in the CFP and YFP being in close proximity. When in this conformation, excitation at 433 nm will cause an energy transfer from CFP to YFP and an emission at the higher wavelength of 575 nm. This process is known as fluorescence energy resonance transfer (FRET).

In collaboration with the Nakamura laboratory, which provided the original wild-type Raichu-Rab7 (hereafter referred to as Raichu-Rab7^{Wt}), I created Rab7 point mutants for S72A (Raichu-Rab7^{S72A}) and S72E (Raichu-Rab7^{S72E}). These

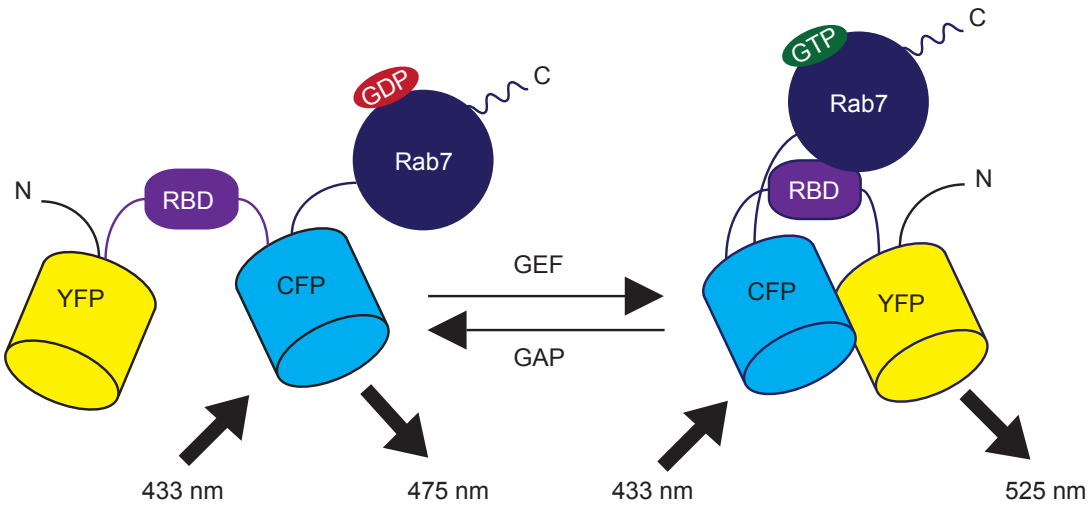

Figure 3.12. Design of the Raichu-Rab7 FRET sensor.
Structure of the Raichu-Rab7 probe, showing the YFP-RBD-CFP-Rab7 confirmation in the inactive and active states. In the inactive GDP-Rab7 state, excitation of CFP at 433 nm results in emission at 475 nm, whereas in the GTP-Rab7 state, binding of Rab7 to the RBD domain brings CFP and YFP in close proximity resulting in FRET and emission at the higher YFP emission wavelength of 525 nm.

constructs were transfected in wild-type MEFs for 48 h, following which they were imaged using a Zeiss LSM inverted 780 microscope. The cytosol and endosomal FRET ratios were quantified and compared between Raichu-Rab7^{Wt}, Raichu-Rab7^{S72A} and Raichu-Rab7^{S72E} (Figure 3.14). As Raichu-Rab7^{S72E} is completely cytosolic (Figure 3.13), there was no endosomal measurement. Intensities were quantified using ImageJ software and the ratios were subjected to one-way ANOVA, followed by Sidak's multiple comparisons test, comparing endosomal-to-endosomal and cytosolic-to-cytosolic ratios between each group. The results revealed that there was a significant decrease in the cytosolic FRET ratio between Raichu-Rab7^{S72E} and the other two probes. In contrast, there were no significant differences between endosomal and cytosolic Raichu-Rab7^{Wt} and Raichu-Rab7^{S72A} FRET ratios.

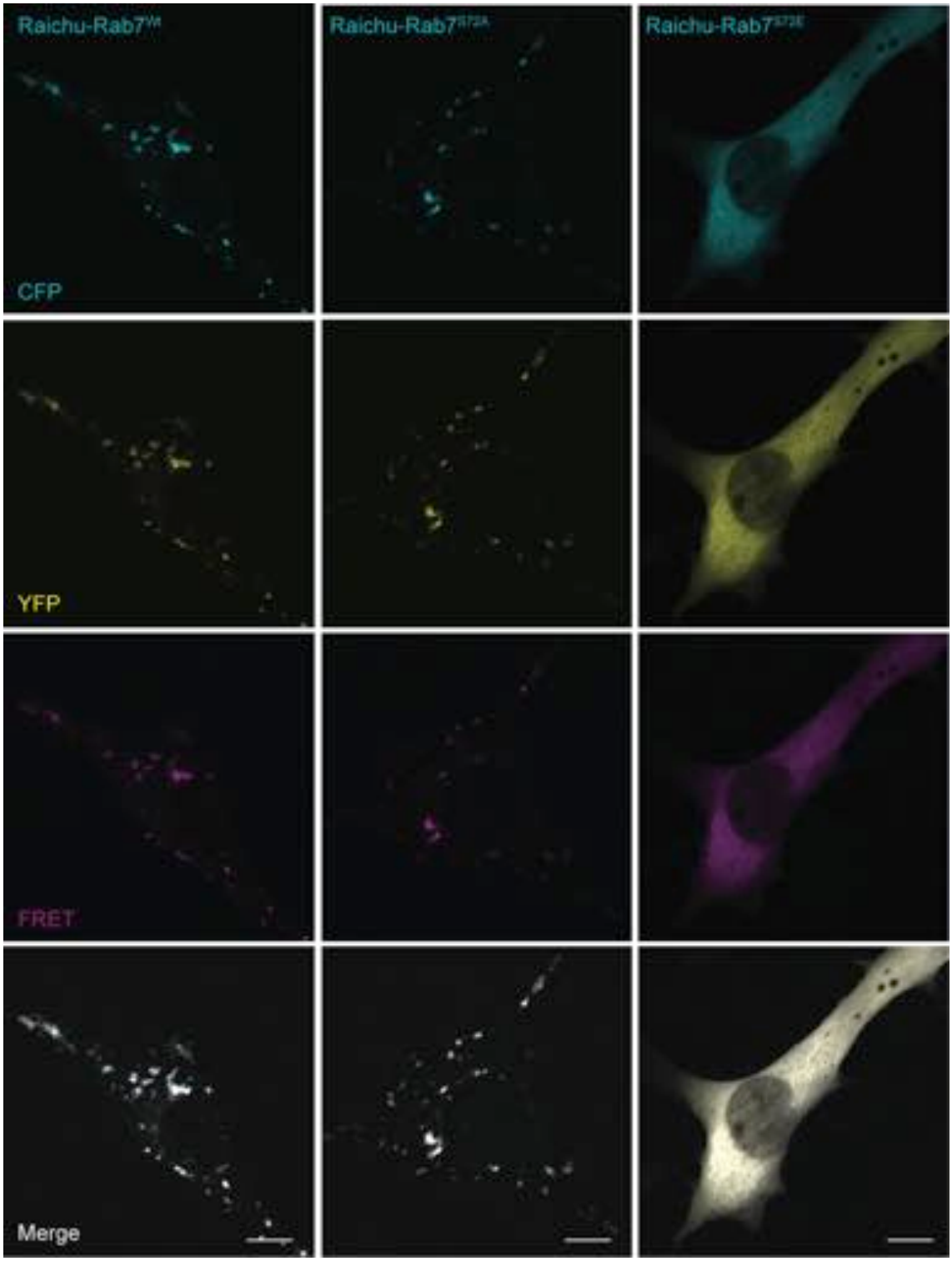

Figure 3.13. Localisation of Raichu-Rab7^{Wt}, Raichu-Rab7^{S72A} and Raichu-Rab7^{S72E} FRET probes.

Raichu-Rab7^{Wt}, Raichu-Rab7^{S72A} and Raichu-Rab7^{S72E} were transfected for 48 h in MEFs, following which they were fixed and imaged by confocal microscopy. The

subcellular localisation of each Raichu-Rab7 probe was similar to the profiles obtained with the GFP-tagged versions of Rab7^{Wt}, Rab7^{S72A} and Rab7^{S72E} (Figure 3.3), indicating that the YFP-RBD-CFP-tag at the N-terminus did not affect Rab7 function.

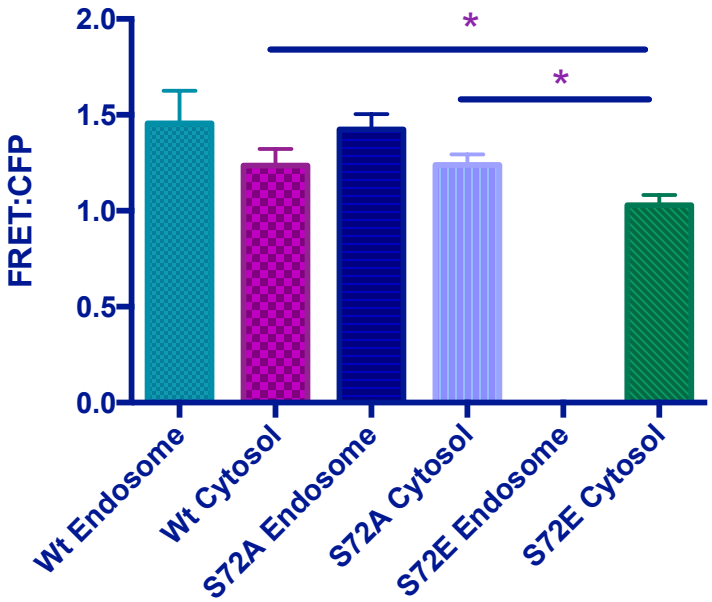

Figure 3.14. Quantification of FRET ratios for endosomal and cytosolic Raichu-Rab7^{Wt}, Raichu-Rab7^{S72A} and Raichu-Rab7^{S72E}.

Raichu-Rab7^{Wt}, Raichu-Rab7^{S72A} and Raichu-Rab7^{S72E} were transfected for 48 h in MEFs, following which they were imaged by confocal microscopy. FRET, CFP and YFP intensities were measured using ImageJ software and the mean FRET:CFP ratios were subjected one-way ANOVA using GraphPad Prism.

3.8 Discussion

Previous members of the MNP laboratory identified Rab5 and Rab7 as key components of endocytic sorting and axonal retrograde signalling (Deinhardt et al., 2006; Schmieg et al., 2014) They found that Rab5 is essential for an early step in sorting but is absent from axonal signaling endosomes, whereas Rab7 is essential for the transport of fast retrograde vesicles. This conversion of Rab5 to Rab7 on endosomes is a commonly agreed upon mechanism for endosomal maturation and targeting of cargo towards the degradative pathway. While numerous proteins have been identified that regulate Rab7 activity, none of these regulate it by phosphorylation. This is quite surprising as Rab7 has been identified in a number of phosphoproteomic screens as being phosphorylated on 11 different sites, with Y183 and S72 being the most frequently found. However, none of these studies further investigated Rab7 and no studies have been published on any of these phosphorylation sites. In contrast, previous studies have identified phosphorylation sites on a number of other Rabs, including Rab4, which is phosphorylated on S196 during mitosis to promote its accumulation in the cytosol (van der Sluijs et al., 1992).

From a sequence and structural point of view, the S72 site of Rab7 appears to be extremely important for Rab7 function, as so much of the surrounding sequence is very well conserved, even in plants (*Arabidopsis thaliana*) and yeast (*Saccharomyces cerevisiae*). In addition, the severe phenotype of the $Rab7^{S72P}$ mouse indicates that this residue is essential for life. However, the $Rab7^{S72P}$ mutation is not ideal since it is too drastic to provide key information. The $Rab7^{S72P}$ mutation is predicted to stabilize the switch II region, which may prevent interaction with the switch I region for GTP-binding and activation. This could potentially lock the structure in a GDP-bound form. The $Rab7^{S72P}$ mutation may also block interaction with REP1, thereby inhibiting the C-terminal prenylation of Rab7 and preventing it entering the GTPase cycle. The mass spectrometry facility at the London Research Institute attempted to detect prenylation of $Rab7^{Wt}$, but as they were unsuccessful, we did not have any

effective means to test the prenylation status of the Rab7^{S72P} mutant. Furthermore, as this mutation is lethal so early in embryogenesis, there was no logic for investigating this any further.

The mechanisms by which Rab7^{S72P} function is inhibited may also be applied to the phosphomimetic mutation Rab7^{S72E}, as it too displays a similar cytosolic localisation (Figure 3.3). As Rab7^{S72E} is never seen localised to vesicular structures in when overexpressed, the initial hypothesis was that phosphorylation of Rab7 at S72 inhibits Rab7 function, preventing its recruitment to endosomal membranes; however, this was disproved in later experiments, which will be discussed in the following chapters. The hypothesis was strengthened by fact that both Rab7^{Wt} and the phosphodeficient Rab7^{S72A} display numerous puncta throughout the cell, reminiscent of late endosomes/multivesicular bodies and lysosomes, with some clustering in the perinuclear region. In addition, both Rab7^{Wt} and Rab7^{S72A} also display some cytosolic localisation, but to only a fraction of the Rab7^{S72E} and Rab7^{S72P} proteins. This localisation of Rab7^{Wt} and Rab7^{S72A} both on vesicles and in the cytosol indicates that they are freely able to cycle through the active GTP- and inactive GDP-bound forms.

In light of the striking differences between Rab7^{Wt} and Rab7^{S72A} compared to Rab7^{S72E}, it was expected that overexpression of these proteins may affect the progression of cargo along the endocytic pathway or the dynamics of endosomal organelles. However, none of the endocytic markers examined exhibited a change in localisation upon expression of the three Rab7 forms, tagged with either GFP (Figure 3.4–3.7) or HA (not shown). In addition, the overall expression levels of LAMP2 and Vps26 were examined by FACS, as comparison of their overall intensities in GFP-positive cells is complicated because the punctate distribution of Rab7^{Wt} and Rab7^{S72A} makes it difficult to create a mask using GFP that would outline the entire cell and restrict the quantification to only GFP-Rab7-positive cells. The results showed that there

were no differences in expression of LAMP2 or Vps26 between Rab7^{Wt} and any of the mutants.

Believing that the cells may require more than 24 h to adjust to the expression of these plasmids, I created stable cell lines expressing the GFP-Rab7 constructs. Unfortunately, after selecting stable populations from high and low expressing clones with similar levels of GFP-Rab7^{Wt}, GFP-Rab7^{S72A} and GFP-Rab7^{S72E}, I found that the cells began to cleave the GFP within one or two weeks of culture. After this, I used human siRNA to knockdown endogenous Rab7 in HEK283 cells, so that they could then be transfected with the GFP-Rab7 constructs, as they were produced from the canine sequence, and were thus resistant to siRNA. However, following transfection, the morphology of the cells changed dramatically and they began to form clusters in the dishes and detached easily when changing the media. Ideally these experiments would have been performed in Rab7$^{-/-}$ MEFs, but as these were only recently obtained there was no time to perform these experiments.

As the localisation of the phosphomimetic and phosphodeficient proteins indicate that phosphorylation may prevent Rab7 recruitment to endosomal membranes, I performed EGFR degradation assays to determine the effect these mutation might have. Indeed, the Rab7^{S72E} mutation appeared to decrease EGFR degradation, while still allowing for receptor activation and the induction of neosynthesis, which I believe occurred as the levels at 90 min were much higher than the initial levels without stimulation. In contrast, the Rab7^{S72A} mutation increased EGFR degradation at 15 and 30 min. While this does appear to be very quick, the EGFR has been shown to colocalise with Rab7 at 15 min (Gomez-Suaga et al., 2014). This decrease in EGFR degradation for Rab7^{S72E} indicates that phosphorylation at S72 inhibits Rab7 activity. This could be by locking it in a GDP-bound form in the cytoplasm by blocking interaction of the switch I and II regions or it could abolish the interaction with certain effects, such as RILP, which has been shown to be involved in EGFR degradation (Progida et al., 2007).

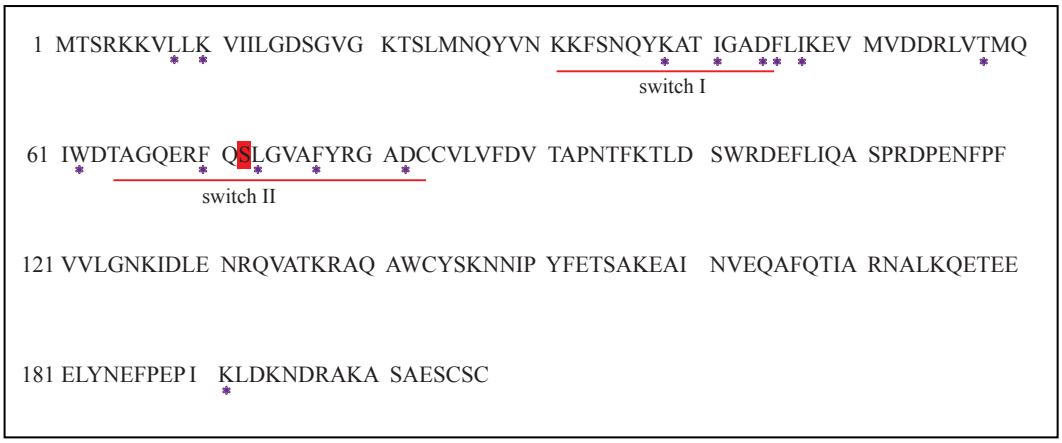

Figure 3.15. Interaction sites of RILP with Rab7.
Sequence of the human Rab7 protein showing the residues interacting with RILP (labelled as *). The S72 of Rab7 is highlighted in red and is located in close proximity to a number of known interaction sites.

Analysis of the crystal structures of the Rab7:RILP and Rab7:REP1 complexes revealed that the S72 site of Rab7 and the surrounding region play important roles in these interactions. However, S72 was never mutated in either of these studies to determine if it has any effect on binding of these interactors. The S72 site was shown to interact with REP1, but as inhibition of this interaction would only affect newly synthesised Rab7, I decided to examine the interaction with RILP first. Although there was no interaction shown in the Rab7:RILP complex at S72, phosphorylation of this residue could still affect binding, as it may inhibit interaction between the switch regions required for Rab7 activation and binding of RILP. Furthermore, other resides in the surrounding region (F70, L73 and L77) form binding sites within the Rab7:RILP complex and phosphorylation could their interaction (Figure 3.15). Indeed the results revealed that the phosphomimetic Rab7^{S72E} inhibited RILP binding by approximately 80% (Figure 3.10). If phosphorylation of Rab7 at S72 inhibits RILP binding, this could also affect microtubule minus end-directed transport of late endosomes/lysosomes and/or acidification. In contrast, the interaction of Rab7 with ORP1L was not affected by the phosphomimetic or phosphodeficient mutation (Figure 3.11).

Unfortunately, as FYCO1 did not immunoprecipitate with any of the Rab7 proteins expressed, there is not enough data to speculate whether phosphorylation is a mechanism of regulating transport in a particular direction.

Finally, the comparison of the FRET ratios between Raichu-Rab7^{Wt}, Raichu-Rab7^{S72A} and Raichu-Rab7^{S72E} indicates that the phosphomimetic mutation decreases the affinity of Rab7 for the GEF, as there was a significant decrease cytosolic ratio for Raichu-Rab7^{S72E} compared with both Raichu-Rab7^{Wt} and Raichu-Rab7^{S72A}. Furthermore, as there was no significant difference in the cytosolic or endosomal FRET ratios for Raichu-Rab7^{Wt} and Raichu-Rab7^{S72A}, this indicates that both have similar interaction profiles with GEF and GAPs, and hence similar activities overall.

Overall, the results obtained with the phosphomimetic and phosphodeficient Rab7 proteins indicate that phosphorylation at S72 decreases Rab7 activity, possibly by inhibiting its interaction with certain effectors, such as RILP.

Chapter 4. Phosphorylation of Rab7 by the non-canonical IKK family members TBK1 and IKKε

4.1 An *in vitro* kinase screen to identify candidates for Rab7 phosphorylation at serine 72

To determine the kinases that phosphorylate Rab7 at S72, we expressed and purified recombinant His-tagged $Rab7^{Wt}$ and $Rab7^{S72P}$ proteins in *E. coli* BL-21, which were subsequently sent to ProQuinase GmbH (Germany) for testing of 190 Ser/Thr kinases in *in vitro* kinase assays. The results of each assay are expressed as the ratio between Rab7 activity (cpm) and kinase autophosphorylation (cpm). As can be seen from the results in Figures 4.1–4.5 and the summarised potential hits in Table 4.1, TBK1 and IKKε were the only two kinases out of the 190 tested that showed a significant decrease in phosphorylation between $Rab7^{Wt}$ and $Rab7^{S72P}$. A number of other kinases, listed in Table 4.1, may also phosphorylate Rab7 but as the differences between $Rab7^{Wt}$ and $Rab7^{S72P}$ are negligible, they most likely phosphorylate at different sites.

Notably, a number of protein kinase C (PKC) family members were potential hits in the screen for phosphorylating Rab7 at sites other than S72. A previous publication has investigated the possible role of PKCδ as an activator of Rab7 (Romero Rosales et al., 2009). In this publication they showed that PKCδ inhibition causes lysosomal fragmentation comparable to when Rab7 is directly inhibited. Furthermore, PKCδ inhibition promotes growth factor-independent cell survival, which is reversed by expression of the constitutively active Rab7 mutant, $Rab7^{Q67L}$. Thus, as PKCδ expression is highly induced upon growth factor withdrawal and the amount of Rab7-GTP simultaneously increases, they was hypothesised that PKCδ could function as a Rab7 activator. We tested PKCα, PKCδ, PKCε and PKCζ in *in vitro* kinases assays in our lab and found that while all appeared to phosphorylate Rab7 to a certain extent, none were specific for the S72 residue. Thus, phosphorylation of Rab7 at alternative

residues to S72 by PKC family members could be alternative mechanisms of regulating Rab7 function.

Table 4.1. Hits from the *in vitro* kinase screen

Name	WT	S72P	WT-S72P	Protein Family
IKK-ε	2.03	0.85	1.18	Ser/Thr protein kinase
TBK1	2.56	0.67	1.89	Ser/Thr protein kinase
IRAK4	1.32	4.73	-3.4	TKL Ser/Thr protein kinase
ACV-R1	1.5	4.11	-2.61	TKL Ser/Thr protein kinase
MST1/STK4	4.73	5.69	-0.96	STE Ser/Thr protein kinase
MST2/STK3	9.13	11.04	-1.9	STE Ser/Thr protein kinase
DYRK3	1.11	2.05	-0.94	CMGC Ser/Thr protein kinase
MARK3/PAR-1a	1.69	2.08	-0.39	CAMK Ser/Thr protein kinase
NEK1	3.61	4.2	-0.59	NEK Ser/Thr protein kinase
PKCα	2.26	2.8	-0.53	AGC Ser/Thr protein kinase
PKCβ1	3.39	3.37	0.02	AGC Ser/Thr protein kinase
PKCβ2	4.56	4.6	-0.05	AGC Ser/Thr protein kinase
PKCδ	3.29	3.9	-0.61	AGC Ser/Thr protein kinase
PKCζ	1.97	2.65	-0.67	AGC Ser/Thr protein kinase
ROCK2	1.5	3.28	-1.78	AGC Ser/Thr protein kinase
CAMK2D	1.95	2.86	-0.91	CAMK Ser/Thr protein kinase
PHKG1	1.56	2.6	-1.04	CAMK Ser/Thr protein kinase
PIM3	2.39	3.05	-0.66	CAMK Ser/Thr protein kinase
TSSK1	1.67	2.19	-0.52	CAMK Ser/Thr protein kinase

Values are presented as activity/kinase autophosphorylation (cut off > 2).

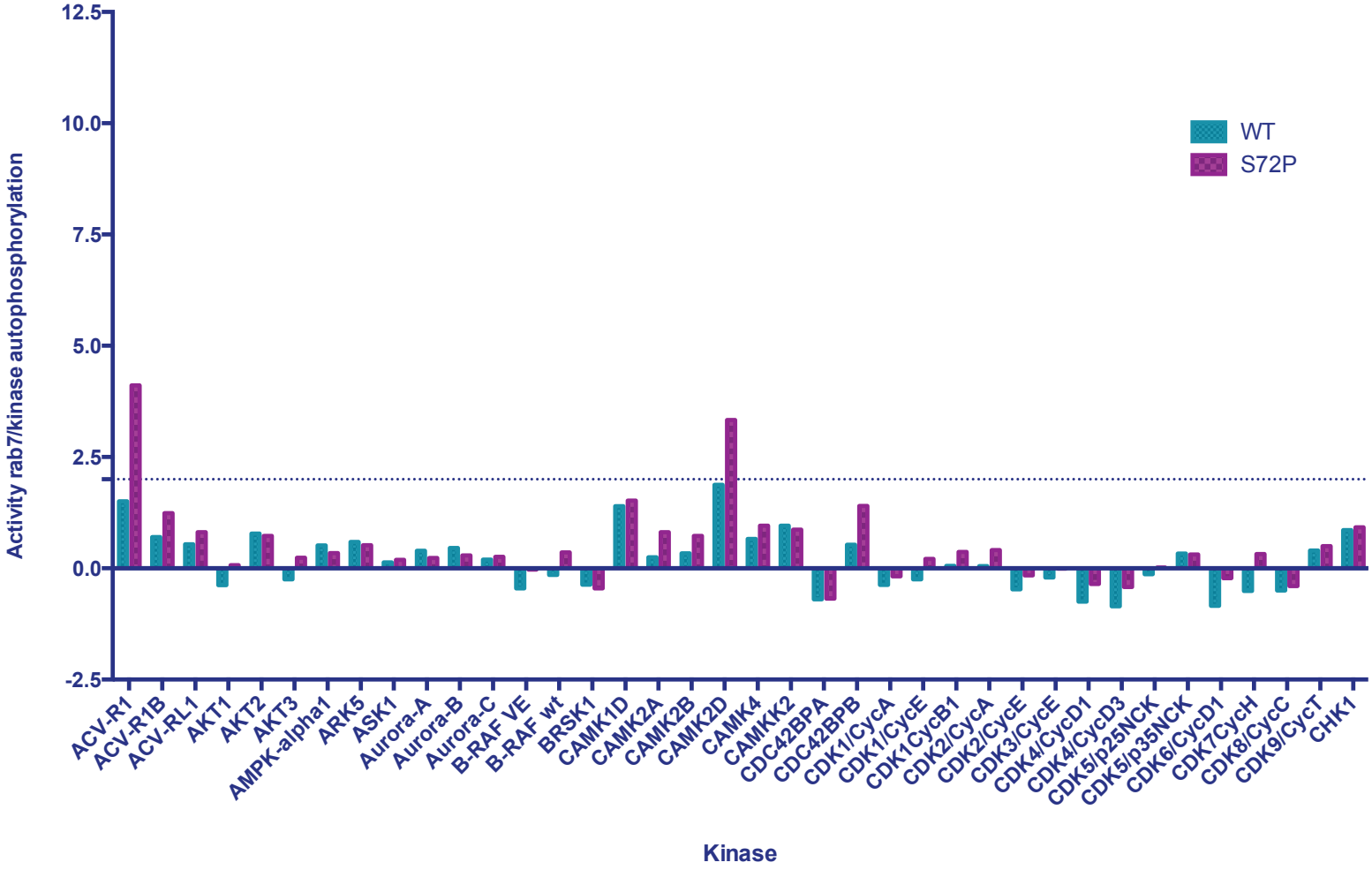

Figure 4.1. ProQuinase screen results 1.

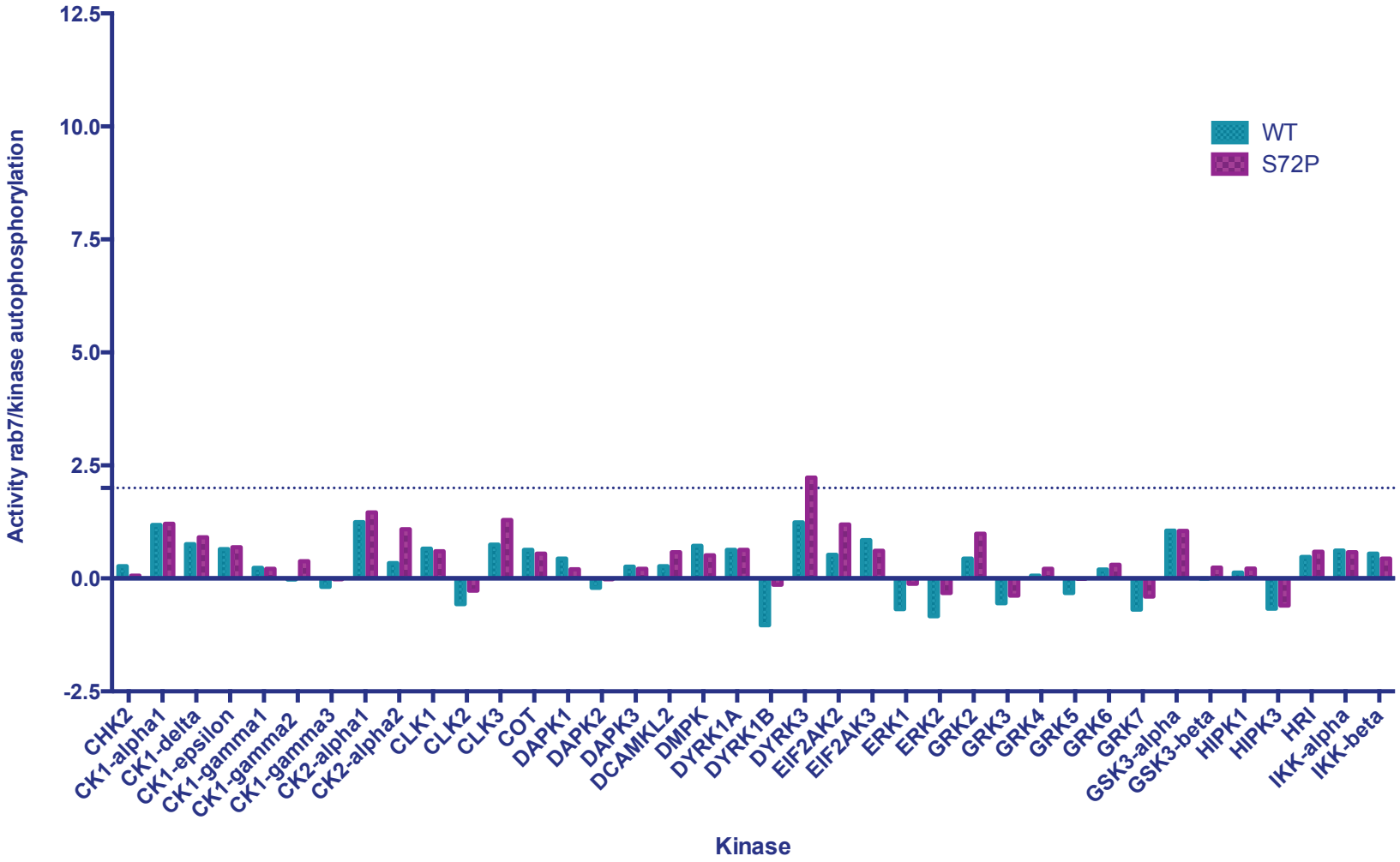

Figure 4.2. ProQuinase screen results 2.

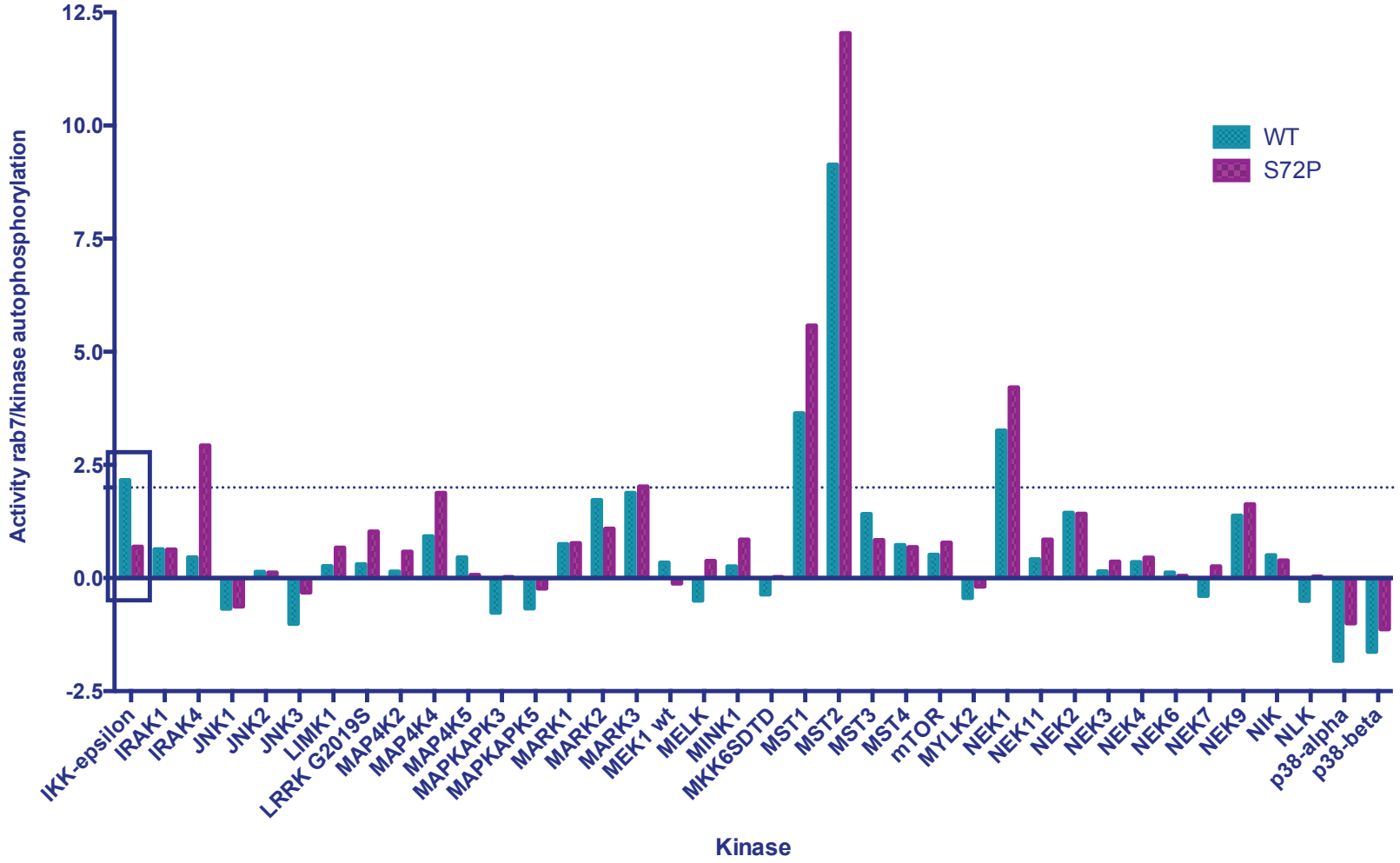

Figure 4.3. ProQuinase screen results 3.

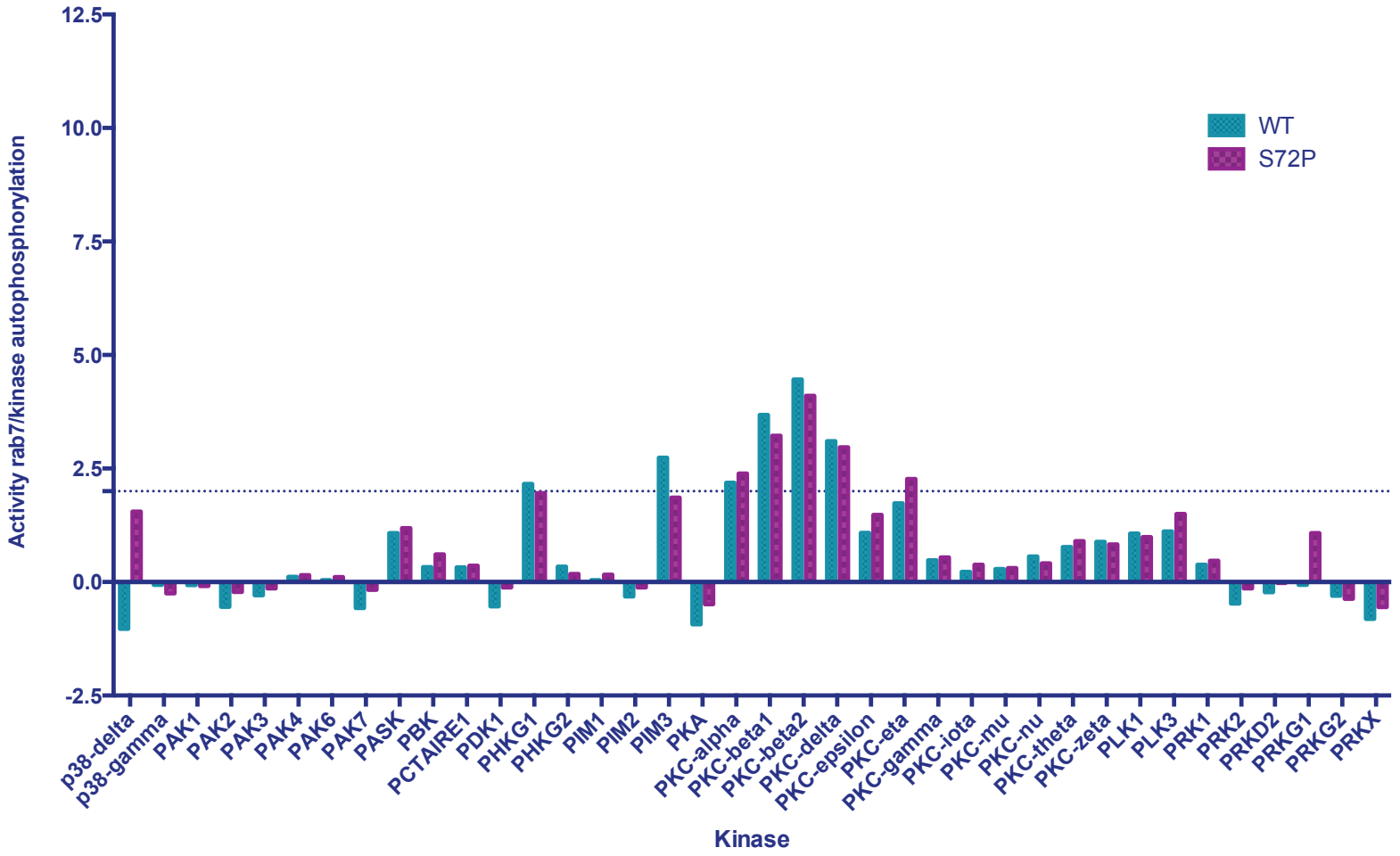

Figure 4.4. ProQuinase screen results 4.

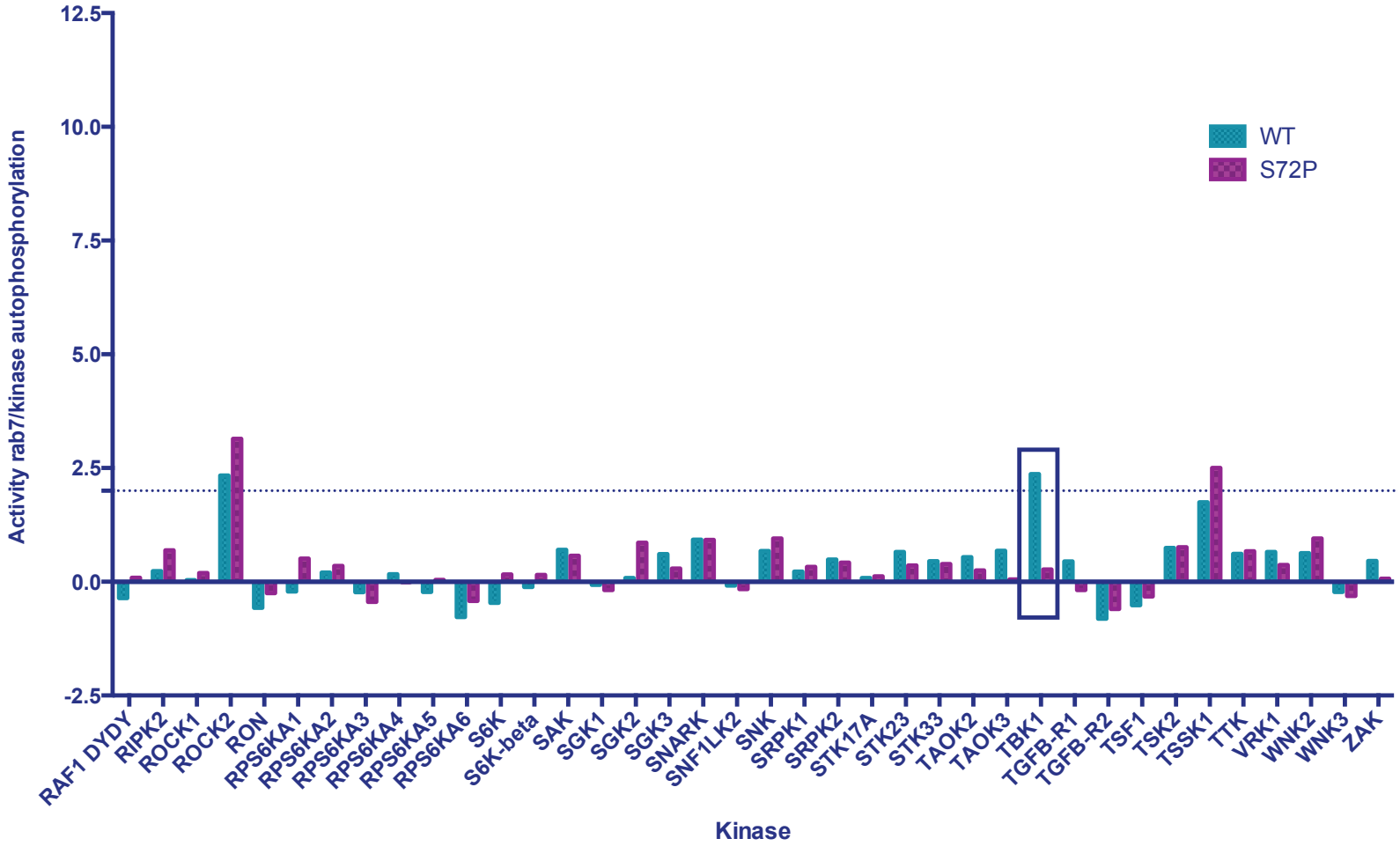

Figure 4.5. ProQuinase screen results 5.

4.1.1 The inhibitor of NF-κB kinase family

TBK1 and IKKε are members of the IκB [inhibitor of NF-κB (nuclear factor κB)] kinase family, which are key regulators of the NF-κB and interferon (IFN) regulatory factor (IRF) families of transcription factors. The IKK family is composed of four members, which are grouped into two subgroups based on sequence homology and substrate specificity (Figure 4.6). IKKα and IKKβ are known as the canonical IKKs, whereas TBK1 and IKKε are the non-canonical IKKs. Within the IKK family, IKKα and IKKβ share 52% identity with one another, while TBK1 and IKKε share 61%. In contrast, sequence identity between the noncanonical and canonical kinases is only 24-27%. Furthermore, within the catalytic kinase domain, the noncanonical and canonical kinases share only 33% identity between groups. This difference in homology in the kinases domain most likely accounts for the different specificities of the two groups: while all four members are involved in regulation of the NF-κB pathway, only TBK1 and IKKε are also involved in IRF-3 and IRF-7 signalling.

The NF-κB pathway is involved in a number of different processes, including immunity, survival, development and activity of a number of different tissues, including the nervous system (Mincheva-Tasheva and Soler, 2013). Pathological dysregulation of NF-κB, and the IKKs, has been linked to inflammatory and autoimmune diseases, obesity and cancer (Weissmann et al., 2014) (Mincheva-Tasheva and Soler, 2013). NF-κB is a transcriptional factor that regulates the expression of pro-inflammatory cytokines, such as TNF-α, IL-1 and IL-12, inducible nitric oxide synthase (iNOS), cyclooxygenase 2 (COX-2), growth factors, inhibitors of apoptosis and effector enzymes, following stimulation of receptors that include members of the Toll-like receptor/interleukin-1 receptor (TLR/IL-1R) superfamily. In mammals, the NF-κB family is composed of five members: p50, p52, RelA (p65), RelB and c-Rel (Moynagh 2005; Hoffmann et al., 2006). These factors are all related and can form homodimers or heterodimers through binding of their N-terminal Rel

homology domain (RHD). In unstimulated cells, NF-κB transcriptional activity is silenced by interaction with inhibitory IκB proteins present in the cytoplasm. Activation of the NF-κB pathway results in phosphorylation of IκB, leading to its dissociation from NF-κB, which subsequently translocates to the nucleus and induces the transcription of its target genes.

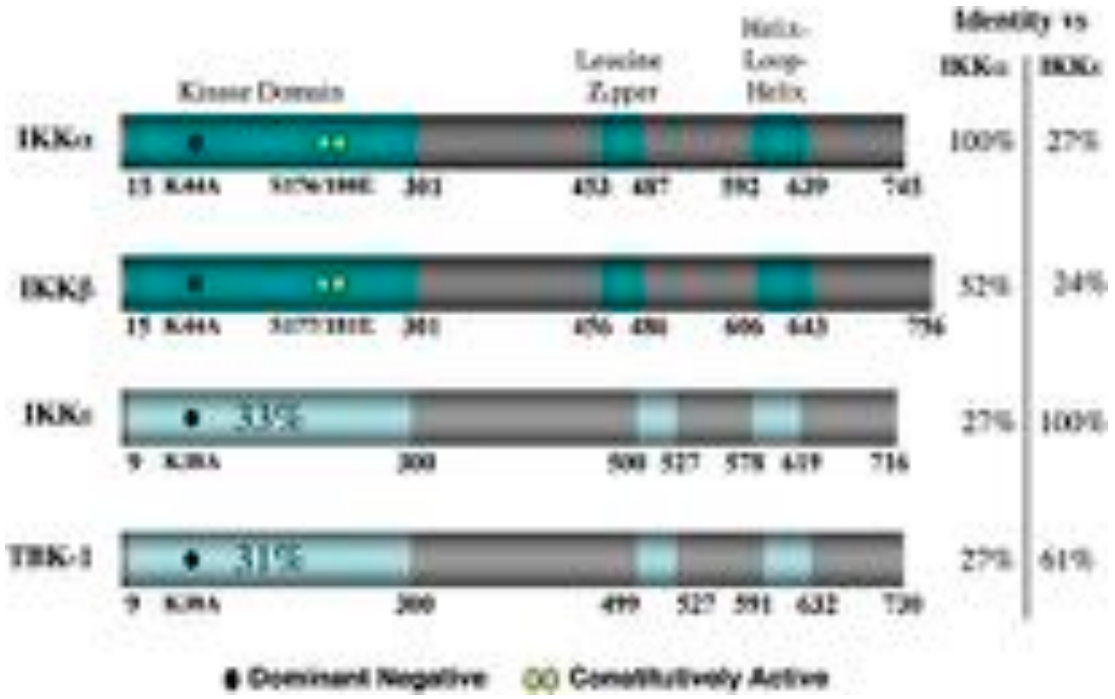

Figure 4.6. Comparison of the IKK family members.
Schematic structure of the IKK family members. The kinase domain is located at the N-terminus, where K44A (IKKα and IKKβ) or K38A (IKKα and TBK-1) mutations within the ATP-binding pocket generates dominant-negative kinases; whereas S176/180E (IKKα) or S177/181E (IKKβ) phosphomimetic mutations within the kinase activation loop generates constitutively active kinases. There are no constitutively active IKKα or TBK-1 mutations. Adapted from Hiscott *et al.*, 2006.

Activation of the NF-kB pathway by the IKKs occurs by a number of different routes. The canonical pathway involves stimulation of tumour necrosis factor receptors (TNFRs), IL-1R and TLRs. The TNFR superfamily is composed of 19 members that play key roles in both the adaptive and innate immune responses,

through binding of TNFR associated factors (TRAFs) to activate both the NF-κB and mitogen-activated protein kinase (MAPK) pathways. Dysregulation of the TNFR pathway has been linked to a number of diseases, including autoimmune disorders and Alzheimer's disease (Jacob et al., 1991) (Culpan et al., 2009). Furthermore, the ability of the TNFR ligands TNF, FasL, and TRAIL to induce apoptotic cell death has been widely exploited in various cancer immunotherapies (Bremer, 2013).

TLRs recognise pathogen-associated molecular patterns (PAMPs), which are present on the surface of invading pathogens, or danger-associated molecular patterns (DAMPs), which are endogenous molecules released from necrotic or dying cells. There are 13 TLRs (TLR1-13) shown in Figure 4.7, all of which recognise specific PAMPs (e.g. TLR7 recognises viral ssRNA in the endosome, whereas TLR5 recognises the bacterial protein flagellin on the plasma membrane) (Tsan, 2006). Of the 13 TLRs, 10 have been characterised in humans (TLR1–10) and 12 in mice (TLR1–9, TLR11–13). While IKKα and IKKβ are activated by stimulation of all TLRs, TBK1 and IKKε are activated only by stimulation of TLR3 and TLR4 with extracellular viral double-stranded RNA (dsRNA) and bacterial LPS, a lipoglycan found in the cell walls of Gram-negative bacteria, respectively. However, TBK1 and IKKε are also activated downstream of melanoma differentiation-associated gene 5 (MDA5) and retinoic acid-inducible gene-I (RIG-I), which are cytoplasmic sensors for viral dsRNA and ssRNA, respectively (Chau et al., 2008).

Both TLRs and IL-1Rs have a conserved region known as the Toll/IL-1R (TIR) domain, which signals through a pathway involving myeloid differentiation primary response gene 88 (MyD88), IL-1R-associated kinase (IRAK)1, IRAK4, transforming growth factor beta-activated kinase 1 (TAK1), TAK1-binding protein (TAB)1, TAB2, and TNFR-associated factor 6 (TRAF6) (Lin et al., 2010). This results in the formation of the IKK complex, consisting of IKKα, IKKβ and

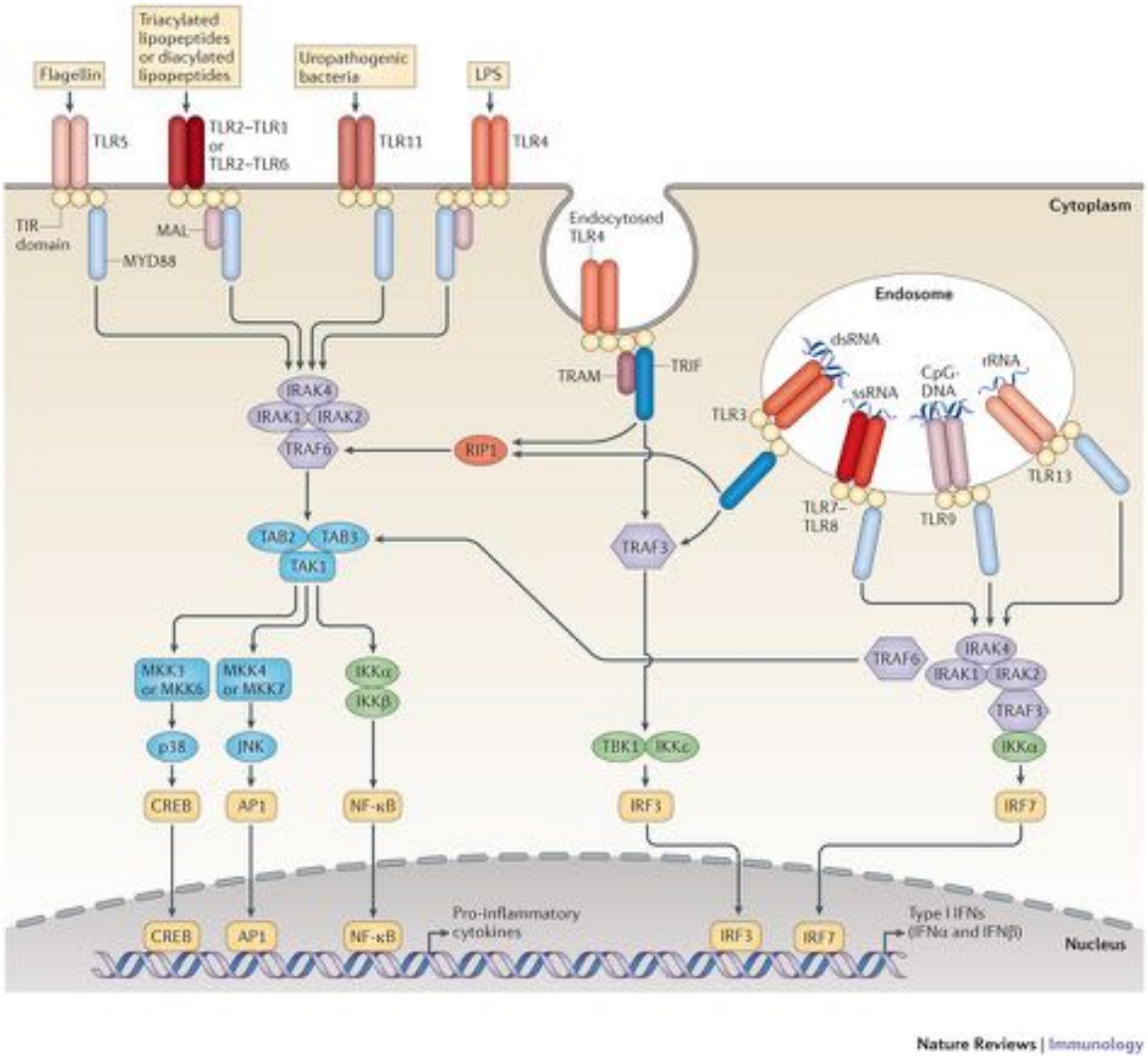

Figure 4.7. Toll-like receptor signalling pathways.

Innate immune pathways are activated by stimulation of Toll-like receptors (TLRs) either on the plasma membrane or in endosomal compartments. These pathways lead to the induction of NF-κB- and/or IRF-dependent transcription of type I interferons and/or proinflammatory cytokines. Figure generated from O'Neill *et al*., 2013.

the scaffolding protein NF-κB essential modulator (NEMO). The IKK complex directly phosphorylates IκBα and targets it for degradation by the proteasome. Activation of TLRs by this route is known as the My88-dependent pathway. TLR3 is the only TLR that cannot activate the MyD88-dependent pathway. Furthermore, this pathway also activates the p38 mitogen-activated protein kinase (MAPK) and c-Jun N-terminal kinase (JNK) cascade (Janssens and Beyaert, 2002).

Unlike other TLRs, TLR4 is the only member that can signal from both the plasma membrane and the endosome (Figure 4.7). Binding of the bridging factor MyD88 adaptor-like protein (Mal), also known as TIR-associated protein (TIRAP), to TLR4 on the plasma membrane allows signalling via the MyD88-dependent pathway that leads to activation of the IKK complex. However, following internalisation, TLR4 recruits another bridging factor, TRIF-related adaptor molecule (TRAM), to activate a MyD88-independent pathway that leads to activation of TRAF3 and the subsequent activation of TBK1 and IKKε (Fitzgerald et al., 2003).

TLR3 also signals via the MyD88-independent pathway. It is initially synthesized as a signalling-deficient full-length (~100 kDa) protein in the endoplasmic reticulum. Following stimulation of cells with viral dsRNA, it is rapidly transported to endolysosomes, where it is cleaved into the active form (~70 kDa) by cathespins B and H. Once cleaved and activated, TLR3 forms a homodimer that directly binds TIR domain-containing adapter inducing IFN-β (TRIF) to activate both TRAF3- and TRAF6-dependent pathways (Garcia-Cattaneo et al., 2012) (Yamamoto et al., 2002). Both TLR3- and TLR4-mediated activation of TBK1 and IKKε, and their subsequent phosphorylation and activation of the transcriptional factor IRF3, occurs via TRAF3 (Figure 4.7).

A previously published large-scale analysis of protein-protein interactions in human cells used >400 bait proteins to pull down specific interactors for each

bait protein (Ewing et al., 2007). When they used IKKε and TRAF6 as bait proteins, Rab7 was identified as an interactor for both. In their analysis the authors used a cut-off of 0.3, where anything above was of high confidence and anything below was a low confidence hit; a value of 0 indicated that the prey protein was present at the lowest acceptable score. When they used IKKε as the bait protein, the confidence score for the interaction with Rab7 was 0.271, whereas when they used TRAF6 the score was 0 (Ewing et al., 2007). Thus, neither interaction of IKKε or TRAF6 with Rab7 was investigated any further. Although both interactions were below the cut-off, the interaction between IKKε and Rab7 was close enough that it could be a realistic interaction, especially following the results of our screen.

4.2 Rab7 is phosphorylated *in vitro* by the noncanonical IKK family members, TBK1 and IKKε

The results of the ProQuinase kinase screen were subsequently validated in our laboratory by Giampietro Schiavo using [γ-32P]ATP *in vitro* kinase assays for TBK1 and IKKε. The other two members of the IKK family, IKKα and IKKβ, were also tested for phosphorylation at S72 to ensure the results of the screen were accurate and confirm specificity. Results revealed that $Rab7^{Wt}$ was phosphorylated by both TBK1 and IKKε, whereas neither phosphorylated $Rab7^{S72P}$ (Figure 4.8). Furthermore, neither IKKα nor IKKβ had any effect on the phosphorylation status of $Rab7^{Wt}$ or $Rab7^{S72P}$.

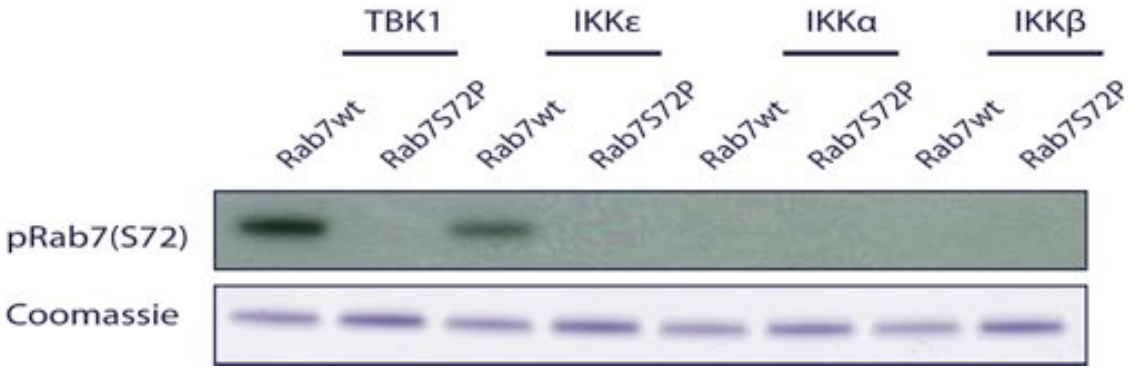

Figure 4.8. *In vitro* kinase assay for the phosphorylation of Rab7 at S72 by the IKK family members, IKK-α, IKK-β, TBK1 and IKK-ε.
Recombinant $Rab7^{Wt}$ and $Rab7^{S72P}$ (control), 2 µg each, were incubated fro 1 h at room temperature in the presence of ^{32}P, and analysed by SDS-PAGE and autoradiography. TBK1 and IKK-ε phosphorylated Rab7 specifically at S72, whereas IKKα and IKKβ did not phosphorylate anywhere. The lower panel is the Coomassie staining of the gel to show that equal amounts of protein were loaded in each lane.

4.3 Antibody testing

Following confirmation that TBK1 and IKKε phosphorylate Rab7 at S72, I decided to test the specificity of two anti-pRab7(S72) antibodies that were produced by inoculating two rabbits with a short peptide containing the phosphorylated Ser72 within the wild-type human sequence (CERFQpSLGVA-$CONH_2$). Following inoculation, phosphatases present in the blood and tissue dephosphorylate some of the peptide, yielding sera containing antibodies against both the nonphosphorylated (Rab7-OH) and S72-phosphorylated Rab7 (pRab7(S72)) peptides. The levels of each antibody can vary, so their specificity was firstly tested by ELISA against the phosphopeptide used for immunization and the corresponding nonphosphorylated CERFQSLGVA-$CONH_2$ peptide. The final bleed from each rabbit was examined, using the corresponding prebleeds as controls. The results of the ELISA can be seen in Figure 4.9, which shows that the antiserum from the rabbit designated 192 is more specific than rabbit 191.

Following the ELISA, I tested whether this serum was specific for recombinant full-length Rab7 phosphorylated at S72. Recombinant His-tagged $Rab7^{WT}$ was phosphorylated *in vitro* with TBK1 and analysed by SDS-PAGE and western blot. The anti-pRab7(S72) antibody was incubated with 1 mg/ml of the unphosphorylated peptide for 2 h at 4°C prior to use to saturate the nonphospho-antibody. The antibody was used at a 1:500 dilution and incubated overnight at 4°C. As can be seen in Figure 4.9, the antibody recognized only the phosphorylated protein. The blot was reprobed with a mouse anti-Rab7 antibody to confirm that equal amounts of phosphorylated and non-phosphorylated protein were loaded (Figure 4.9), thus confirming that the antibody is specific for pRab7(S72).

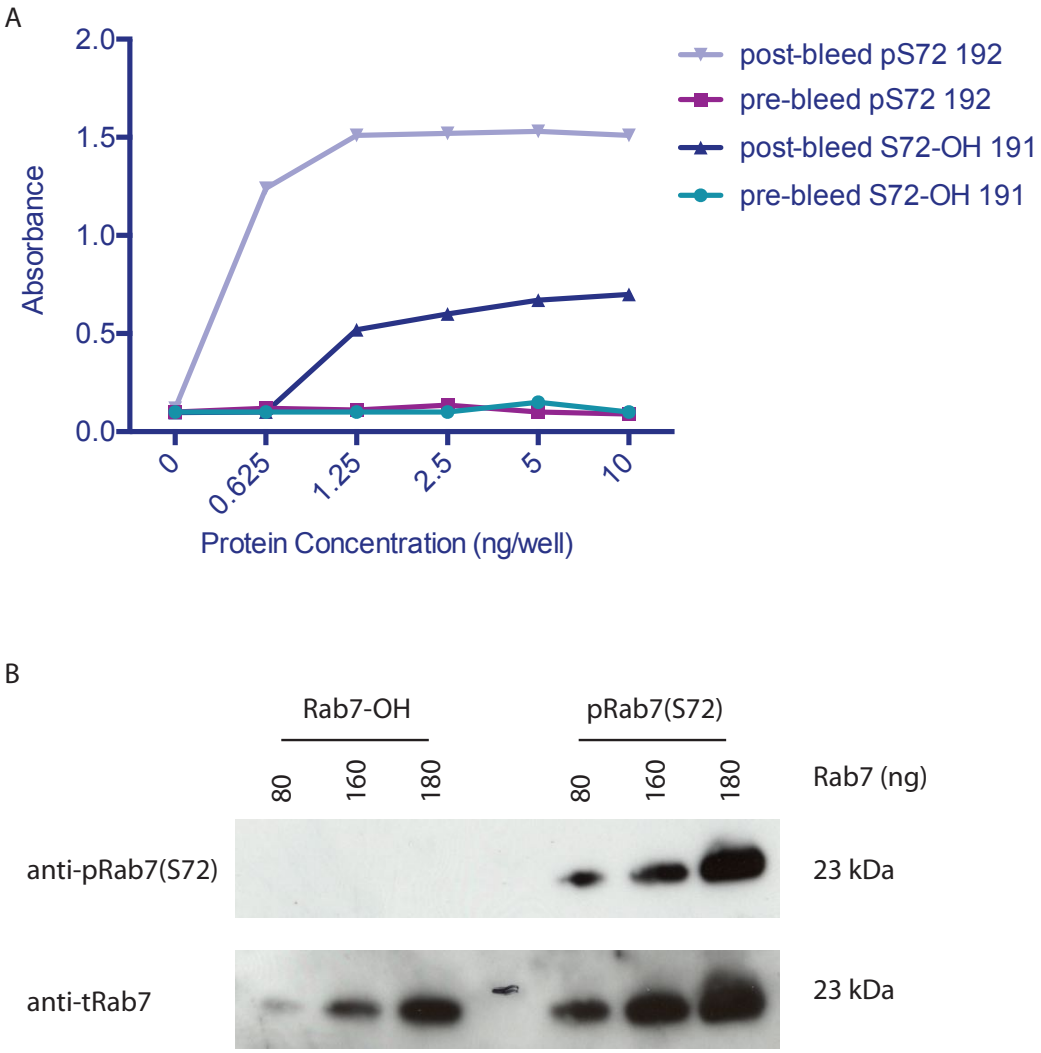

Figure 4.9. Testing specificity of the anti-pRab7(S72) antibody.

A. Antibody specificity of the anti-phospho-Rab7 (S72) antibody was examined by ELISA using the phosphorylated and non-phosphorylated versions of the peptide used for immunisation the rabbit. **B.** After saturating the non-phosphoantibody with 1 mg/ml unphosphorylated peptide, the antibody was tested on recombinant Rab7 that had been *in vitro* phosphorylated with TBK1. Non-phosphorylated recombinant Rab7 was used as a control. As can be seen from the blots the antibody was highly specific for the phosphorylated Rab7.

4.4 BX795 and MRT67306 inhibit TBK1- and IKKε-mediated phosphorylation of Rab7 at serine 72 *in vitro*

BX795 and MRT67307 are two published chemical inhibitors of TBK1 and IKKε (Clark et al., 2011; Clark et al., 2009). BX795 was originally discovered as a potent inhibitor of TBK1- and IKKε-mediated phosphorylation and activation of IRF3 and the subsequent production of IFNβ, without inhibiting NF-κB activation by IKKα and IKKβ. Although it blocked the autophosphorylation of both kinases, it did not inhibit phosphorylation at their active site (S172) following stimulation of mouse RAW264.7 macrophages with poly(I:C), LPS, TNFα or IL-1α, but actually enhanced phosphorylation of this residue (Clark et al., 2009). Furthermore, it also had off target effects as it suppressed the activation of JNK and p38α MAPK by LPS or poly(I:C). Thus, BX795 was modified to create the improved inhibitor MRT67307, which no longer suppressed the activation of JNK or p38α MAPK by inflammatory stimuli, such as poly(I:C) and IL-1 (Clark et al., 2011).

Both inhibitors were tested to determine if they could suppress TBK1 and IKKε phosphorylation of Rab7 at S72 *in vitro*. BX795 and MRT67307 are both recommended for use at a concentration of 2 μM in cellular assays. Thus, to ensure sufficient activity *in vitro*, they were both examined at 0.2, 2 and 20 μM. Following incubation at 30°C for 30 min, samples were subjected to SDS-PAGE and western blot with the anti-pRab7(S72) antibody.

The results revealed that BX795 was more effective at inhibiting TBK1 phosphorylation of Rab7, but the differences at 2 μM were not significant, with both inhibiting phosphorylation by >95% (Figure 4.10).

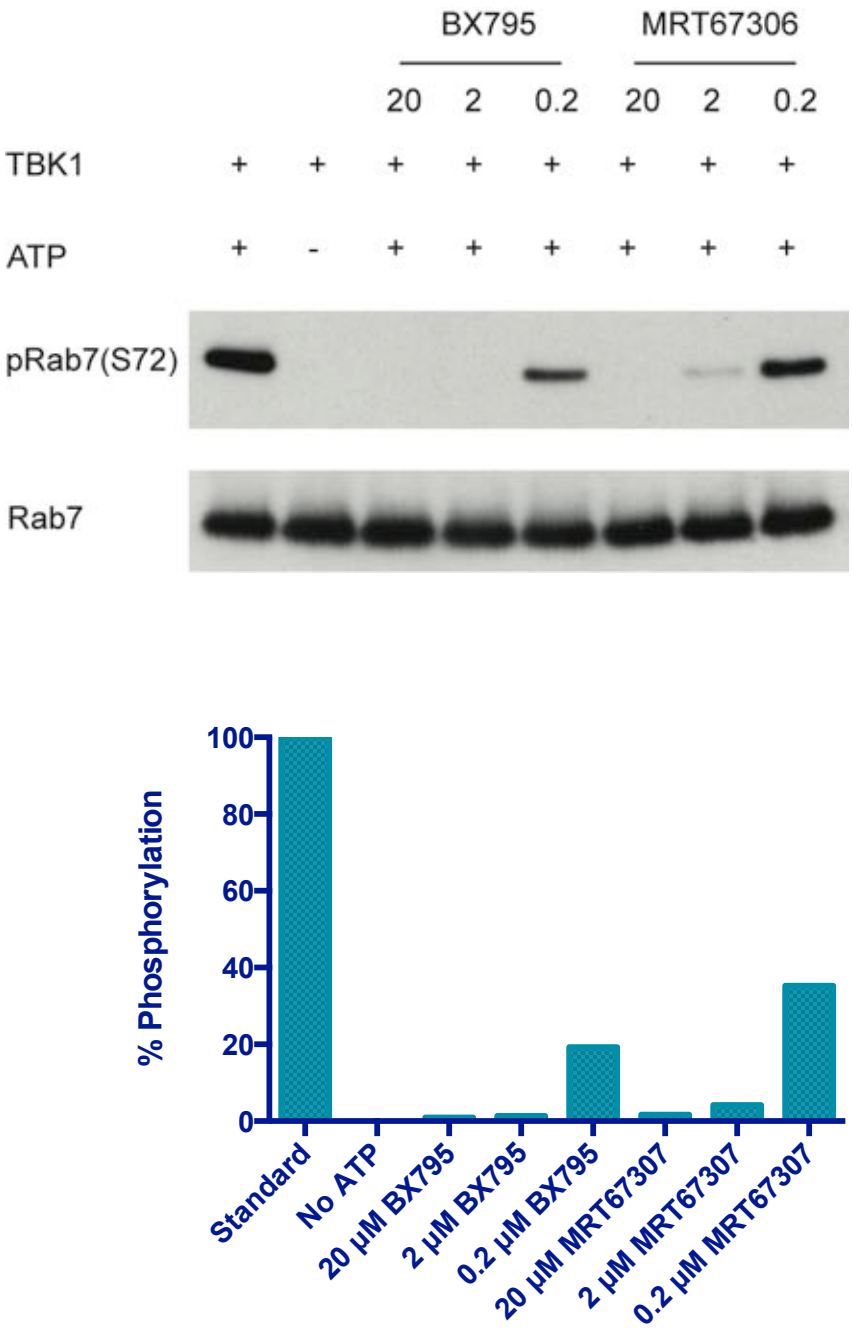

Figure 4.10. Inhibition of TBK1-mediated phosphorylation of Rab7 at S72 with BX795 and MRT67306.

Rab7 phosphorylation at S72 by TBK1 was performed under increasing concentrations of the two inhibitors of TBK1 and IKKε, BX795 and MRT67307. Both inhibitors were highly effective at concentrations of 2 μM and 20 μM, with BX795 exhibiting slightly stronger inhibition at 2 and 0.2 μM.

4.5 Rab7 is phosphorylated at serine 72 following stimulation of the viral dsRNA-activated toll-like receptor, TLR3

Following the results of these *in vitro* experiments, I wanted to examine whether phosphorylation of Rab7 at S72 could be stimulated in a cellular model. It has been previously shown that TLR3 signalling requires endosomal acidification, as pre-treatment with chloroquine or bafilomycin A1 inhibits TLR3-induced cytokine secretion and IFN-β promoter activation (Funami et al., 2004; Itoh et al., 2008). Thus, as TLR3 signalling is dependent on the endolysosomal system and possibly Rab7 activity, I decided to firstly determine if phosphorylation at S72 occurs following stimulation of TLR3 with poly(I:C), a synthetic analog of dsRNA. The experiment was performed in MEFs, as they have been previously shown to express TLRs 1-9 and transfect much better than immune lineage cells (Kurt-Jones et al., 2004).

As there was no reliable Rab7 antibody for immunoprecipitation available, with GFP-Rab7^{WT} was transfected in MEFs overnight, following which cells were stimulated with 10 μg/ml poly(I:C) for 30, 60 and 90 min. Unstimulated and serum-starved controls were included to compare basal levels of phosphorylation between the samples. One sample was also preincubated with BX795, an inhibitor of TBK1 and IKKε, for 2 h at 37°C to determine if it the basal levels of phosphorylation could be affected. Following stimulation with poly(I:C), GFP-Rab7^{WT} was immunoprecipitated from cell lysates using GFP-trap beads and analysed by SDS-PAGE and western blot using the rabbit anti-pRab7(S72) antibody. Blots were probed with a mouse anti-Rab7 antibody (Abcam) for quantification of phosphorylation relative to the levels of transfection.

Results were analysed using one-way ANOVA, followed by Dunnett's multiple comparisons test to compare each sample with the untreated control. There was a steady increase in phosphorylation at S72 over the 180 min period, with a 3.6-fold increase compared to basal levels at the final time point. All poly(I;C)-stimulated samples showed significant increases in phosphorylation compared

with the control sample, with the strength of significance increasing with time. There was very little difference in the starved condition, while there was a slight increase in phosphorylation in the cells treated with BX795.

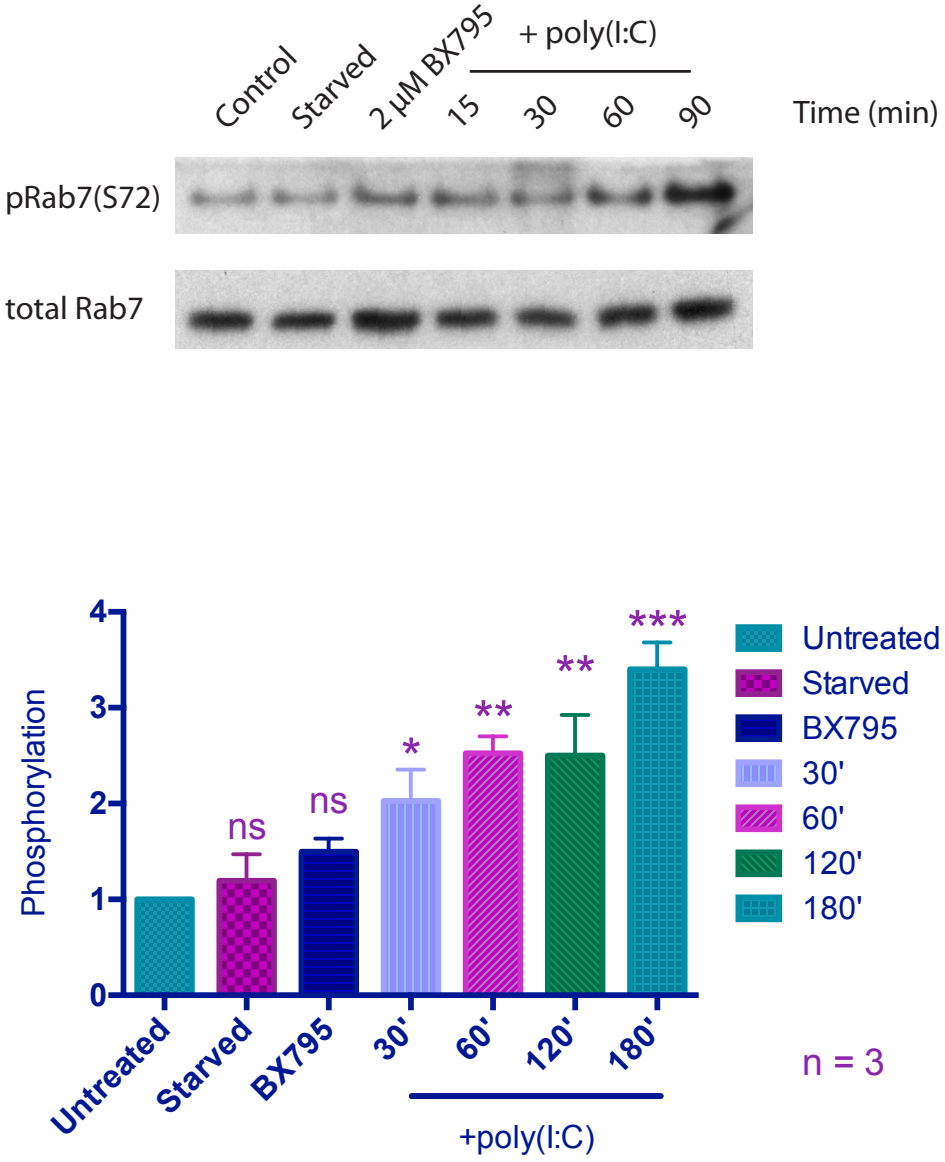

Figure 4.11. poly(I:C)-induced phosphorylation of GFP-Rab7 at S72 in MEFs. MEFs overexpressing GFP-Rab7 were stimulated with 10 μg/ml poly(I:C) for 30, 60, 120 and 180 min to determine phosphorylation of Rab7 at S72. The BX795 inhibitor of TBK1 and IKKε was included as a control but it increased the levels of phosphorylation rather than decrease them. A starved control was also

included as cells were starved for 2 h prior to stimulation. Poly(I:C) stimulation caused a steady increase in phosphorylation at S72 up to 180 min.

BX795 is a pharmacological inhibitor of TBK1 and IKKε that has been shown to blocks the phosphorylation, nuclear translocation, and transcriptional activity of IRF3 and, consequently, the production of IFN-β in macrophages stimulated with poly(I:C) or LPS (Clark et al., 2009). Activation of TBK1 and IKKε requires phosphorylation of S172 in their active site. BX795 does not block phosphorylation of this residue, but actually enhances it in response to LPS, poly(I:C), IL-1α, or TNFα. Furthermore, BX795 inhibited the activation of JNK and p38α MAPK by inflammatory stimuli, thus limiting its use as a probe for IKKє and TBK1. Thus, BX795 was modified to produce MRT67307, which inhibited IRF3 phosphorylation and IFNβ production in macrophages, but no longer suppressed the activation of JNK or p38 MAPK (Clark et al., 2011). Similar to BX795, MRT67307 treatment of macrophages enhanced poly(I:C)- and LPS-stimulated phosphorylation of TBK1 at Ser172, and enhanced the catalytic activity of IKKє and TBK1 in *in vitro* enzymatic assays, following their immunoprecipitation from extracts of poly(I:C)-stimulated cells.

After obtaining the improved TBK1 and IKKε inhibitor, MRT67307, I tested whether it could inhibit Rab7 phosphorylation at S72 following stimulation of MEFs with 10 μg/ml poly(I:C). Surprisingly, there was increased phosphorylation of Rab7 at S72 in cells treated with the inhibitor compared to the control. As there was also an increased basal level of phosphorylation at S72 when cells were incubated with the first generation inhibitor, BX795, the inhibitors were abandoned for future experiments. While these inhibitors inhibit IRF3 phosphorylation, they may not affect the activity of TBK1 and IKKε for other substrates.

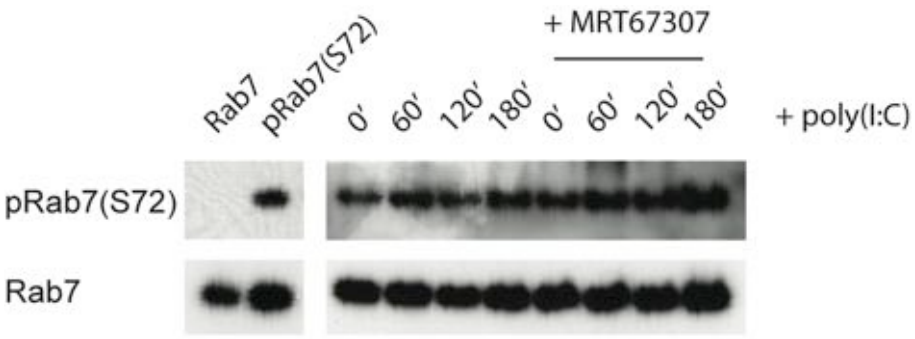

Figure 4.12. Testing MRT67307 inhibition of poly(I:C)-induced phosphorylation of Rab7 at S72.

MEFs overexpressing GFP-Rab7 were treated with 2 μM MRT67307 to inhibit TBK1 and IKKε activity or vehicle control for 2 h prior to stimulation with 10 μg/ml poly(I:C) for 60, 120 and 180 min. Results revealed that there was increased phosphorylation in cells treated with the inhibitor compared to those without.

4.6 Rab7 is phosphorylated at serine 72 following stimulation of the bacterial LPS-activated toll-like receptor, TLR4

As mentioned previously, TLR4 is a membrane-bound receptor that recognises bacterial LPS on the surface of immune and epithelial cells. It is the only TLR that requires a co-receptor, the small lipid-binding glycoprotein myeloid differentiation factor 2 (MD-2), to bind its ligand. After activation of TLR4 at the plasma membrane, signalling via the MyD88-dependent pathway occurs within minutes of binding the Mal-MyD88 adaptor pair; however, approximately 30 min later, TLR4 is internalised, where it interacts with the TRAM-TRIF complex to signal via the MyD88-independent pathway in endosomes and lysosomes (Kagan et al., 2008). Signalling through the MyD88-dependent pathway results in activation of IKKα and IKKβ, whereas signalling via the MyD88-independent pathway results in activation of TBK1 and IKKε.

To ensure activation of the noncanonical IKKs, 0, 1, 2 and 4 h time points were used for stimulation with 1 μg/ml LPS from *E. coli* 0111:B4. As can be seen from the results in Figure 4.13, LPS caused a 1.7-fold increase in Rab7 phosphorylation at S72 after 1 h stimulation, which increased to 2.4-fold at 2 and 4 h.

Unfortunately, at the time I was unable to repeat this experiment and when I thawed the next set of MEFs, they were SV40-immortalised, which the original cells were not, and did not respond to stimulation with LPS. The original cells were spontaneously immortalised in culture and had been given to me by a previous member of the group. Unfortunately, there were no vials of these left in the stocks when I went to repeat these experiments.

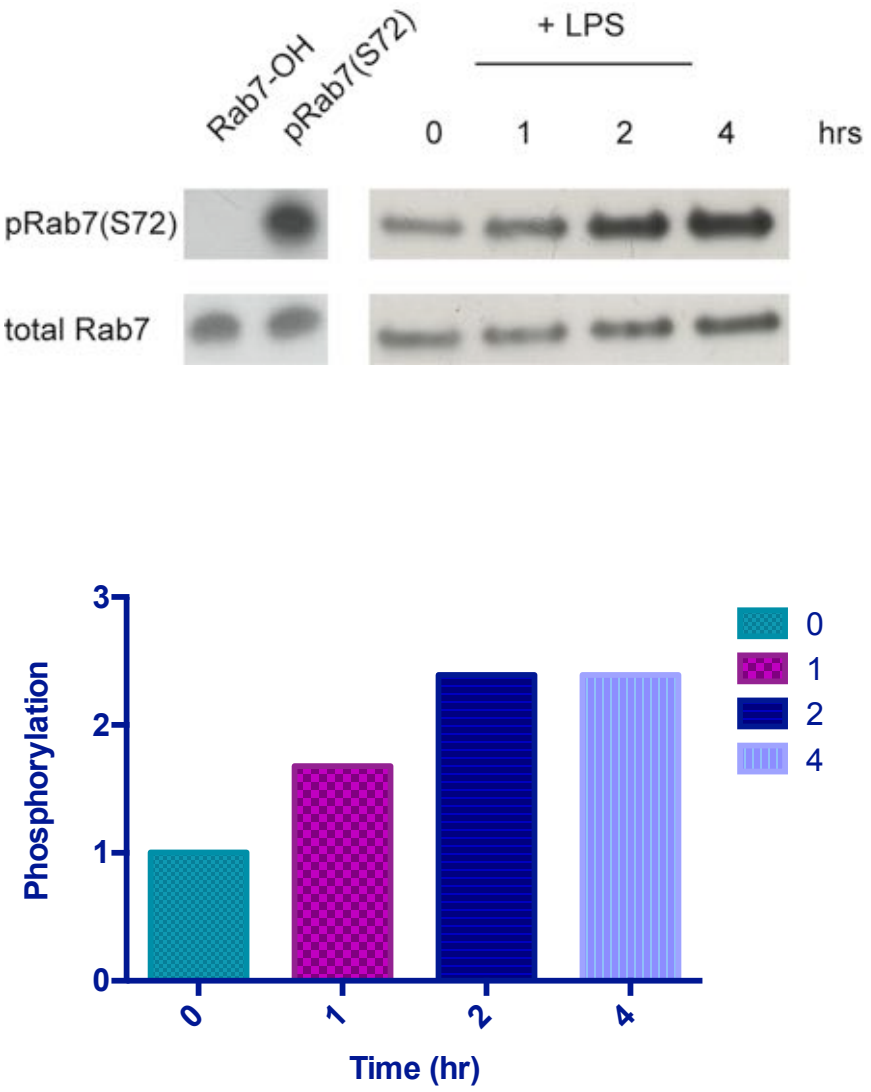

Figure 4.13. LPS stimulation of TLR4 in MEFs.

MEFs overexpressing GFP-Rab7 were stimulated with 1 µg/ml LPS from *E. coli* 0111:B4 for 1, 2 and 4 h to determine phosphorylation of Rab7 at S72. Levels were compared to the basal levels in unstimulated cells (0 h). LPS stimulation caused 2.4-fold increase in phosphorylation at S72 at 2 h, and remained constant at 4 h.

4.7 Discussion

Rab7 has been previously identified in phosphoproteomic screens as being phosphorylated on 11 different sites, with S72 and Y183 showing up in the highest number of screens, indicating that these are physiologically important and regulated by widespread-activated kinases. Phosphorylation of Rab7 at S72 was identified in various screens in human cells, including TBK1 signalling in lung cancer cells (Kim et al., 2013), the DNA damage response (Bennetzen et al., 2010), the mitotic phosphoproteome (Olsen et al., 2010), and T cell receptor signalling (Mayya et al., 2009), while in mouse cells it was identified in screens including TLR4-stimulated macrophages (Weintz et al., 2010), IFN-γ-activated macrophages (Trost et al., 2009), and mTORC1-mediated inhibition of growth factor signalling (Hsu et al., 2011). S72 phosphorylation has also been identified in screens investigating the phosphoproteome of various tissues under basal conditions, including the brain, lung, liver, pancreas, spleen and testis (Huttlin et al., 2010). However, all of the publications identifying S72 as a possible site for phosphorylation on Rab7 excluded it from their main hits as it was below the study threshold values or undetected in repeat experiments, and thus it was never investigated in more detail.

In this study, 190 serine/threonine kinases were screened for phosphorylation of $Rab7^{Wt}$ at S72, using $Rab7^{S72P}$ as a control. The screen identified only two kinases, TBK1 and IKKε, which specifically phosphorylate Rab7 at S72 *in vitro*. Most of the literature on TBK1 and IKKε has been focused on their roles in NF-κB and IRF3/IRF7 signalling via activation of TLR3 and TLR4. Interestingly, a number of other kinases involved in pathways regulated by TBK1 and IKKε were also examined in the screen. IRAK4, an important regulator of the MyD88-dependent pathway that is activated following TLR4 stimulation at the plasma membrane was also identified as a potential hit, but as it phosphorylated the $Rab7^{S72P}$ protein higher than $Rab7^{Wt}$, it most likely phosphorylates Rab7 elsewhere (Table 4.1). It would be interesting to determine if IRAK4 phosphorylates Rab7 at another site and whether this has any effect on Rab7

activity as activation of the MyD88-dependent pathway promotes the degradation of TRAF3, an important regulator of TBK1 and IKKε activity.

In unstimulated cells, TRAF3 is constitutively bound to NIK, an essential activator of the alternative NF-κB pathway, which is activated during the generation of B and T lymphocytes following ligation of lymphotoxin-β receptor (LTβR), B cell-activating factor receptor (BAFFR), and CD40R. NIK activates IKKα, which phosphorylates of IκB, resulting in its dissociation from NF-κB, which subsequently translocates to the nucleus and induces the transcription of its target genes. IKKα, IKKβ and NIK were all tested in the ProQuinase screen, but all three were well below the threshold and exhibited no differential phosphorylation between $Rab7^{Wt}$ and $Rab7^{S72P}$ (Figures 4.1–4.5).

All four members of the IKK family were subsequently tested in [γ-32P]ATP *in vitro* kinase assays to confirm their phosphorylation activity on S72 and ensure specificity was restricted to the noncanonical IKKs. The results revealed that both TBK1 and IKKε phosphorylated Rab7 at S72, while neither IKKα nor IKKβ phosphorylated Rab7 at S72 or any position (Figure 4.8). TBK1 and IKKε are activated mainly by the MyD88-independent pathway following stimulation of TLR3, TLR4, MDA-5 and RIG-I. Indeed, stimulation of TLR3 with poly(I:C) in MEFs resulted 3.6-fold increase in phosphorylation of Rab7 at S72 after 180 min, whereas stimulation of TLR4 with LPS resulted in a 2.4-fold increase after 120 min. The increase in phosphorylation following LPS stimulation did not increase between 120 and 240 min, although this could be a result of saturation of the signal, as only a fraction of Rab7 is likely to be on this compartment at steady state. When these were repeated in SV40-immortalised cells they were unresponsive to stimulation.

After showing phosphorylation of Rab7 at S72 increases in wild-type MEFs following stimulation of TLR3 and TLR4, the next step was to inhibit TBK1 and IKKε to see if this decreased phosphorylation following stimulation. Although the TBK1 inhibitors, BX795 and MRT67307, inhibited phosphorylation of Rab7 at

S72 *in vitro* and have previously been shown to inhibit TBK1- and IKKε-mediated phosphorylation of IRF3 in macrophages, they did not reduce basal levels of Rab7 phosphorylation, even when incubated overnight in the presence of the inhibitors. This could be the result of other kinase(s) phosphorylating Rab7 at S72 under basal conditions. Further investigation is required to determine if there are other kinases responsible for phosphorylating under these conditions. Phosphorylation was also examined in TBK1$^{-/-}$ MEFs following stimulation of TLR3 and TLR4. However, the behaviour of the TBK1$^{-/-}$ MEFs in comparison to their wild-type littermates was completely different. The TBK1$^{-/-}$ MEFs transfected approximately five times their wild-type littermates and appeared to proliferate at a faster speed, thus making it very difficult to estimate the same levels of transfection and amount of protein when performing GFP-Rab7 immunoprecipitation. There were also increased levels of phosphorylation at S72 after 8 h in the TBK1$^{-/-}$ MEFs, with a corresponding increase in pIRF3. This could be a result of the induction of IKKε expression that occurs at ~8 h following infection.

Ideally, these experiments should be performed in macrophages as they are much more responsive to LPS and poly(I:C) stimulation; however, as they do not transfect well this limits their use. Macrophages are programmed to remove exogenous DNA they have engulfed and therefore the optimal mechanism for transfecting them is to use viral vectors. However, viral vectors may activate the pathways regulating TBK1 and IKKε activity. To address this limitation, viral vectors could be used to create stable cell lines. Once the DNA has integrated into the genome, the cells should switch off virally activated pathways allowing for their subsequent activation using exogenous stimuli. In macrophages Rab7, along with its effectors FYCO1 and RILP, have been shown to be required for lysosomal tubulation following stimulation with LPS (Mrakovic et al., 2012). FYCO1 is responsible for plus-end directed transport of late endosome/lysosome, whereas RILP interacts with the p150(Glued) subunit of the dynactin motor for minus end-directed transport (Pankiv et al., 2010) (Johansson et al., 2007b). Thus, as was seen in Chapter 3 (Figure 3.10) RILP

binding was significantly reduced by approximately 80% to the phosphomimetic Rab7^{S72E}, compared to Rab7^{Wt} and Rab7^{S72A}. Thus, phosphorylation of Rab7 at S72 could be a mechanism for promoting association with specific effectors, and inhibiting association with others, such as RILP, which are more important for homeostatic functions. Furthermore, as kinesin has been shown to be paramount for the formation of tubular lysosomes in macrophages, this could support the hypothesis that inhibition of Rab7 binding to RILP occurs by increased phosphorylation of Rab7 at S72 following stimulation of TBK1- and IKKε-activating pathways during infection.

Another process where Rab7 has been shown to be important and could be regulated by phosphorylation at S72 is MHC class II antigen presentation. When exogenous antigens are taken up into B cells, dendritic cells and macrophages they are exposed to an environment of increasing acidity and proteolytic activity as they progress along the endosomal pathway (Bertram et al., 2002). In the late endosomal compartment, these antigenic peptides associate with MHC class II molecules, which are then transported to the cell surface for presentation to CD4+ T cells. During this process these MHC class II-positive compartments form tubular structures, which originate from late endosome/lysosomes and polarize toward the T cell via retrograde transport (Chow et al., 2002). Furthermore, overexpression of Rab7 was shown to increase the rate of antigen processing and presentation in B cells (Bertram et al., 2002). These results also support a hypothesis in which phosphorylation of Rab7 at S72 could be a mechanism for redirecting Rab7 function from normal homeostatic functions toward being an essential component of the innate immune response. Future investigation should examine whether phosphorylation of Rab7 at S72 occurs on endosomal membranes of antigen-presenting cells and examining the interactors required for the formation of tubular structures.

Chapter 5. Differential activities of pRab7(S72) and unphosphorylated Rab7

5.1 Membrane-associated Rab7 is preferentially phosphorylated compared to cytosolic Rab7

While the phosphomimetic Rab7^{S72E} mutant is completely cytosolic, it is still unclear whether this mutant is an effective reporter of the effect phosphorylation at S72 would have on Rab7. The cytosolic localisation of Rab7^{S72E} could be caused by inhibition of its interaction with REP1, as REP1 interacts with Rab7 at S72, which would thereby prevent C-terminal prenylation and subsequent recruitment to endosomal membranes. This, however, is not an optimal indicator of what occurs *in vivo*, as inhibition of the REP1 interaction, following phosphorylation of Rab7 at S72 by TBK1 and IKKε, would only affect newly-synthesised Rab7, whereas the increases observed following poly(I:C) and LPS stimulation by western blot would suggest that a much larger population is phosphorylated. Thus, I decided to perform subcellular fractionation to determine the localisation of pRab7(S72).

GFP-Rab7^{Wt} was transfected for 48 h in MEFs, following which they were stimulated with 10 μg/ml poly(I:C) for 4 h. Cells were lysed by allowing them to swell under hyperosmotic stress in a sucrose-containing buffer, following which they were passed through a 17.5-gauge needle (15-20 times). Nuclei and any remaining whole cells were removed by two centrifugations at 1000 × *g*, for 10 min each. Cleared lysates were centrifuged at 100,000 × *g* for 1 h at 4°C to obtain the cytosolic (supernatant) and membrane (pellet) fractions. The membrane pellet was washed once in the sucrose-containing buffer, following which the membranes were dissolved in RIPA buffer. Both the cytosolic and membrane fractions were then treated with GFP-Trap® beads to

immunoprecipitate GFP-Rab7^{Wt}, following which SDS-PAGE and western blots were performed to determine the ratios of pRab7(S72) to total Rab7.

In the initial experiments, the total cytosolic and membrane fractions were analysed by western blot. However, as can be seen from Figure 5.1.A, the cytosolic fraction contained 10–20-fold more total Rab7 than the membrane fraction. While there was some pRab7(S72) in the cytosolic fraction it was a tiny amount in comparison to the membrane fraction. Furthermore, following stimulation with poly(I:C) there appeared to be a decrease in the pRab7(S72) associated with the membrane. These experiments were performed using one 10-cm dish per sample, which is the same condition as what had been used previously with the poly(I:C) and LPS stimulation experiments for total cellular changes in pRab7(S72). However, due to the different conditions used for the subcellular fractionation, a significant amount of material seemed to be lost during the experiment. To combat this, the amount of material was increased to one 20-cm dish per sample. Furthermore, the amount of material loaded from the cytosolic fraction was decreased to approximately 10% of the overall volume, so that the total Rab7 for each sample was similar. After increasing the amount of material used for the subcellular fractionation, it was clear that the overall ratio of pRab7(S72) to total Rab7 was significantly higher in the membrane fraction compared to the cytosolic fraction.

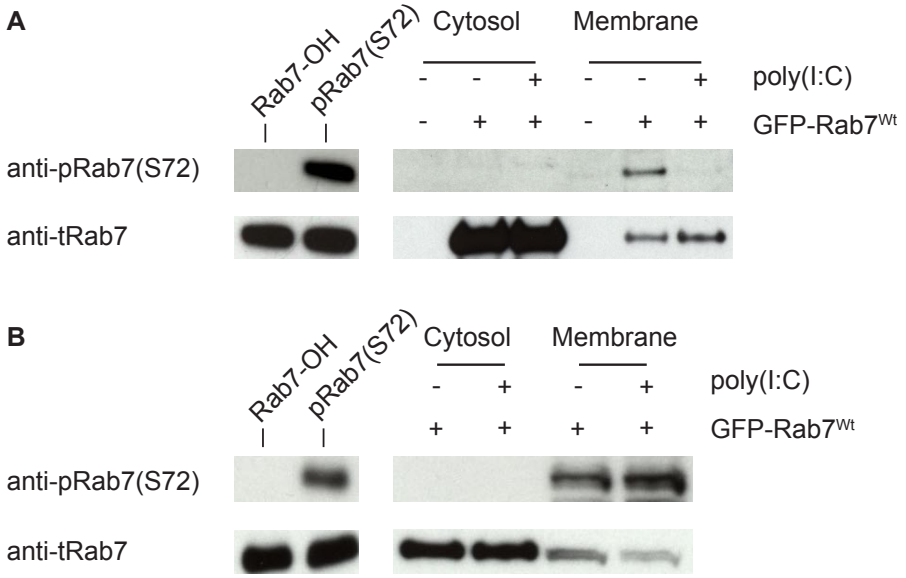

Figure 5.1. Subcellular fractionation of GFP-Rab7 in MEFs stimulated with poly(I:C).

GFP-Rab7^{Wt} was transfected in MEFs for 48 h, following which cells subjected to subcellular fraction by centrifugation at 100,000 × g for 1 h at 4°C. The entire membrane and cytosolic fractions were subjected to GFP-trap to immunoprecipitate the GFP-Rab7^{Wt}, following which the entire fractions were loaded in (A) and approximately 10% of the cytosolic fraction was loaded in (B). pRab7(S72) was detected using the rabbit anti-pRab7(S72) antibody, following which the blots were stripped and reprobed with a mouse total (t)Rab7 antibody. From both experiments we can see a much higher ration or pRab7(S72) to total Rab7 is found in the membrane fraction compared to the cytosol.

Following the results of the subcellular fractionation, I purified the anti-pRab7(S72) antibody to examine pRab7(S72) localisation by immunofluorescence. This had been previously attempted but we did not have a good antibody for total Rab7 to confirm that the staining was specific.

MEFs were stained with the rabbit anti-pRab7(S72) antibody (1:500) for 2 h, followed by and anti-rabbit AlexaFlour 488 secondary antibody. The cells were post-fixed for 5 mins in 4% PFA. Following this, the cells were stained for total Rab7 using a rabbit anti-Rab7 antibody and anti-rabbit AlexaFlour 555 secondary antibody. This method prevents the secondary antibody used for the anti-pRab7(S72) antibody from accessing the total anti-Rab7 antibody. Thus, any colocalisation would not be a result of non-specific staining of the anti-pRab7(S72) antibody. The control sample was performed in the same manner, with the incubation with the total Rab7 antibody being substituted for PBS containing 1% BSA.

From the results it is clear that a large proportion of the pRab7(S72) pool is located on punctate structures, all of which co-stain for Rab7. However, only a minority of all of the Rab7-positive puncta are positive for pRab7(S72). This indicates that the pRab7(S72)-positive structures are a subpool of the total Rab7 population of late endosomes/MVB or lysosomes. The control sample shows high background, but no punctate staining reminiscent of the pRab7(S72) staining.

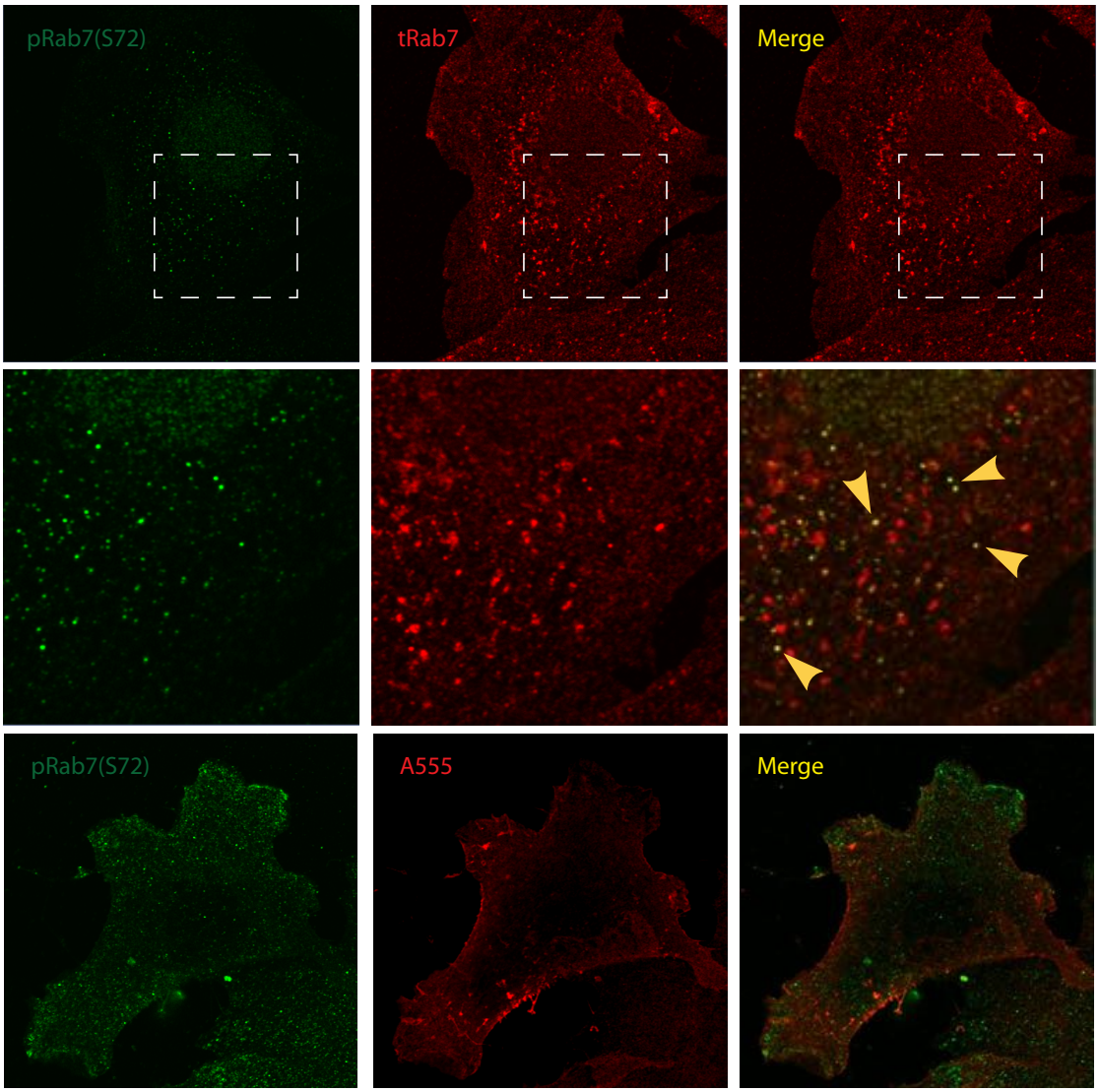

Figure 5.2. Localisation of pRab7(S72) by immunofluorescence.

MEFs were stained for pRab7(S72), followed by a total Rab7 antibody. The pRab7(S72) pool of organelles appear to be a sub-population of the total Rab7-positive compartment. The middle panel shows the double- and single-positive organelles highlighted by boxes in the top panel. The bottom panel shows control staining incorporating both secondary antibodies, but excluding the total Rab7 antibody, which is most notable in the perinuclear region.

5.2 Phosphorylation of Rab7 at S72 increases the rate of GTP hydrolysis *in vitro*

Inactivation of all Rab proteins occurs via hydrolysis of the γ-phosphate of GTP to yield GDP, mainly through interaction with a GAP. GDP is then removed by interaction with a GEF. However, some Rabs have GAP-independent intrinsic activities for GTP hydrolysis, which is catalysed by a conserved glutamine residue (Q67 for Rab7), and GDP dissociation. It has been previously shown that the constitutively active mutation Q67L exhibits decreased intrinsic GTP hydrolysis, with no impairment in GTP binding (Spinosa et al., 2008). This mutation is in close proximity to the S72 residue, which, when phosphorylated, may also affect GTP hydrolysis and/or binding.

His-tagged Rab7^{Wt} was phosphorylated *in vitro* with IKKε at 30°C for 30 min. Following this, unphosphorylated and IKKε-phosphorylated Rab7^{Wt} were bound to Ni^{2+} beads, loaded with [α-P^{32}]GTP and incubated at 37°C for various time points to allow GTP hydrolysis to occur. The assay was performed in the absence of excess cold GTP. This will allow dissociation of GDP and further binding of [α-P^{32}]GTP. This method is more efficient when looking at GTP hydrolysis, whereas performing the incubation step in excess cold GTP allows analysis of the hydrolysis rate per binding event and the nucleotide dissociation activity, as only the bound [α-P^{32}]GTP would be hydrolysed and following dissociation of GDP, Rab7 would be more likely to bind cold GTP.

The results revealed that phosphorylation of Rab7 at S72 caused a steady increase in GTP hydrolysis compared to the unphosphorylated control, which was significantly increased at both 60 (P = 0.0035) and 120 min (P = 0.0002). Furthermore, binding of [α-P^{32}]GTP was increased in pRab7(S72). The assay was also performed in excess cold GTP (10 mM), but there was very little hydrolysis of [α-P^{32}]GTP and difference between the unphosphorylated and pRab7(S72) proteins was not significant (n = 2, not shown). Statistical analysis

was performed using two-way ANOVA followed by Sidak's multiple comparisons test.

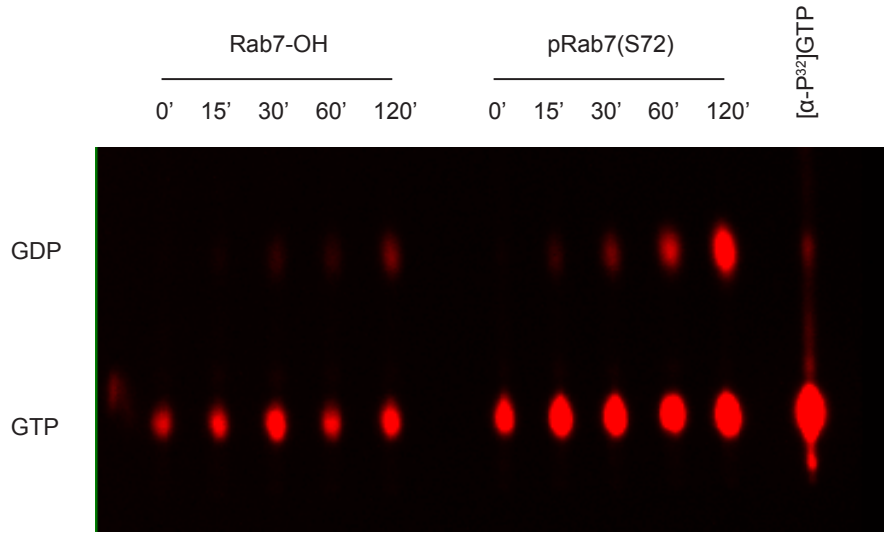

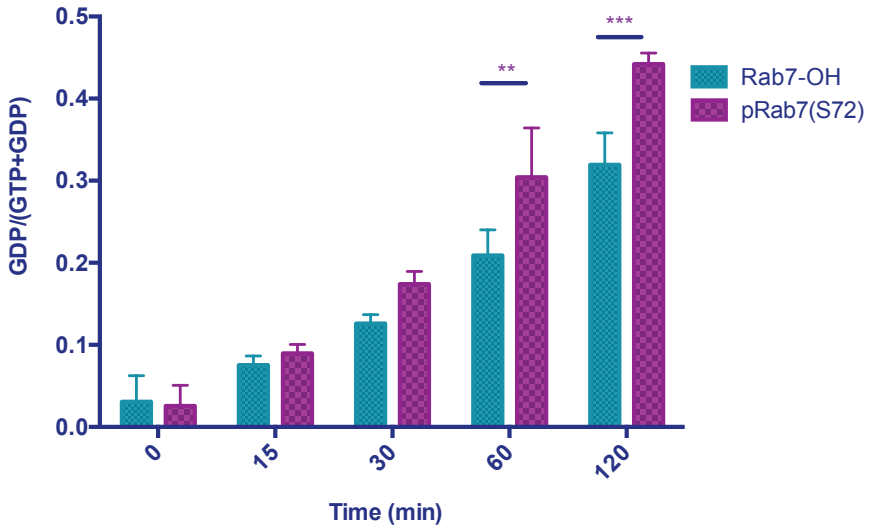

Figure 5.3. *In vitro* [α-P^{32}]GTP hydrolysis activity of unphosphorylated and S72-phosphorylated Rab7.

The intrinsic GTP hydrolysis activity of pRab7(S72) was compared to unphosphorylated Rab7 using [α-P^{32}]GTP. The top image shows the phosphorimager analysis and the bottom shows the quantification of three independent experiments. pRab7(S72) exhibits increased GTPase activity compared to unphosphorylated Rab7, which is significantly increased at both 60 (P = 0.0035) and 120 min (P = 0.0002). n = 3.

5.3 Pull-down and mass spectrometry of differential interactors of Rab7 following phosphorylation at S72

Following the results of the subcellular fractionation and the immunofluorescence using the anit-pRab7(S72) antibody, which revealed that a significant proportion of pRab7(S72) was membrane-bound, I decided to do a pull-down and mass spectrometry using recombinant GST-Rab7 +/- TBK! phosphorylation to look for differential interactors between unphosphorylated Rab7 and pRab7(S72). In the earlier experiments investigating the differential interactions of $Rab7^{Wt}$, $Rab7^{S72A}$ and $Rab7^{S72E}$ with RILP and ORP1L, ORP1L bound equally to all three proteins, whereas RILP binding to the $Rab7^{S72E}$ mutant was significantly decreased by around 80% (Figure 3.10). However, the phosphomimetic $Rab7^{S72E}$ mutation exhibits a completely cytosolic localisation, which is in complete contrast to the subcellular fractionation and the immunofluorescence results. Thus, the pull-down and mass spectrometry was performed to determine if phosphorylation of Rab7 at S72 affects interaction with different effectors.

GST-Rab7 was bound to GSH-agarose resin, following which it was split into two samples, unphosphorylated and TBK1-phosphorylated GST-Rab7 samples. The pRab7(S72) sample was phosphorylation *in vitro* using His-TBK1 at 30°C for 30 min on a shaking hotblock. Samples were then washed once in TBK1 buffer without kinase. Then, bound nucleotides were removed by washing twice with 1 M guanidine-HCl, and then loaded with GTPγS. Two 10-cm dishes of confluent HEK293 cells were used to prepare lysates, which were mixed together and pre-cleared of nonspecific binding proteins using empty GSH-agarose beads, before splitting in two for the pull-down. Half of the pull-down was used for mass spectrometry and the other half was used for western blot analysis of interactors.

Prior to obtaining the mass spectrometry results, I decided to test the remaining samples from the pull-down for interaction of endogenous interaction RILP and ORP1L with the GST-tagged unphosphorylated Rab7 and pRab7(S72). The results revealed ORP1L interacted with both unphosphorylated Rab7 and pRab7(S72), whereas RILP interacted with only the unphosphorylated protein (Figure 5.4).

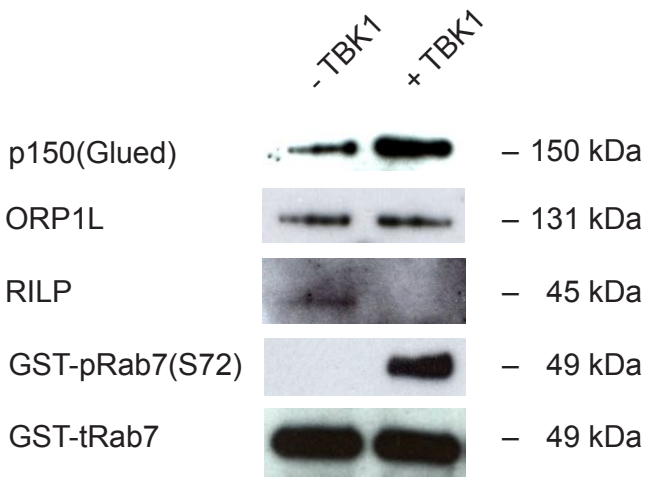

Figure 5.4. Association of endogenous ORP1L and RILP to unphosphorylated and pRab7(S72) .

GST-Rab7 bound to GSH-agarose beads was phosphorylated at S72 using TBK1. Following this both phosphorylated and unphosphorylated GST-Rab7 samples were incubated with HEK283 cell lysates. Half of the sample was used for mass spectrometry and the other half was loaded for western blot analysis. RILP, ORP1L and p150(Glued) were detected using specific antibodies, while total Rab7 was detected using a mouse anti-Rab7 antibody and pRab7(S72) was detected using the rabbit anti-pRab7(S72) antibody.

The mass spectrometry results identified a number of differential interactors for unphosphorylated Rab7 and pRab7(S72) (Table 5.1), as well as a larger number of common interactors (Table 5.2). Surprisingly, although the western blot of the mass spectrometry samples detected ORP1L and RILP interactions, neither was detected in the mass spectrometry analysis. However, the p150(Glued) subunit of the dynactin complex, which binds to ORP1L and RILP for microtubule minus-end directed transport of late endosomes, showed a specific interaction with pRab7(S72) in the mass spectrometry (Figure 5.4). This interaction was confirmed by western blot, which showed 2.7 time more p150(Glued) associated with pRab7(S72) compared to the unphosphorylated Rab7 (Figure 5.4). The p50 subunit of the dynactin complex interacted with both pRab7(S72) and unphosphorylated Rab7. Cytoplasmic dynein 1 intermediate chain 2 (DC1I2) and cytoplasmic dynein 1 heavy chain 1 (DYHC1) were also detected, with DC1I2 selectively binding unphosphorylated Rab7 and DYHC1 binding both proteins, but with a 2.2-fold higher affinity for pRab7(S72). These results that phosphorylation of Rab7 at S72 seems to bypass the need of RILP for dynein recruitment, which agrees with the study of Vihervaara *et al*., which found that ORP1L was sufficient to recruit p150(Glued) and the dynein motor to Rab7-positive endosomes (Vihervaara et al., 2011).

Other interesting interactors from the mass spectrometry data include TRAF3, TRAF4, REP1 and vimentin. Both REP1 and vimentin are known interactors of Rab7, whereas TRAF3 and TRAF4 are potentially novel binding partners. TRAF3, TRAF4, and REP1 were all only detected in the unphosphorylated Rab7 sample, with TRAF3 being the strongest hit.

Identified Proteins	Number of Peptides Rab7-OH	pRab7(S72)
TNF receptor-associated factor 3 (TRAF3)	7	0
Stress-70 protein, mitochondrial (GRP75)	3	0
T-complex protein 1 subunit gamma (CCT3)	2	0
Cytoskeleton-associated protein 4 (CKAP4)	2	0
Cytoplasmic dynein 1 intermediate chain 2 (DC1I2)	2	0
Rab escort protein 1 (REP1)	1	0
TNF receptor-associated factor 4 (TRAF4)	1	0
Transitional endoplasmic reticulum ATPase (TERA)	0	5
Leucine-rich PPR motif-containing protein (LPPRC)	0	5
Spectrin beta chain, non-erythrocytic 1 (SPTB2)	0	4
Dynactin subunit 1 (p150(Glued)) - DCTN1	0	3
Transportin-1	0	3
Death-inducer obliterator 1 (DIDO1)	0	3
CCAR1	0	2
Developmentally-regulated GTP-binding protein 1	0	2
Importin subunit beta-1 (IMB1)	0	2
RRP12-like protein (RRP12)	0	2
Transformer-2 protein homolog beta (TRA2)	0	2
Rab1A	0	2
Arginine/serine-rich coiled-coil protein 2	0	2
Neutrophil defensin 1 (DEF1)	0	2
Rab34	0	1

Table 5.1. Mass spectrometry results of the proteins found to differentially interact with unphosphorylated Rab7 and pRab7(S72).

A number of differential interactors were identified by mass spectrometry for unphosphorylated Rab7 and pRab7(S72). The list includes hits proteins with >3 peptides detected and interesting hits for those with <3 peptides. The proteins highlighted in yellow are known interactors of Rab7, while the proteins in red are interesting hits as TRAF3 is involved in TBK1 and IKKε activation downstream of TLR3 and TLR4 signalling.

Identified Proteins	Rab7-OH	pRab7(S72)
Ataxin-2-like protein (ATX2L)	27	22
Clathrin heavy chain 1	30	15
Bcl-2-associated transcription factor 1 (BCLF1)	11	10
Thyroid hormone receptor-associated protein 3	12	11
Desmoplakin	4	16
Actin, cytoplasmic 1	6	8
Prohibitin-2	9	8
Tubulin alpha-1B chain (TBA1B)	8	9
Myosin-10	8	12
Fatty acid synthase (FAS)	5	13
Constitutive coactivator of PPAR-gamma-like protein 1	11	9
Interleukin enhancer-binding factor 3 (ILF3)	5	7
Prohibitin	8	7
Protein LSM14 homolog A (LS14A)	7	3
Exportin-2	3	7
Endoplasmin	1	4
Vimentin	8	5
Cytoplasmic dynein 1 heavy chain 1 (DYHC1)	4	9
Dynactin 2 (p50) - DCTN2	1	1
AP-2 complex subunit beta	5	11
AP-2 complex subunit alpha-1	5	9
Fragile X mental retardation protein 1 (FMR1)	6	6
Fragile X mental retardation syndrome-related protein 2	13	16
Nuclear fragile X mental retardation-interacting protein 2	20	19
Ras GTPase-activating protein-binding protein 1	9	6
Ras GTPase-activating protein-binding protein 2	10	8
Rab6C	1	1

Table 5.2. Mass spectrometry results of common interactors of unphosphorylated Rab7 and pRab7(S72).

A large number of common interactors were identified by mass spectrometry for unphosphorylated Rab7 and pRab7(S72). The table shows the highest hits of the analysis. The proteins highlighted in yellow are known interactors of Rab7.

5.4 Discussion

The initial hypothesis of this project, conceived from experiments using GFP-Rab7^{Wt}, GFP-Rab7^{S72A} and GFP-Rab7^{S72E}, was that phosphorylation of Rab7 at S72 inhibited Rab7 recruitment to the membrane for activation. This hypothesis was supported by experiments showing that GFP-Rab7^{S72E} is completely cytosolic (Figure 3.3) and appeared to decrease in EGFR degradation (Figure 3.9). However, as the S72 residue is located in the switch II region of Rab7, on a site known to interact with REP1, I hypothesised that the Rab7^{S72E} mutation could prevent interaction of newly synthesised Rab7^{S72E} with REP1, thereby preventing its C-terminal prenylation, which would block its recruitment to the membrane and function. After the *in vitro* kinase screen and subsequent validation of the hits revealed that TBK1 and IKKε were the only two kinases of the 190 tested that phosphorylated Rab7 at S72, it was unclear why this would only affect newly synthesised Rab7, especially with the diversity of the phosphoproteomic screens S72 phosphorylation was detected in.

To determine if the cytosolic localisation of Rab7^{S72E} was a good indicator of the localisation of pRab7(S72) and not an artefact caused by an inhibition of its C-terminal prenylation, subcellular fractionation was performed of GFP-Rab7^{Wt} expressing MEFs to determine the correct localisation. Surprisingly, a large proportion of pRab7(S72) was located on the membrane compared to the cytosolic proportion (Figure 5.1). This result was confirmed by immunofluorescence using the anti-pRab7(S72) antibody (Figure 5.2). Interestingly, the anti-pRab7(S72) antibody staining revealed that only a subpool of the Rab7-positive organelles were positive for pRab7(S72). Future experiments should be performed to determine the identity of these endosomes, using labels such as Lysotracker or a pulse-chase experiment using fluorescently-labelled EGF.

Following these results, it was clear that the original hypothesis that phosphorylation inhibited Rab7 activity was most likely wrong; so two new hypotheses were generated as follows:

1. Phosphorylation of Rab7 at S72 affects its GTPase activity.

2. Phosphorylation of Rab7 at S72 affects Rab7 interaction with specific effectors.

To test the first hypothesis, an *in vitro* kinase assay was performed using [α-P^{32}]GTP to determine if there was a difference in the intrinsic GTPase activities of pRab7(S72) and unphosphorylated Rab7. The results revealed that over a 120-min period, there was an increasing rate of GTP hydrolysis in pRab7(S72), which was statistically significant at both 60 (P = 0.0035) and 120 min (P = 0.0002). Furthermore, binding of [α-P^{32}]GTP was increased in pRab7(S72) compared to unphosphorylated Rab7 (Figure 5.3). If phosphorylation of Rab7 at S72 were to weaken or inhibit the interaction between the switch I and II regions, the open conformation could allow for increased GTP association. Following GTP binding, intrinsic GTP hydrolysis would occur via the catalytic Q67 residue, allowing for GDP dissociation, followed by further binding of [α-P^{32}]GTP and its subsequent hydrolysis. This experiment addresses the binding and rate of GTP hydrolysis. In a cellular context, other factors, such as recruitment of specific GEF or GAP, may further modulate GTP status of pRab7(S72). However, the results do provide good evidence that phosphorylation of Rab7 at S72 affects the interaction of the switch I and II regions, which could cause an inhibition of Rab7 function or it could affect binding of certain effectors that require interaction between these regions, such as RILP, which binds numerous residues within both regions when in the GTP-bound conformation.

To test the second hypothesis, recombinant pGST-Rab7(S72) and unphosphorylated GST-Rab7 were used to for a pull-down and mass spectrometry analysis of differential interactors. Although a number of known interactors, including RILP and ORP1L, were not detected in the mass

spectrometry results, they were detected by western blot of the same samples used for the mass spectrometry pull-down. RILP was detected only in the unphosphorylated sample, whereas ORP1L was detected in both (Figure 5.4).

Both RILP and ORP1L are involved in recruitment of the dynein-dynactin motor to late endosomes and lysosomes. The results of the mass spectrometry screen also detected both the p150(Glued) and p50(Dynamitin) subunits of the dynactin complex, along with cytoplasmic dynein heavy chain 1 (DHC1), cytoplasmic dynein 1 intermediate chain 2 (DC1I2) and cytoplasmic dynein 2 light intermediate chain 1 (DC2L1). The p150(Glued) subunit was detected only in the pRab7(S72) sample, along with 2.1-fold more DHC1 compared to the unphosphorylated sample; p50(Dynamitin) and DC2L1 were detected equally in both; and DC1I2 was only detected in the unphosphorylated sample (Table 5.1, Table 5.2). Studies have shown differential requirements for different components of the dynein-dynactin motor for specific functions. Tan *et al.* showed that cytoplasmic dynein 1 light intermediate chain 1 (DC1L10, which was not detected in our study, is involved in recruitment of dynein to lysosomes and late endosomes, independent of RILP-dependent recruitment of dynactin (Tan et al., 2011).

According to most studies published on the recruitment of p150(Glued) to Rab7-positive late endosomes and lysosomes, this occurs by its direct binding to RILP; however, evidence that p150(Glued) is not recruited in the absence of RILP is not very strong. Jordens *et al.* originally claimed that expression of the C-terminal half of RILP reduced p150(Glued) recruitment to lysosomes compared to overexpressed full-length RILP; however, the immunofluorescence images showing this are at a lower magnification than the full-length and do not appear to be very different from each other (Jordens et al., 2001). Furthermore, the absence of p150(Glued) from their subcellular fractionation analysis of p50(Dynamitin), Rab7 and α-tubulin localisation in cells overexpressing both forms of RILP raises questions as to why it was omitted. Vihervaara *et al.* ORP1L is capable of recruiting p150(Glued) to late endosomes/lysosomes

independent of RILP (Vihervaara et al., 2011). More recently, Kant *et al.*, showed that RILP binds the HOPS complex and p150(Glued), and most mutations in RILP that affect HOPS subunit binding also affected RILP binding (van der Kant et al., 2013). They also found that the highest affinity for binding of p150(Glued) to Rab7-RILP was in the presence of the HOPS complex. Thus, RILP does not does not appear to be the major determinant of p150(Glued) recruitment to Rab7, and may be recruited to the complex by other factors. The increased interaction of p150(Glued) with pRab7(S72) could be a result of increased recruitment of other effectors required for the formation of a complex with Rab7-p150(Glued) that would be inhibited by the presence of RILP. Furthermore, as this experiment used recombinant Rab7 that was phosphorylated *in vitro* with TBK1, it is not known how much of the sample was indeed phosphorylated at S72 and was most likely a mixture of both unphosphorylated and phosphorylated Rab7. Thus, the presence of certain effectors in the pRab7(S72) sample at lower levels than unphosphorylated Rab7 could be an effect of them binding to Rab7 that has not been phosphorylated by TBL1 *in vitro*. However, these results still provide novel information on differential interactions with effectors as a result of Rab7 phosphorylation at S72, which has never been investigated previously.

Johansson *et al.* showed that binding of ORP1L promotes binding of the ORP1L-Rab7–RILP–p150(Glued) complex to membrane-associated αI-βIII spectrin, which then binds to the Arp1 subunit of dynactin (Johansson et al., 2007a). Interestingly, this study also found that ORP1L but not RILP, is required for dynein-mediated transport of late endosomes, by mediating interaction between ORP1L and βIII spectrin. While βIII spectrin was not detected in the mass spectrometry results, αI spectrin, also known as spectrin alpha chain, non-erythrocytic 1 (SPTN1), and βII spectrin, or spectrin beta chain, non-erythrocytic 1 (SPTB2), were detected (>4 peptides for each). βII spectrin was only detected in the pRab7(S72) sample, while αI spectrin was detected in both. Spectrin itself is a large, heterodimeric protein composed of α and β subunits. In humans, there are two α (αI and αII) and five β (βI–βV) subunits. Unfortunately,

the function of βII spectrin is not very well established, but it has been shown to be involved in hepatocyte proliferation through the transforming growth factor-β (TGFβ) signalling pathway by functioning as a Smad3/4 adaptor protein (Thenappan et al., 2011). TGFβ signals in early endosomes and is degraded via the proteasome and lysosome, indicating that Rab7 interaction with spectrin subunits could be involved in the regulation of TGFβ signalling (Kavsak et al., 2000).

Two of the most interesting hits from the mass spectrometry results were TRAF3 and REP1, both of which were specific interactors for unphosphorylated Rab7 (Table 5.1). The lack of the interaction of REP1 with the pRab7(S72) suggests that the concerns about Rab7^{S72E} giving false indications because it does not interact with REP1, and as a consequence never gets prenylated, are most likely true. TRAF3 interaction with unphosphorylated Rab7 was the most surprising result for the entire analysis, as TRAF3 is a key regulator of IRF3/7 signalling, upstream of TBK1 and IKKε. Unfortunately, I did not have time to confirm this by western blot, but the fact that TRAF4 also interacts specifically with unphosphorylated Rab7 is a good indicator that this is correct. Furthermore, TRAF6 has previously been identified as a Rab7 interactor in a large-scale analysis of protein-protein interactions in human cells, and TRAF6 is required for TrkA polyubiquitination and internalization, and NGF-dependent neurite outgrowth (Ewing et al., 2007). The possible significance of the interaction of Rab7 with TRAF3 will be discussed in more detail in the following Discussion chapter.

Chapter 6. Discussion

6.1 Mechanisms of Rab7 regulation

While many studies use phosphomimetic and phosphodeficient mutations to examine the effects phosphorylation at a specific residue may have on a proteins function, it is evident from the results of this study that the phosphomimetic Rab7^{S72E} does not mimic the behaviour of a constitutively phosphorylated Rab7 at S72. Rab7^{S72E} appears to be inactive, whereas the results of subcellular fractionation, immunofluorescence and pull-down all indicate that a large proportion of pRab7(S72) is located on endosomal membranes and is capable of interaction with certain effectors. Binding of RILP to Rab7 is believed to lock Rab7 in an active state, whereas phosphorylation appears to inhibit RILP binding and increase GDP/GPT turnover of Rab7. Thus, phosphorylation of Rab7 at S72 could increase the intrinsic GTPase activity of Rab7, but it may also be a mechanism of promoting interaction with certain effectors over others. As the S72 residue is also located in the switch II region, adjacent to sites required for the interaction with the switch I region upon GTP-binding, this could also affect the active state of Rab7. It would be very interesting to see if the interaction between the switch I and II regions is maintained in the crystallisation of pRab7(S72) in the GTP-bound form.

6.2 Phosphorylation of Rab7 at serine 72 via toll-like receptor signalling

In this study, both TBK1 and IKKε were identified as kinases that phosphorylate Rab7 at S72 *in vitro*. Furthermore, stimulation of TLR3 and TLR4, both of which are upstream receptors responsible for the activation of TBK1 and IKKε, causes increased phosphorylation of Rab7 at S72 in MEFs. Interestingly, one of the biggest hits of the mass spectrometry analysis, of differential interactors for unphosphorylated Rab7 and pRab7(S72), was TRAF3, which specifically bound

to the unphosphorylated Rab7 sample (Table 5.1). TRAF3 is activated by TLRs that signal via the endosomal pathway. TLR3, 7, 8 and 9 are all internal receptors that recognise bacterial and viral nucleic acids, whereas the plasma membrane receptors recognise surface markers of invading pathogens (Janssens and Beyaert, 2002). TLR4 is the only plasma membrane-associated TLR that can activate the IRF3 pathway, and does so following internalisation and activation of TRAF3. The remaining plasma membrane TLRs (TLR1, 2, 5 and 6) all signal from the cell surface.

TLR3, 7, 8 and 9 all reside within the ER of resting cells and traffic to endosomes/lysosomes upon activation (Latz et al., 2004). It was originally believed that TLRs in the ER quickly traffic to endosomes upon activation; however, it is now believed that TLR7 and 9 pass through the Golgi, based on analysis of the carbohydrates of these TLRs in endosomes (Chockalingam et al., 2009). It is believed that TLR3 also passes through the Golgi for proteolytic processing in endosomes (Qi et al., 2012). This proteolytic processing is dependent on Unc93b1, and ER-localised molecular chaperone responsible for the trafficking of TLRs to endosomes/lysosomes. However, TLR3 is also found in the full-length form in endosomes/lysosomes and is signalling competent, but its half-life in HEK293 cells is approximately 3 h, compared to over 7 h for the cleaved form (Qi et al., 2012). This suggests that TLR3 could traffic to via two different mechanisms, one via the Golgi and the other direct from the ER to endosomes/lysosomes.

Recently, there has increasing amount of evidence for substantial contact between endosomes and the ER, with some studies indicating that these contacts sites increase with endosomal maturation. Friedman *et al.* measured the association of early and late endosomes with the ER and found that 50% of early endosomes tracked over a 2-min period remained in contact with the ER, compared to >95% of late endosomes, in both COS-7 and U2OS cells (Friedman et al., 2013). Both early and late endosomes coupled to the ER were also found to be in contact with microtubules for transport towards the

perinuclear region as they mature (Friedman et al., 2013). This close association Rab7-positive organelles with the ER has been proposed as contact sites for the transfer of cholesterol to lysosomes, but could also allow for the transfer of TLRs and other proteins to the endocytic pathway, and the interaction of Rab7 with ORP1L could be a key regulator of this process (Rocha et al., 2009). For TLR3, this could explain why it is present in full-length and cleaved forms in endosomes/lysosomes, as the full-length may bypass the Golgi apparatus and traffic directly via contacts sites with the ER, following stimulation of the cleaved form that is already present in endosomes. Thus, this mechanism would allow for attenuation of the IRF3 signalling pathway following recruitment of full-length TLR3 from the ER much faster than if it were to pass through the Golgi.

Binding of TRAF3 to Rab7 could allow faster recruitment of TRAF3 to activated TLR3 or TLR4, where it would bind TRIF (Figure 6.1). Activated TRAF3 could then bind TBK1 and IKKε to form a complex, which in turn could phosphorylate Rab7 on the membrane. A previous study investigating the role of the 26S proteasome adaptor Ecm29 in TLR3 signalling, found that an absence of Ecm29 attenuated TLR3 signalling, TRAF3 abundance, TBK1 activation and IRF3 translocation into the nucleus (Gorbea et al., 2013). More interestingly, they also found increased colocalisation of TBK1 and Rab7. Previously, I transfected GFP-TBK1 or GFP-IKKε with HA-Rab7 in HeLa cells to monitor their colocalisation, but was unsuccessful. Overexpression of TBK1 and IKKε results in their autophosphorylation in the catalytic domain, but this was insufficient to induce phosphorylation of Rab7. However, if Rab7 interacts with TBK1 and IKKε in a complex containing TRAF3, which is recruited to TLR3 or TLR4 in endosomes/lysosomes, then this would not occur in HeLa cells, as these do not express endogenous TLR3 or TLR4. It would be interesting ascertain the extent of colocalisation of pRab7(S72), Rab7, TBK1, IKKε, and TRAF3, before and after stimulation of TR3 or TLR4 in macrophage or dendritic cells, which express these constituents at higher levels than most other cell types.

6.3 Phosphorylation of Rab7 at serine 72 as a possible mechanism of controlling lysosomal tubulation

An alternative hypothesis for the role of Rab7 phosphorylation at S72 could be a mechanism that allows for the formation of tubular lysosomes in macrophages and dendritic cells following infection. Stimulation of macrophages and dendritic cells with LPS causes the remodelling of the class II major histocompatibility complex (MHCII) compartment, a lysosome-related organelle, from a punctate morphology into tubular network that is believed to be involved in antigen presentation (Mrakovic et al., 2012). The formation of these tubular lysosomes requires Rab7, and its effectors RILP and FYCO1, as well as Arl8b, and its effector SKIP. RILP and FYCO1 regulate the dynein- and kinesin-mediated transport of lysosomes, respectively. Arl8b is another small GTPase that is also involved in the microtubule plus end-directed transport of lysosomes through regulation of the kinesin motor (Mrakovic et al., 2012). Expression of the dominant-negative GFP-Rab7^{T22N} resulted in a significant reduction (67 ± 5%) in the number of tubular lysosomes per cell compared to GFP-Rab7^{Wt}. Interestingly, overexpression of GFP-RILP also caused a significant reduction (51 ± 7%) in the number of tubular lysosomes compared to untransfected cells, even though it was still recruited to the few that were present. This indicates that the balance between Rab7-RILP and Rab7-FYCO1 is extremely important for tubulation.

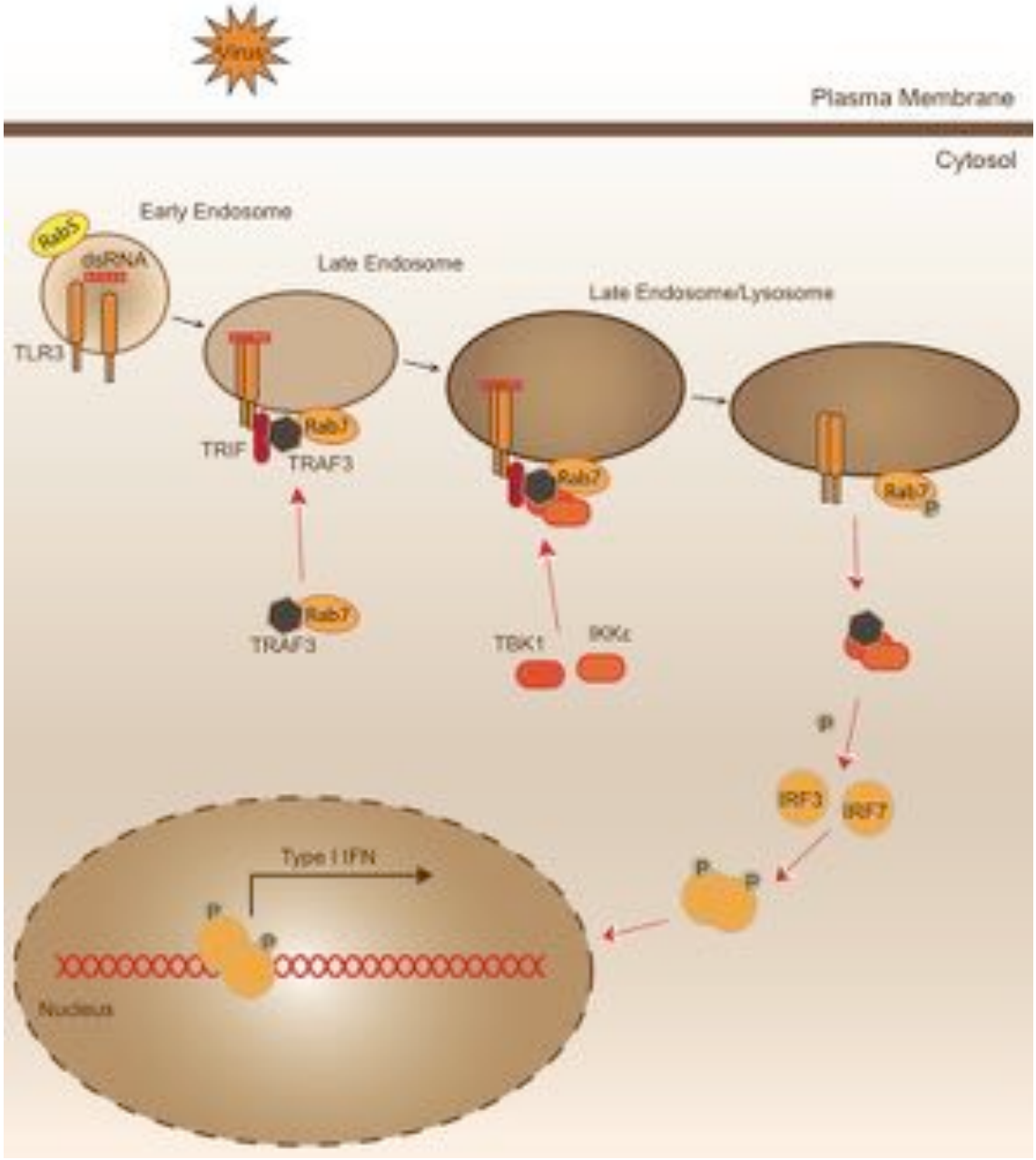

Figure 6.1. Model of Rab7-dependent recruitment of TRAF3 to TLR3 in endosomes/lysosomes.

Activation and dimerization of TLR3 occurs by binding of dsRNA in the early endosome. Signalling of TLR3 requires endosomal acidification, and the exchange of Rab5 for Rab7. TLR3 requires binding of TRIF to activate the downstream signalling pathway. Rab7 could then bring TRAF3, which can bind unphosphorylated Rab7, to the late endosome/lysosome, where it can then bind TRIF. TBK1 and IKKε then bind and form a complex with TRAF3, which could then phosphorylate Rab7 at S72. The TRAF3-TBK1-IKKε complex phosphorylates IRF3 and/or IRF7, which dimerise and translocate to the nucleus to induce production of type I interferon.

Furthermore, it has been previously shown that Rab7 is expressed at low levels in resting B cells, but is upregulated following stimulation with CD40 ligand (CD40L) or bacterial LPS. Furthermore, overexpression of Rab7 in B cells also results in an increased rate of MHCII antigen presentation (Bertram et al., 2002). This function of Rab7 appears to be different to its normal homeostatic functions, which could implicate a requirement for differential regulation. Phosphorylation of Rab7 at S72 could inhibit RILP recruitment, thus allowing for the recruitment of other effectors, such as FYCO1, to allow for lysosomal tubulation and antigen processing. Indeed, increased phosphorylation of Rab7 at S72 has been previously detected in a number of immunological screens, including LPS stimulation of macrophages (Weintz et al., 2010). Furthermore, in this study, LPS and poly(I:C) stimulation of MEFs increased phosphorylation of Rab7 at S72. In future work, it would be interesting to see if there was a subset of the pRab7(S72) localised to tubular lysosomes in macrophages and if this subset colocalised with other markers, such as RILP and FYCO1. Unfortunately, as FYCO1 did not bind to pRab7(S72) or unphosphorylated Rab7 during the pull-down, it is still unclear if the working model is sound.

6.4 TBK1 & IKKε regulation of vesicular transport

While most of the research into TBK1 and IKKε to date has investigated their roles in NF-κB and IRF signalling, both kinases may also be involved in the regulation of endosomal trafficking. IKKε plays an important role in the elongation of *Drosophila* mechanosensory bristle growth, by phosphorylating Nuf, a Rab11 effector, to control the trafficking of recycling endosomes in and out of the bristle tip (Otani et al., 2011). This phosphorylation of Nuf appears to inhibit dynein recruitment to incoming recycling endosomes, thereby promoting recruitment of Rab11 and their subsequent recycling. Knockdown of IKKε in *Drosophila* results in shortened bristle length, branching and cytoskeleton disorganization. The same study also showed that IKKε phosphorylates the mammalian homolog of Nuf, Rab11-FIP3.

TBK1 has also been shown to interact with the ESCRT-I subunit VPS37C, in a kinase activity-independent manner, indicating that it is an auxiliary subunit of the ESCRT-I complex (Da et al., 2011). As ESCRT-I is required for HIV-1 budding, the authors examined the role of TBK1 in this process and found that knockdown of TBK1 results in more efficient budding of the virus. Although this process does involve activation of innate immunity, TBK1 did coimmunoprecipitate with ESCRT-I in unstimulated cells, indicating that it may play another role in regulating this complex.

Thus, although most of the studies investigating TBK1 and IKKε activity have focused on their role in innate immunity, both kinases may play much larger roles in the regulation of intracellular vesicular transport pathways. This could also explain why there is phosphorylation of Rab7 at S72 under basal conditions, both in the unstimulated controls in the poly(I:C) (Figure 4.11) and LPS experiments (Figure 4.13), and in the phosphoproteomic screens where it was discovered in numerous tissues under basal conditions (Huttlin et al., 2010).

IKKε and TBK1 are also abundantly expressed in the nervous system, where the NF-κB pathway important for neuronal survival, neuroprotection and the suppression of neuronal inflammation (Emmanouil et al., 2011; Mincheva et al., 2011; Moser et al., 2011). Dysregulation of the NF-κB pathway has been associated with Huntington's disease, multiple sclerosis and other neurodegenerative disorders, where Rab7 has also been implicated (Khoshnan and Patterson, 2011). It has been shown that the NF-κB pathway is activated by neurotrophins to promote cell survival in embryonic motor neurons *in vitro* (Mincheva et al., 2011). Unfortunately the authors did not examine whether TBK1 or IKKε were involved in this process; however, the expression of both TBK1 and particularly IKKε, which is predominantly induced following activation of the innate immune response, suggests that these kinases function in other mechanisms in the nervous system. It would be interesting to see if TBK1 and/or IKKε played a role in the axonal transport of signalling endosomes and in

establishing polarity and growth of neurons, similar to the effects seen in *Drosophila* bristles.

6.5 An alternative mechanism of Rab7 regulation

Another kinase tested in the *in vitro* kinase, the G2019S mutant of leucine-rich repeat kinase 2 ($LRRK2^{G2019S}$), which is the most common Parkinson's disease mutation, has been shown to promote Rab7-dependent perinuclear clustering of lysosomes (Dodson et al., 2012). While in the *in vitro* kinase screen, there was no increase in phosphorylation of Rab7 at S72 with $LRRK2^{G2019S}$, it did appear to phosphorylate elsewhere. In the original screen, which did not include the $Rab7^{S72P}$ control, $LRRK2^{G2019S}$ was one of the main hits; however, in the two subsequent rescreens it appeared to phosphorylate the $Rab7^{S72P}$ mutant more. $LRRK2^{Wt}$ has been implicated in a number of processes, including has been shown to regulate synaptic vesicle trafficking, endocytosis, macroautophagy, and retromer-dependent transport from late endosomes to the trans-Golgi network (Gomez-Suaga et al., 2014). The $LRRK2^{G2019S}$ mutation increases the kinase activity of LRRK2 and the effect of this mutation on lysosome positioning appears to require both microtubules and cytoplasmic dynein, indicating that LRRK2 is an inhibitor of Rab7-dependent microtubule minus-end directed transport (Dodson et al., 2012). Another recent study also showed that $LRRK2^{G2019S}$ decreases Rab7 activity and inhibits EGFR degradation (Gomez-Suaga et al., 2014). The phosphorylation of Rab7 by $LRRK2^{G2019S}$ may represent another mechanism of Rab7 regulation by phosphorylation.

6.6 Future work

While it is clear that pRab7(S72) is present on endosomal membranes, it is unknown exactly what subset of Rab7-positive membranes this pool is. Future work should investigate the nature of this endocytic compartment that is decorated with pRab7(S72). Unfortunately, as $Rab7^{S72E}$ does not localise to membranes we were unable to examine whether this phosphomimetic mutation has any effect on the speed or direction of transport of late endosomes/lysosomes containing this protein. To address this, it may be interesting to investigate the localisation of pRab7(S72) on tubulated lysosomes, following stimulation of macrophages or dendritic cells with LPS. This may allow visualisation of pRab7(S72) on a subdomain of these structures. Colocalisation with specific effectors could also provide further insight into the role of this phosphorylation on Rab7.

Future investigation should also examine the interaction of Rab7 with TRAF3, REP1 and FYCO1, to determine if phosphorylation at S72 affects binding of these interactors in an isolated system. It would also be interesting to see if Rab7, TRAF3 and TBK1/IKKε colocalise in dendritic cells following stimulation of TRL3 or TLR4 by immunofluorescence and if they can form a complex *in vitro* using recombinant proteins.

Finally, I believe it is important to confirm if TBK1 and IKKε are in fact responsible for phosphorylation at S72 in cells following stimulation of TLR3 and/or TLR4. It would also be also interesting to see if stimulation of other receptors, such as the cytosolic MDA-5/RIG-I receptors caused phosphorylation of Rab7 at S72.

6.7 Concluding Remarks

The major conclusions of this study are as follows:

- Phosphorylation of Rab7 at S72 occurs following stimulation of TLR3 and TLR4 with viral dsRNA and bacterial LPS, respectively, possibly through TBK1 and IKKε, which both phosphorylate Rab7 at S72 *in vitro*

- TRAF3 has been identified as a new potential interactor of unphosphorylated Rab7, which may affect recruitment of TRAF3 to membranes following viral infection and subsequent activation of TBK1 and IKKε.

- Phosphorylation of Rab7 at S72 promotes differential binding of known interactors, including RILP, p150(Glued) and REP1, while having no effect others, such as ORP1L. The enrichment of S72-phosphorylated Rab7 on endosomal membranes also supports a role of phosphorylation in the regulation of interaction with effectors.

- Phosphorylation at S72 increases the intrinsic GTPase activity of Rab7, which may affect cycling of Rab7 from the cytosol to endosomal membranes and its activation state.

Reference List

Ali, B.R., Wasmeier, C., Lamoreux, L., Strom, M., and Seabra, M.C. (2004). Multiple regions contribute to membrane targeting of Rab GTPases. J Cell Sci *117*, 6401-6412.

Alonso-Curbelo, D., Riveiro-Falkenbach, E., Perez-Guijarro, E., Cifdaloz, M., Karras, P., Osterloh, L., Megias, D., Canon, E., Calvo, T.G., Olmeda, D.*, et al.* (2014). RAB7 controls melanoma progression by exploiting a lineage-specific wiring of the endolysosomal pathway. Cancer cell *26*, 61-76.

Balderhaar, H.J., and Ungermann, C. (2013). CORVET and HOPS tethering complexes - coordinators of endosome and lysosome fusion. J Cell Sci *126*, 1307-1316.

Bennetzen, M.V., Larsen, D.H., Bunkenborg, J., Bartek, J., Lukas, J., and Andersen, J.S. (2010). Site-specific phosphorylation dynamics of the nuclear proteome during the DNA damage response. Molecular & cellular proteomics : MCP *9*, 1314-1323.

Bertram, E.M., Hawley, R.G., and Watts, T.H. (2002). Overexpression of rab7 enhances the kinetics of antigen processing and presentation with MHC class II molecules in B cells. International immunology *14*, 309-318.

Beyenbach, K.W., and Wieczorek, H. (2006). The V-type H+ ATPase: molecular structure and function, physiological roles and regulation. The Journal of experimental biology *209*, 577-589.

Billcliff, P.G., and Lowe, M. (2014). Inositol lipid phosphatases in membrane trafficking and human disease. The Biochemical journal *461*, 159-175.

Bilsland, L.G., Sahai, E., Kelly, G., Golding, M., Greensmith, L., and Schiavo, G. (2010). Deficits in axonal transport precede ALS symptoms in vivo. Proceedings of the National Academy of Sciences of the United States of America *107*, 20523-20528.

Bremer, E. (2013). Targeting of the tumor necrosis factor receptor superfamily for cancer immunotherapy. ISRN oncology *2013*, 371854.

Cabrera, M., Nordmann, M., Perz, A., Schmedt, D., Gerondopoulos, A., Barr, F., Piehler, J., Engelbrecht-Vandre, S., and Ungermann, C. (2014). The Mon1-

Ccz1 GEF activates the Rab7 GTPase Ypt7 via a longin-fold-Rab interface and association with PI3P-positive membranes. J Cell Sci *127*, 1043-1051.

Cantalupo, G., Alifano, P., Roberti, V., Bruni, C.B., and Bucci, C. (2001). Rab-interacting lysosomal protein (RILP): the Rab7 effector required for transport to lysosomes. Embo J *20*, 683-693.

Carlton, J., Bujny, M., Peter, B.J., Oorschot, V.M., Rutherford, A., Mellor, H., Klumperman, J., McMahon, H.T., and Cullen, P.J. (2004). Sorting nexin-1 mediates tubular endosome-to-TGN transport through coincidence sensing of high- curvature membranes and 3-phosphoinositides. Current biology : CB *14*, 1791-1800.

Ceresa, B.P., and Bahr, S.J. (2006). rab7 activity affects epidermal growth factor:epidermal growth factor receptor degradation by regulating endocytic trafficking from the late endosome. The Journal of biological chemistry *281*, 1099-1106.

Chau, T.L., Gioia, R., Gatot, J.S., Patrascu, F., Carpentier, I., Chapelle, J.P., O'Neill, L., Beyaert, R., Piette, J., and Chariot, A. (2008). Are the IKKs and IKK-related kinases TBK1 and IKK-epsilon similarly activated? Trends in biochemical sciences *33*, 171-180.

Chen, L., Hu, J., Yun, Y., and Wang, T. (2010). Rab36 regulates the spatial distribution of late endosomes and lysosomes through a similar mechanism to Rab34. Molecular membrane biology *27*, 23-30.

Chevallier, J., Chamoun, Z., Jiang, G., Prestwich, G., Sakai, N., Matile, S., Parton, R.G., and Gruenberg, J. (2008). Lysobisphosphatidic acid controls endosomal cholesterol levels. The Journal of biological chemistry *283*, 27871-27880.

Chockalingam, A., Brooks, J.C., Cameron, J.L., Blum, L.K., and Leifer, C.A. (2009). TLR9 traffics through the Golgi complex to localize to endolysosomes and respond to CpG DNA. Immunol Cell Biol *87*, 209-217.

Chow, A., Toomre, D., Garrett, W., and Mellman, I. (2002). Dendritic cell maturation triggers retrograde MHC class II transport from lysosomes to the plasma membrane. Nature *418*, 988-994.

Chu, Y., Dodiya, H., Aebischer, P., Olanow, C.W., and Kordower, J.H. (2009). Alterations in lysosomal and proteasomal markers in Parkinson's disease: relationship to alpha-synuclein inclusions. Neurobiology of disease *35*, 385-398.

Clark, K., Peggie, M., Plater, L., Sorcek, R.J., Young, E.R., Madwed, J.B., Hough, J., McIver, E.G., and Cohen, P. (2011). Novel cross-talk within the IKK family controls innate immunity. The Biochemical journal *434*, 93-104.

Clark, K., Plater, L., Peggie, M., and Cohen, P. (2009). Use of the pharmacological inhibitor BX795 to study the regulation and physiological roles of TBK1 and IkappaB kinase epsilon: a distinct upstream kinase mediates Ser-172 phosphorylation and activation. The Journal of biological chemistry *284*, 14136-14146.

Cogli, L., Progida, C., Bramato, R., and Bucci, C. (2013). Vimentin phosphorylation and assembly are regulated by the small GTPase Rab7a. Biochimica et biophysica acta *1833*, 1283-1293.

Culpan, D., Cram, D., Chalmers, K., Cornish, A., Palmer, L., Palmer, J., Hughes, A., Passmore, P., Craig, D., Wilcock, G.K.*, et al.* (2009). TNFR-associated factor-2 (TRAF-2) in Alzheimer's disease. Neurobiology of aging *30*, 1052-1060.

D'Souza, R.S., Semus, R., Billings, E.A., Meyer, C.B., Conger, K., and Casanova, J.E. (2014). Rab4 Orchestrates a Small GTPase Cascade for Recruitment of Adaptor Proteins to Early Endosomes. Current Biology *24*, 1187-1198.

Da, Q., Yang, X.M., Xu, Y.L., Gao, G.X., Cheng, G.H., and Tang, H. (2011). TANK-Binding Kinase 1 Attenuates PTAP-Dependent Retroviral Budding through Targeting Endosomal Sorting Complex Required for Transport-I. Journal of immunology *186*, 3023-3030.

De Luca, M., Cogli, L., Progida, C., Nisi, V., Pascolutti, R., Sigismund, S., Di Fiore, P.P., and Bucci, C. (2014). RILP regulates vacuolar ATPase through interaction with the V1G1 subunit. J Cell Sci *127*, 2697-2708.

De Vos, K.J., Grierson, A.J., Ackerley, S., and Miller, C.C.J. (2008). Role of axonal transport in neurodegenerative diseases. Annu Rev Neurosci *31*, 151-173.

Deinhardt, K., Salinas, S., Verastegui, C., Watson, R., Worth, D., Hanrahan, S., Bucci, C., and Schiavo, G. (2006). Rab5 and Rab7 control endocytic sorting along the axonal retrograde transport pathway. Neuron *52*, 293-305.

Deneka, M., Neeft, M., Popa, I., van Oort, M., Sprong, H., Oorschot, V., Klumperman, J., Schu, P., and van der Sluijs, P. (2003). Rabaptin-5 alpha/rabaptin-4 serves as a linker between rab4 and gamma(1)-adaptin in membrane recycling from endosomes. Embo J *22*, 2645-2657.

Dephoure, N., Zhou, C., Villen, J., Beausoleil, S.A., Bakalarski, C.E., Elledge, S.J., and Gygi, S.P. (2008). A quantitative atlas of mitotic phosphorylation. Proceedings of the National Academy of Sciences of the United States of America *105*, 10762-10767.

DeSelm, C.J., Miller, B.C., Zou, W., Beatty, W.L., van Meel, E., Takahata, Y., Klumperman, J., Tooze, S.A., Teitelbaum, S.L., and Virgin, H.W. (2011). Autophagy proteins regulate the secretory component of osteoclastic bone resorption. Developmental cell *21*, 966-974.

Ding, J., Soule, G., Overmeyer, J.H., and Maltese, W.A. (2003). Tyrosine phosphorylation of the Rab24 GTPase in cultured mammalian cells. Biochem Bioph Res Co *312*, 670-675.

Dodson, M.W., Zhang, T., Jiang, C., Chen, S., and Guo, M. (2012). Roles of the Drosophila LRRK2 homolog in Rab7-dependent lysosomal positioning. Human molecular genetics *21*, 1350-1363.

Dumas, J.J., Zhu, Z., Connolly, J.L., and Lambright, D.G. (1999). Structural basis of activation and GTP hydrolysis in Rab proteins. Structure *7*, 413-423.

Emmanouil, M., Taoufik, E., Tseveleki, V., Vamvakas, S.S., and Probert, L. (2011). A Role for Neuronal NF-kappa B in Suppressing Neuroinflammation and Promoting Neuroprotection in the CNS. Adv Exp Med Biol *691*, 575-581.

Ewing, R.M., Chu, P., Elisma, F., Li, H., Taylor, P., Climie, S., McBroom-Cerajewski, L., Robinson, M.D., O'Connor, L., Li, M.*, et al.* (2007). Large-scale mapping of human protein-protein interactions by mass spectrometry. Molecular systems biology *3*, 89.

Fitzgerald, K.A., Rowe, D.C., Barnes, B.J., Caffrey, D.R., Visintin, A., Latz, E., Monks, B., Pitha, P.M., and Golenbock, D.T. (2003). LPS-TLR4 signaling to

IRF-3/7 and NF-kappaB involves the toll adapters TRAM and TRIF. The Journal of experimental medicine *198*, 1043-1055.

Flinn, R.J., Yan, Y., Goswami, S., Parker, P.J., and Backer, J.M. (2010). The Late Endosome is Essential for mTORC1 Signaling. Molecular biology of the cell *21*, 833-841.

Friedman, J., DiBenedetto, J., West, M., Rowland, A., and Voeltz, G.K. (2013). Endoplasmic reticulum–endosome contact increases as endosomes traffic and mature. Molecular biology of the cell *24*, 1030-1040.

Funami, K., Matsumoto, M., Oshiumi, H., Akazawa, T., Yamamoto, A., and Seya, T. (2004). The cytoplasmic 'linker region' in Toll-like receptor 3 controls receptor localization and signaling. International immunology *16*, 1143-1154.

Ganley, I.G., Carroll, K., Bittova, L., and Pfeffer, S. (2004). Rab9 GTPase regulates late endosome size and requires effector interaction for its stability. Molecular biology of the cell *15*, 5420-5430.

Garcia-Cattaneo, A., Gobert, F.X., Muller, M., Toscano, F., Flores, M., Lescure, A., Del Nery, E., and Benaroch, P. (2012). Cleavage of Toll-like receptor 3 by cathepsins B and H is essential for signaling. Proceedings of the National Academy of Sciences of the United States of America *109*, 9053-9058.

Gomez-Suaga, P., Rivero-Rios, P., Fdez, E., Blanca Ramirez, M., Ferrer, I., Aiastui, A., Lopez De Munain, A., and Hilfiker, S. (2014). LRRK2 delays degradative receptor trafficking by impeding late endosomal budding through decreasing Rab7 activity. Human molecular genetics.

Gorbea, C., Rechsteiner, M., Vallejo, J.G., and Bowles, N.E. (2013). Depletion of the 26S proteasome adaptor Ecm29 increases Toll-like receptor 3 signaling. Science signaling *6*, ra86.

Gu, F., Crump, C.M., and Thomas, G. (2001). Trans-Golgi network sorting. Cellular and Molecular Life Sciences *58*, 1067-1084.

Gutierrez, M.G., Master, S.S., Singh, S.B., Taylor, G.A., Colombo, M.I., and Deretic, V. (2004). Autophagy is a defense mechanism inhibiting BCG and Mycobacterium tuberculosis survival in infected macrophages. Cell *119*, 753-766.

Haglund, K., and Dikic, I. (2012). The role of ubiquitylation in receptor endocytosis and endosomal sorting. J Cell Sci *125*, 265-275.

Hehnly, H., and Doxsey, S. (2014). Rab11 endosomes contribute to mitotic spindle organization and orientation. Developmental cell *28*, 497-507.

Henne, W.M., Buchkovich, N.J., and Emr, S.D. (2011). The ESCRT pathway. Developmental cell *21*, 77-91.

Henriksen, L., Grandal, M.V., Knudsen, S.L., van Deurs, B., and Grovdal, L.M. (2013). Internalization mechanisms of the epidermal growth factor receptor after activation with different ligands. PloS one *8*, e58148.

Hsu, P.P., Kang, S.A., Rameseder, J., Zhang, Y., Ottina, K.A., Lim, D., Peterson, T.R., Choi, Y., Gray, N.S., Yaffe, M.B.*, et al.* (2011). The mTOR-regulated phosphoproteome reveals a mechanism of mTORC1-mediated inhibition of growth factor signaling. Science *332*, 1317-1322.

Husebye, H., Halaas, O., Stenmark, H., Tunheim, G., Sandanger, O., Bogen, B., Brech, A., Latz, E., and Espevik, T. (2006). Endocytic pathways regulate Toll-like receptor 4 signaling and link innate and adaptive immunity. Embo J *25*, 683-692.

Hutagalung, A.H., and Novick, P.J. (2011). Role of Rab GTPases in membrane traffic and cell physiology. Physiol Rev *91*, 119-149.

Huttlin, E.L., Jedrychowski, M.P., Elias, J.E., Goswami, T., Rad, R., Beausoleil, S.A., Villen, J., Haas, W., Sowa, M.E., and Gygi, S.P. (2010). A tissue-specific atlas of mouse protein phosphorylation and expression. Cell *143*, 1174-1189.

Ikawa, K., Satou, A., Fukuhara, M., Matsumura, S., Sugiyama, N., Goto, H., Fukuda, M., Inagaki, M., Ishihama, Y., and Toyoshima, F. (2014). Inhibition of endocytic vesicle fusion by Plk1-mediated phosphorylation of vimentin during mitosis. Cell cycle *13*, 126-137.

Itoh, K., Watanabe, A., Funami, K., Seya, T., and Matsumoto, M. (2008). The clathrin-mediated endocytic pathway participates in dsRNA-induced IFN-beta production. Journal of immunology *181*, 5522-5529.

Jacob, C.O., Lewis, G.D., and McDevitt, H.O. (1991). MHC class II-associated variation in the production of tumor necrosis factor in mice and humans:

relevance to the pathogenesis of autoimmune diseases. Immunologic research *10*, 156-168.

Jager, S., Bucci, C., Tanida, I., Ueno, T., Kominami, E., Saftig, P., and Eskelinen, E.L. (2004). Role for Rab7 in maturation of late autophagic vacuoles. J Cell Sci *117*, 4837-4848.

Janssens, S., and Beyaert, R. (2002). A universal role for MyD88 in TLR/IL-1R-mediated signaling. Trends in biochemical sciences *27*, 474-482.

Johansson, M., Rocha, N., Zwart, W., Jordens, I., Janssen, L., Kuijl, C., Olkkonen, V.M., and Neefjes, J. (2007a). Activation of endosomal dynein motors by stepwise assembly of Rab7-RILP-p150(Glued), ORP1L, and the receptor beta III spectrin. Journal of Cell Biology *176*, 459-471.

Johansson, M., Rocha, N., Zwart, W., Jordens, I., Janssen, L., Kuijl, C., Olkkonen, V.M., and Neefjes, J. (2007b). Activation of endosomal dynein motors by stepwise assembly of Rab7-RILP-p150Glued, ORP1L, and the receptor betalll spectrin. The Journal of cell biology *176*, 459-471.

Jordens, I., Fernandez-Borja, M., Marsman, M., Dusseljee, S., Janssen, L., Calafat, J., Janssen, H., Wubbolts, R., and Neefjes, J. (2001). The Rab7 effector protein RILP controls lysosomal transport by inducing the recruitment of dynein-dynactin motors. Current biology : CB *11*, 1680-1685.

Kagan, J.C., Su, T., Horng, T., Chow, A., Akira, S., and Medzhitov, R. (2008). TRAM couples endocytosis of Toll-like receptor 4 to the induction of interferon-beta. Nature immunology *9*, 361-368.

Kaniuk, N.A., Canadien, V., Bagshaw, R.D., Bakowski, M., Braun, V., Landekic, M., Mitra, S., Huang, J., Heo, W.D., Meyer, T.*, et al.* (2011). Salmonella exploits Arl8B-directed kinesin activity to promote endosome tubulation and cell-to-cell transfer. Cellular microbiology *13*, 1812-1823.

Karniguian, A., Zahraoui, A., and Tavitian, A. (1993). Identification of Small Gtp-Binding Rab Proteins in Human Platelets - Thrombin-Induced Phosphorylation of Rab3b, Rab6, and Rab8 Proteins. Proceedings of the National Academy of Sciences of the United States of America *90*, 7647-7651.

Kavsak, P., Rasmussen, R.K., Causing, C.G., Bonni, S., Zhu, H.T., Thomsen, G.H., and Wrana, J.L. (2000). Smad7 binds to Smurf2 to form an E3 ubiquitin ligase that targets the TGF beta receptor for degradation. Mol Cell *6*, 1365-1375.

Khoshnan, A., and Patterson, P.H. (2011). The role of I kappa B kinase complex in the neurobiology of Huntington's disease. Neurobiology of disease *43*, 305-311.

Kim, J.Y., Welsh, E.A., Oguz, U., Fang, B., Bai, Y., Kinose, F., Bronk, C., Remsing Rix, L.L., Beg, A.A., Rix, U.*, et al.* (2013). Dissection of TBK1 signaling via phosphoproteomics in lung cancer cells. Proceedings of the National Academy of Sciences of the United States of America *110*, 12414-12419.

Klopper, T.H., Kienle, N., Fasshauer, D., and Munro, S. (2012). Untangling the evolution of Rab G proteins: implications of a comprehensive genomic analysis. BMC biology *10*, 71.

Kurt-Jones, E.A., Sandor, F., Ortiz, Y., Bowen, G.N., Counter, S.L., Wang, T.C., and Finberg, R.W. (2004). Use of murine embryonic fibroblasts to define Toll-like receptor activation and specificity. Journal of endotoxin research *10*, 419-424.

Kyei, G.B., Dinkins, C., Davis, A.S., Roberts, E., Singh, S.B., Dong, C., Wu, L., Kominami, E., Ueno, T., Yamamoto, A.*, et al.* (2009). Autophagy pathway intersects with HIV-1 biosynthesis and regulates viral yields in macrophages. The Journal of cell biology *186*, 255-268.

Latz, E., Schoenemeyer, A., Visintin, A., Fitzgerald, K.A., Monks, B.G., Knetter, C.F., Lien, E., Nilsen, N.J., Espevik, T., and Golenbock, D.T. (2004). TLR9 signals after translocating from the ER to CpG DNA in the lysosome. Nature immunology *5*, 190-198.

Lin, M.G., and Zhong, Q. (2011). Interaction between small GTPase Rab7 and PI3KC3 links autophagy and endocytosis: A new Rab7 effector protein sheds light on membrane trafficking pathways. Small GTPases *2*, 85-88.

Lin, S.C., Lo, Y.C., and Wu, H. (2010). Helical assembly in the MyD88-IRAK4-IRAK2 complex in TLR/IL-1R signalling. Nature *465*, 885-890.

Manczak, M., Anekonda, T.S., Henson, E., Park, B.S., Quinn, J., and Reddy, P.H. (2006). Mitochondria are a direct site of A beta accumulation in Alzheimer's disease neurons: implications for free radical generation and oxidative damage in disease progression. Human molecular genetics *15*, 1437-1449.

Mayinger, P. (2012). Phosphoinositides and vesicular membrane traffic. Bba-Mol Cell Biol L *1821*, 1104-1113.

Mayya, V., Lundgren, D.H., Hwang, S.I., Rezaul, K., Wu, L., Eng, J.K., Rodionov, V., and Han, D.K. (2009). Quantitative phosphoproteomic analysis of T cell receptor signaling reveals system-wide modulation of protein-protein interactions. Science signaling *2*, ra46.

McCray, B.A., Skordalakes, E., and Taylor, J.P. (2010). Disease mutations in Rab7 result in unregulated nucleotide exchange and inappropriate activation. Human molecular genetics *19*, 1033-1047.

Merithew, E., Stone, C., Eathiraj, S., and Lambright, D.G. (2003). Determinants of Rab5 interaction with the N terminus of early endosome antigen 1. The Journal of biological chemistry *278*, 8494-8500.

Mincheva, S., Garcera, A., Gou-Fabregas, M., Encinas, M., Dolcet, X., and Soler, R.M. (2011). The Canonical Nuclear Factor-kappa B Pathway Regulates Cell Survival in a Developmental Model of Spinal Cord Motoneurons. Journal of Neuroscience *31*, 6493-6503.

Mincheva-Tasheva, S., and Soler, R.M. (2013). NF-kappaB signaling pathways: role in nervous system physiology and pathology. The Neuroscientist : a review journal bringing neurobiology, neurology and psychiatry *19*, 175-194.

Mitchell, D.J., Blasier, K.R., Jeffery, E.D., Ross, M.W., Pullikuth, A.K., Suo, D., Park, J., Smiley, W.R., Lo, K.W., Shabanowitz, J.*, et al.* (2012). Trk activation of the ERK1/2 kinase pathway stimulates intermediate chain phosphorylation and recruits cytoplasmic dynein to signaling endosomes for retrograde axonal transport. The Journal of neuroscience : the official journal of the Society for Neuroscience *32*, 15495-15510.

Mizuno, K., Kitamura, A., and Sasaki, T. (2003). Rabring7, a novel Rab7 target protein with a RING finger motif. Molecular biology of the cell *14*, 3741-3752.

Moser, C.V., Kynast, K., Baatz, K., Russe, O.Q., Ferreiros, N., Costiuk, H., Lu, R.R., Schmidtko, A., Tegeder, I., Geisslinger, G.*, et al.* (2011). The Protein Kinase IKK epsilon Is a Potential Target for the Treatment of Inflammatory Hyperalgesia. Journal of immunology *187*, 2617-2625.

Mrakovic, A., Kay, J.G., Furuya, W., Brumell, J.H., and Botelho, R.J. (2012). Rab7 and Arl8 GTPases are necessary for lysosome tubulation in macrophages. Traffic *13*, 1667-1679.

Nordmann, M., Cabrera, M., Perz, A., Brocker, C., Ostrowicz, C., Engelbrecht-Vandre, S., and Ungermann, C. (2010). The Mon1-Ccz1 Complex Is the GEF of the Late Endosomal Rab7 Homolog Ypt7. Current Biology *20*, 1654-1659.

Olsen, J.V., Vermeulen, M., Santamaria, A., Kumar, C., Miller, M.L., Jensen, L.J., Gnad, F., Cox, J., Jensen, T.S., Nigg, E.A.*, et al.* (2010). Quantitative phosphoproteomics reveals widespread full phosphorylation site occupancy during mitosis. Science signaling *3*, ra3.

Ong, S.T., Freeley, M., Skubis-Zegadlo, J., Fazil, M.H.U.T., Kelleher, D., Fresser, F., Baier, G., Verma, N.K., and Long, A. (2014). Phosphorylation of Rab5a Protein by Protein Kinase C epsilon Is Crucial for T-cell Migration. Journal of Biological Chemistry *289*, 19420-19434.

Orth, J.D., Krueger, E.W., Weller, S.G., and McNiven, M.A. (2006). A novel endocytic mechanism of epidermal growth factor receptor sequestration and internalization. Cancer Res *66*, 3603-3610.

Otani, T., Oshima, K., Onishi, S., Takeda, M., Shinmyozu, K., Yonemura, S., and Hayashi, S. (2011). IKK epsilon Regulates Cell Elongation through Recycling Endosome Shuttling. Developmental cell *20*, 219-232.

Owen, D.J., Collins, B.M., and Evans, P.R. (2004). Adaptors for clathrin coats: structure and function. Annual review of cell and developmental biology *20*, 153-191.

Pankiv, S., Alemu, E.A., Brech, A., Bruun, J.A., Lamark, T., Overvatn, A., Bjorkoy, G., and Johansen, T. (2010). FYCO1 is a Rab7 effector that binds to LC3 and PI3P to mediate microtubule plus end-directed vesicle transport. The Journal of cell biology *188*, 253-269.

Peralta, E.R., Martin, B.C., and Edinger, A.L. (2010). Differential Effects of TBC1D15 and Mammalian Vps39 on Rab7 Activation State, Lysosomal Morphology, and Growth Factor Dependence. Journal of Biological Chemistry *285*, 16814-16821.

Pereira-Leal, J.B., Strom, M., Godfrey, R.F., and Seabra, M.C. (2003). Structural determinants of Rab and Rab Escort Protein interaction: Rab family motifs define a conserved binding surface. Biochem Biophys Res Commun *301*, 92-97.

Pons, V., Luyet, P.P., Morel, E., Abrami, L., van der Goot, F.G., Parton, R.G., and Gruenberg, J. (2008). Hrs and SNX3 functions in sorting and membrane invagination within multivesicular bodies. Plos Biol *6*, 1942-1956.

Poteryaev, D., Datta, S., Ackema, K., Zerial, M., and Spang, A. (2010). Identification of the switch in early-to-late endosome transition. Eur J Cell Biol *89*, 28-28.

Progida, C., Malerod, L., Stuffers, S., Brech, A., Bucci, C., and Stenmark, H. (2007). RILP is required for the proper morphology and function of late endosomes. J Cell Sci *120*, 3729-3737.

Qi, R., Singh, D., and Kao, C.C. (2012). Proteolytic processing regulates Toll-like receptor 3 stability and endosomal localization. The Journal of biological chemistry *287*, 32617-32629.

Riggs, K.A., Hasan, N., Humphrey, D., Raleigh, C., Nevitt, C., Corbin, D., and Hu, C. (2012). Regulation of integrin endocytic recycling and chemotactic cell migration by syntaxin 6 and VAMP3 interaction. J Cell Sci *125*, 3827-3839.

Rocha, N., Kuijl, C., van der Kant, R., Janssen, L., Houben, D., Janssen, H., Zwart, W., and Neefjes, J. (2009). Cholesterol sensor ORP1L contacts the ER protein VAP to control Rab7-RILP-p150 Glued and late endosome positioning. The Journal of cell biology *185*, 1209-1225.

Romero Rosales, K., Peralta, E.R., Guenther, G.G., Wong, S.Y., and Edinger, A.L. (2009). Rab7 activation by growth factor withdrawal contributes to the induction of apoptosis. Molecular biology of the cell *20*, 2831-2840.

Roy, S.G., Stevens, M.W., So, L., and Edinger, A.L. (2013). Reciprocal effects of rab7 deletion in activated and neglected T cells. Autophagy *9*, 1009-1023.

Sakane, A., Hatakeyama, S., and Sasaki, T. (2007). Involvement of Rabring7 in EGF receptor degradation as an E3 ligase. Biochem Bioph Res Co *357*, 1058-1064.

Saxena, S., Bucci, C., Weis, J., and Kruttgen, A. (2005). The small GTPase Rab7 controls the endosomal trafficking and neuritogenic signaling of the nerve growth factor receptor TrkA. Journal of Neuroscience *25*, 10930-10940.

Schaefer, M.R., Wonderlich, E.R., Roeth, J.F., Leonard, J.A., and Collins, K.L. (2008). HIV-1 Nef targets MHC-I and CD4 for degradation via a final common beta-COP-dependent pathway in T cells. PLoS pathogens *4*, e1000131.

Schmieg, N., Menendez, G., Schiavo, G., and Terenzio, M. (2014). Signalling endosomes in axonal transport: travel updates on the molecular highway. Seminars in cell & developmental biology *27*, 32-43.

Seaman, M.N.J., Harbour, M.E., Tattersall, D., Read, E., and Bright, N. (2009). Membrane recruitment of the cargo-selective retromer subcomplex is catalysed by the small GTPase Rab7 and inhibited by the Rab-GAP TBC1D5. J Cell Sci *122*, 2371-2382.

Semerdjieva, S., Shortt, B., Maxwell, E., Singh, S., Fonarev, P., Hansen, J., Schiavo, G., Grant, B.D., and Smythe, E. (2008). Coordinated regulation of AP2 uncoating from clathrin-coated vesicles by rab5 and hRME-6. Journal of Cell Biology *183*, 499-511.

Seto, S., Matsumoto, S., Ohta, I., Tsujimura, K., and Koide, Y. (2009). Dissection of Rab7 localization on Mycobacterium tuberculosis phagosome. Biochem Biophys Res Commun *387*, 272-277.

Smith, G.A., Rocha, E.M., McLean, J.R., Hayes, M.A., Izen, S.C., Isacson, O., and Hallett, P.J. (2014). Progressive axonal transport and synaptic protein changes correlate with behavioral and neuropathological abnormalities in the heterozygous Q175 KI mouse model of Huntington's disease. Human molecular genetics *23*, 4510-4527.

Spinosa, M.R., Progida, C., De Luca, A., Colucci, A.M., Alifano, P., and Bucci, C. (2008). Functional characterization of Rab7 mutant proteins associated with Charcot-Marie-Tooth type 2B disease. The Journal of neuroscience : the official journal of the Society for Neuroscience *28*, 1640-1648.

Steffan, J.J., Dykes, S.S., Coleman, D.T., Adams, L.K., Rogers, D., Carroll, J.L., Williams, B.J., and Cardelli, J.A. (2014). Supporting a role for the GTPase Rab7 in prostate cancer progression. PloS one *9*, e87882.

Takahashi, S., Kubo, K., Waguri, S., Yabashi, A., Shin, H.W., Katoh, Y., and Nakayama, K. (2012). Rab11 regulates exocytosis of recycling vesicles at the plasma membrane. J Cell Sci *125*, 4049-4057.

Tan, S.C., Scherer, J., and Vallee, R.B. (2011). Recruitment of dynein to late endosomes and lysosomes through light intermediate chains. Molecular biology of the cell *22*, 467-477.

Thenappan, A., Shukla, V., Khalek, F.J.A., Li, Y., Shetty, K., Liu, P., Li, L., Johnson, R.L., Johnson, L., and Mishra, L. (2011). Loss of Transforming Growth Factor beta Adaptor Protein beta-2 Spectrin Leads to Delayed Liver Regeneration in Mice. Hepatology *53*, 1641-1650.

Trost, M., English, L., Lemieux, S., Courcelles, M., Desjardins, M., and Thibault, P. (2009). The phagosomal proteome in interferon-gamma-activated macrophages. Immunity *30*, 143-154.

Tsan, M.F. (2006). Toll-like receptors, inflammation and cancer. Seminars in cancer biology *16*, 32-37.

Tu, C., Ortega-Cava, C.F., Winograd, P., Stanton, M.J., Reddi, A.L., Dodge, I., Arya, R., Dimri, M., Clubb, R.J., Naramura, M.*, et al.* (2010). Endosomal-sorting complexes required for transport (ESCRT) pathway-dependent endosomal traffic regulates the localization of active Src at focal adhesions. Proceedings of the National Academy of Sciences of the United States of America *107*, 16107-16112.

Ungermann, C., Price, A., and Wickner, W. (2000). A new role for a SNARE protein as a regulator of the Ypt7/Rab-dependent stage of docking. Proceedings of the National Academy of Sciences of the United States of America *97*, 8889-8891.

van der Kant, R., Fish, A., Janssen, L., Janssen, H., Krom, S., Ho, N., Brummelkamp, T., Carette, J., Rocha, N., and Neefjes, J. (2013). Late endosomal transport and tethering are coupled processes controlled by RILP and the cholesterol sensor ORP1L. J Cell Sci *126*, 3462-3474.

van der Sluijs, P., Hull, M., Huber, L.A., Male, P., Goud, B., and Mellman, I. (1992). Reversible phosphorylation--dephosphorylation determines the localization of rab4 during the cell cycle. Embo J *11*, 4379-4389.

Verhoeven, K., De Jonghe, P., Coen, K., Verpoorten, N., Auer-Grumbach, M., Kwon, J.M., FitzPatrick, D., Schmedding, E., De Vriendt, E., Jacobs, A.*, et al.* (2003). Mutations in the small GTP-ase late endosomal protein RAB7 cause Charcot-Marie-Tooth type 2B neuropathy. American journal of human genetics *72*, 722-727.

Vihervaara, T., Uronen, R.L., Wohlfahrt, G., Bjorkhem, I., Ikonen, E., and Olkkonen, V.M. (2011). Sterol binding by OSBP-related protein 1L regulates late endosome motility and function. Cellular and molecular life sciences : CMLS *68*, 537-551.

Villen, J., Beausoleil, S.A., Gerber, S.A., and Gygi, S.P. (2007). Large-scale phosphorylation analysis of mouse liver. Proceedings of the National Academy of Sciences of the United States of America *104*, 1488-1493.

Wang, T., and Hong, W. (2002). Interorganellar regulation of lysosome positioning by the Golgi apparatus through Rab34 interaction with Rab-interacting lysosomal protein. Molecular biology of the cell *13*, 4317-4332.

Wang, T., Zhang, M., Ma, Z., Guo, K., Tergaonkar, V., Zeng, Q., and Hong, W. (2012). A role of Rab7 in stabilizing EGFR-Her2 and in sustaining Akt survival signal. Journal of cellular physiology *227*, 2788-2797.

Ward, E.S., Martinez, C., Vaccaro, C., Zhou, J., Tang, Q., and Ober, R.J. (2005). From sorting endosomes to exocytosis: Association of Rab4 and Rab11 GTPases with the fc receptor, FcRn, during recycling. Molecular biology of the cell *16*, 2028-2038.

Weintz, G., Olsen, J.V., Fruhauf, K., Niedzielska, M., Amit, I., Jantsch, J., Mages, J., Frech, C., Dolken, L., Mann, M.*, et al.* (2010). The phosphoproteome of toll-like receptor-activated macrophages. Molecular systems biology *6*, 371.

Weissmann, L., Quaresma, P.G., Santos, A.C., de Matos, A.H., D'Avila Bittencourt Pascoal, V., Zanotto, T.M., Castro, G., Guadgnini, D., Martins da Silva, J., Velloso, L.A.*, et al.* (2014). IKK epsilon is key to induction of insulin resistance in the hypothalamus and its inhibition reverses obesity. Diabetes.

Wild, P., Farhan, H., McEwan, D.G., Wagner, S., Rogov, V.V., Brady, N.R., Richter, B., Korac, J., Waidmann, O., Choudhary, C.*, et al.* (2011). Phosphorylation of the autophagy receptor optineurin restricts Salmonella growth. Science *333*, 228-233.

Wu, M.S., Wang, T.L., Loh, E., Hong, W.J., and Song, H.W. (2005). Structural basis for recruitment of RILP by small GTPase Rab7. Embo J *24*, 1491-1501.

Wurmser, A.E., Sato, T.K., and Emr, S.D. (2000). New component of the vacuolar class C-Vps complex couples nucleotide exchange on the Ypt7 GTPase to SNARE-dependent docking and fusion. Journal of Cell Biology *151*, 551-562.

Yamamoto, M., Sato, S., Mori, K., Hoshino, K., Takeuchi, O., Takeda, K., and Akira, S. (2002). Cutting edge: a novel Toll/IL-1 receptor domain-containing adapter that preferentially activates the IFN-beta promoter in the Toll-like receptor signaling. Journal of immunology *169*, 6668-6672.

Yu, Y.H., Yoon, S.O., Poulogiannis, G., Yang, Q., Ma, X.J.M., Villen, J., Kubica, N., Hoffman, G.R., Cantley, L.C., Gygi, S.P.*, et al.* (2011). Phosphoproteomic Analysis Identifies Grb10 as an mTORC1 Substrate That Negatively Regulates Insulin Signaling. Science *332*, 1322-1326.

Zhang, K., Fishel Ben Kenan, R., Osakada, Y., Xu, W., Sinit, R.S., Chen, L., Zhao, X., Chen, J.Y., Cui, B., and Wu, C. (2013). Defective axonal transport of Rab7 GTPase results in dysregulated trophic signaling. The Journal of neuroscience : the official journal of the Society for Neuroscience *33*, 7451-7462.

Zhang, X.M., Walsh, B., Mitchell, C.A., and Rowe, T. (2005). TBC domain family, member 15 is a novel mammalian Rab GTPase-activating protein with substrate preference for Rab7. Biochem Bioph Res Co *335*, 154-161.